Title	BIAN型共役系高分子/ポリ(アクリル酸リチウム)バインダーを用いたリチウムイオン電池用シリコン/黒鉛負極の安定化
Author(s)	Sameer Nirupam Mishra
Citation	
Issue Date	2024-03
Type	Thesis or Dissertation
Text version	ETD
URL	http://hdl.handle.net/10119/19075
Rights	
Description	Supervisor: 松見 紀佳, 先端科学技術研究科, 博士

Japan Advanced Institute of Science and Technology

Doctoral Dissertation

Stabilization of Si and Graphite based Anodes for LIB Using BIAN
Type Conjugated Polymer/ Poly (lithium acrylate) Binder

Sameer Nirupam Mishra

Supervisor: Noriyoshi Matsumi

Graduate School of Advanced Science and Technology
Japan Advanced Institute of Science and Technology

Materials Science
March 2024

Abstract

Energy storage systems have become integral for sustainable living, moving away from crude oils and fossil fuels. This thesis delves into the hierarchy of primary energy sources, their harvesting methods, associated disadvantages, and environmental impacts, while exploring sustainable alternatives. Focusing on lithium-ion battery (LIB) technology, it examines the evolution of crucial components defining LIB performance, such as the solid electrolyte interphase (SEI), its composition, integrity, and thickness affecting Li ion diffusion and battery efficiency. Emphasis is placed on binders and electrolyte additives influencing SEI development, particularly highlighting BIAN-based polymers and LiPAA for their mechanical and electrochemical characteristics in enhancing fast charging and SEI stabilization. The thesis aims to investigate the structural and chemical qualities of bis(imino)acenaphthene (BIAN) compounds, leveraging them to develop innovative BIAN-based functional polymers as binders for high-performance LIB anodes. Chapter 1 provides an introductory overview, while Chapter 2 details the utilization of a BIAN-LiPAA composite polymer in graphite-based anodes, facilitating extremely Fast Charging (XFC) via strategic modifications. Building upon these successes, Chapter 3 explores the synthesis of another BIAN-based composite polymer to stabilize silicon-based anodes. Chapter 4 consolidates and summarizes the research outcomes, presenting findings from the investigation into BIAN-based polymers and their impact on LIB anode performance. This thesis culminates in a conclusive reflection on the potential and significance of BIAN-based functional polymers as crucial components in advancing the efficiency and stability of high-performance LIBs.

Preface

This thesis encapsulates the culmination of my PhD. research focused on enhancing Si and Graphite-based anodes in lithium-ion batteries (LIBs) through the utilization of a composite binder system comprising BIAN-type polymer and Poly (lithium acrylate). Conducted under the guidance of Prof. Noriyoshi Matsumi at the Graduate School of Advanced Science and Technology, Japan Advanced Institute of Science and Technology from 2018 to 2021, this work delves into crucial aspects influencing the performance and charging capabilities of LIBs.

In the landscape of electrochemical conversion systems and energy storage devices, such as batteries and fuel cells, the shift towards more sustainable energy sources has been pivotal. The significance of lithium-ion battery (LIB) technology stands out prominently in this context. Among the factors governing LIBs' performance, the formation of a passivation layer known as the solid electrolyte interface (SEI) holds paramount importance. The SEI's thickness, integrity, and composition significantly impact the battery's charge diffusion rate and overall performance. Consequently, there has been a concerted effort to engineer an effective SEI by exploring various avenues, including polymer binders, electrolyte additives, and modified electrode materials.

The polymers within the bis-iminoacenaphthene (BIAN) type materials have garnered attention for their exceptional redox behaviors, low LUMO (lowest unoccupied molecular orbitals) enabling n-doping in the anodic environment, and an electron-rich diimine backbone facilitating improved electronic conductivity. However, opportunities exist to further enhance the diffusion coefficient and augment the count of Li ions for facilitating rapid Li ion diffusion. Such enhancements could potentially lead to achieving extremely fast charging (XFC) capabilities. Hence, two composite binders BIAN-LiPAA and BIAN-DHBDN-LiPAA, were prepared by mixing a BIAN based copolymer and poly (lithium acrylate) (LiPAA). This thesis summarizes the synthesis, characterization, and application of two BIAN-based multifunctional composite binders in order to stabilize fast charging graphite and Si anodes by tailoring robust SEI and providing surplus Li ions and mechanical robustness to the electrode matrix as well. The thesis comes to a head with a synopsis of both the studies and providing fundamental understanding on structure activity relationship and potential applications of BIAN-based polymers as binder in LIBs.

Sameer Nirupam Mishra
Graduate School of Advanced Science and Technology
Japan Advanced Institute of Science and Technology
March 2024.

Acknowledgements

Sameer Nirupam Mishra
Graduate School of Advanced Science and Technology
Japan Advanced Institute of Science and Technology
March 2024.

Contents

Chapter 1
Introduction

Abstract

This chapter presents a synopsis of energy storage systems, highlighting their crucial role in our daily lives by offering sustainable and environmentally friendly alternatives to crude oils and fossil fuels. It begins by discussing the hierarchical arrangement of primary energy sources, their harvesting methods, drawbacks, and negative environmental impacts, while also exploring potential sustainable alternatives. Furthermore, it delves into the evolution of research and development in lithium-ion batteries (LIBs) technology, focusing on key components that significantly impact a LIB's performance. The chapter extensively covers the composition, structure, and thickness of the solid-electrolyte interface (SEI), elucidating its influence on lithium-ion diffusion, charging rates, and overall battery performance. Distinctively focused on the crucial role of components such as binders and electrolyte additives in modulating SEI formation. Moreover, the chapter thoroughly discusses binders, emphasizing the significance of BIAN-based polymers and LiPAA as binders due to their diverse mechanical and electrochemical characteristics. These properties are highlighted for their potential in enabling fast charging, stabilizing the SEI, modifying SEI formation, and providing mechanical robustness, particularly in high energy density electrodes.

A path from nonrenewable sources to electrochemical energy sources

In today's world, energy stands as the foundation of economic advancement. The rapid industrialization of the late 18th century heavily relied on easily accessible fossil fuels like oil, natural gas, and coal as primary energy sources. Fossil fuels, products of gradual degradation from a wide array of plants and animals through natural methods inside Earth's crust across many ecological eras.

Over the past three hundred years of globalization, humanity's outlook on existence has undergone a significant transformation. Catering to the ever-improving lifestyle demands has made energy an indispensable necessity. We shifted from dependence on windmills and watermills to non-renewable fossil fuels due to their potential to convert into carbon dioxide and water, generating substantial energy. This energy aided human labor, fueling the development of previously small-scale industries. Coal, historically recognized for its industrial and domestic uses, notably found widespread use in thermal power plants for energy generation.

Human ingenuity has led to substantial technological advancements harnessing various types of fossil fuels such as natural gas and petroleum, serving diverse purposes. Petroleum, commonly known as crude oil, undergoes refinement to produce various supplemental fuels like gasoline, kerosene, diesel, petroleum jelly, extensively utilized in transportation, synthetic materials (chemicals and medicines), and asphalt production. Similarly, non-renewable natural gas plays a crucial role in daily activities such as cooking, plastic manufacturing, and energy generation. The abundant availability of fossil fuels sparked a technological revolution lasting over two centuries.

Regrettably, the uncontrolled utilization of these non-renewable energy sources has raised several concerning issues including environmental pollution, greenhouse gas emissions, acid rain, deforestation, disruption in seasonal cycles impacting habitats, alongside concerns about their finite reserves leading to eventual exhaustion. According to the IEEJ's Asia/World Energy Outlook 2016 analysis, global primary energy consumption is projected to increase by 1.2% annually, reaching 18.9 billion TOE (tons of oil equivalent) by 2040 from 13.7 billion TOE in 2014. By 2040, fossil fuels will continue to be the largest contributors of energy, accounting for 78% of the total[1].

This predictive survey and estimate raise serious concerns about how humanity will strike a balance between the ever-increasing desire for growth and a healthy ecology to ensure the survival of living creatures. As a result, the need for sustainable sources of energy at accessible rates that are environmentally benign and fulfill the energy needs of future generations is critical today[1].

Electrochemical Energy Storage (EES) solutions work by converting and storing electrical energy in materials and devices that can be converted back to electricity when needed. Figure 1 depicts a logical classification of energy storage technologies based on function, storage duration and reaction time[1].
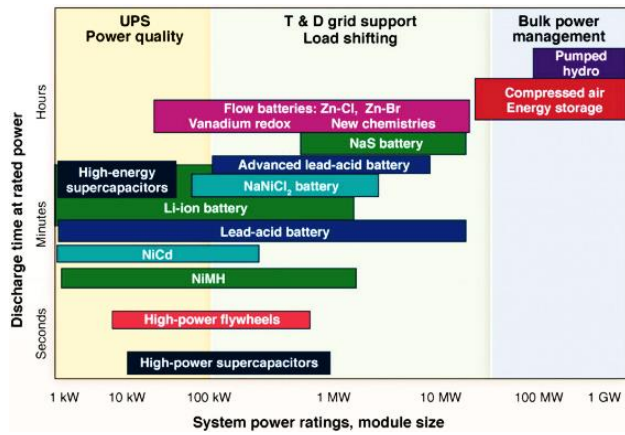
Figure 1 Energy Storage Technologies (EES) and their classification

As shown in figure below, the realm of Energy Storage System (EES) technologies encompasses a variety of storage options based on different forms and modes. However, within the scope of this study, only a select few EES technology modes are discussed here such as capacitors, supercapacitors, fuel cells and batteries.

Despite their differences, the energy-supplying process shares similarities among these three systems as it occurs at the dual phase boundary referred to as the electrode-electrolyte interface. However, what is noteworthy here that the pathways for electron transfer and ion transport vary significantly across these systems, setting them apart in their operational mechanisms and principles.

Capacitors and Supercapacitors
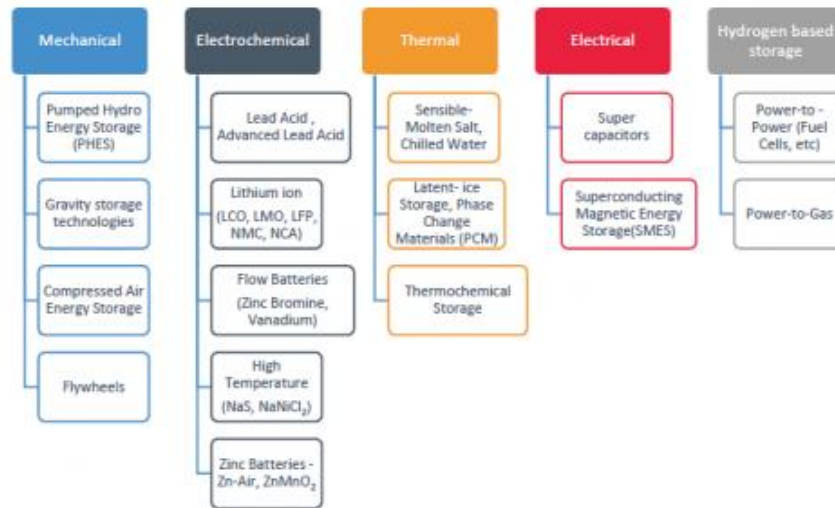
Figure 2 EES devices and various forms and modes of energy storage

Supercapacitors exhibit superior power delivery capabilities compared to batteries, yet they face limitations in storing an equivalent charge within the same volume. Consequently, their current utility is primarily restricted to applications demanding instant power delivery rather than high-capacity energy storage. Their notable attribute lies in their high cycle life, enduring millions of charge-discharge cycles, owing to their charge-storage mechanism involving an electric double layer formed on the electrode

surface, free from irreversible chemical processes. However, the specific charge storage mechanism of supercapacitors mandates operation at low potentials to prevent irreversible degradation of the electrolyte and this precaution is crucial in maintaining the stability and longevity of the supercapacitor's functionality[2].

Electrochemical capacitors, also known as supercapacitors or ultracapacitors, are categorized into three types based on their storage approach and cell configuration: hybrid capacitors (HCs) and electric double layer capacitors (EDLCs), When polarized, EDLCs store energy by creating an electric double layer at the electrode-electrolyte interface [2], enabling the separation of electric charge[2]. Compared to electrostatic capacitors, the high surface area and charge separation within a few angstroms in EDLCs contribute to their elevated capacitance. Pseudo-capacitors, in contrast, exhibit capacitor-like behavior through electrochemical charge storage within electrochemical capacitors (ECs). Hybrid capacitors, on the other hand, amalgamate both physical and chemical charge storage mechanisms.

Fuel cells (FCs)

Fuel cells have gained a lot of acceptance due to their eco-friendly operation, affordability, and high efficiency. Functionally, they offer low noise levels and versatile applications in both portable and stationary power generation. Energy conversion occurs directly from chemical energy to electricity in fuel cells, producing water and heat as byproducts. These cells comprise two electrodes separated by an electrolyte, receiving hydrogen fuel at the anode and oxygen (from the air) at the cathode. Hydrogen fuel continuously degrades into protons at the anode.[2,3]

The electrolyte-membrane functions as an intermediary, permitting the passage of solely positive ions toward the cathode while acting as an electron insulator. Electrons travel via an external circuit to the positive electrode to recombine and uphold the system's charge equilibrium. Consequently, positive and negative ions combine with the oxidant at the cathode, resulting in the generation of depleted oxidant, specifically ultra-pure water[3].

Depending on the electrolyte and fuel used, the fuel cells can be classified into 6 types. They are as follows.

Proton exchange membrane fuel cell (PEMFC):
Direct formic acid fuel cell (DFAFC)
Direct ethanol fuel cell (DEFC)
Alkaline fuel cell (AFC)
Proton ceramic fuel cell (PCFC)

Direct borohydride fuel cell (DBFC)
Phosphoric acid fuel cell (PAFC)
Molten carbonate fuel cell (MCFC)
Solid oxide fuel cell (SOFC)
Direct methanol fuel cell (DMFC)

Industries are developing their approach to fuel-cell technology by attempting to comprehend the present limitations and hurdles that impede its adoption in many aspects of life. Figure 3 depicts the connections/relationships between operational principles, feature-based benefits, and prospective applications of fuel cells.
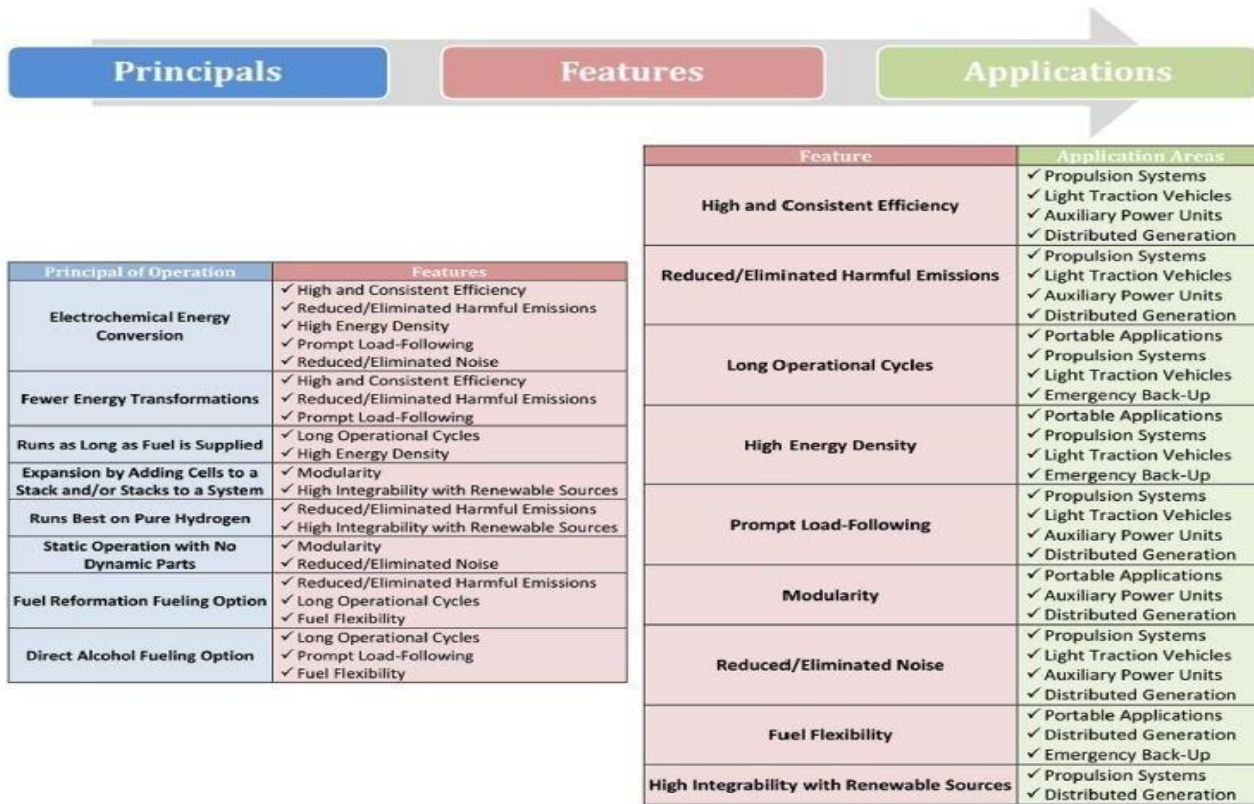
Figure 3 Principle, applications, and feature of the fuel cells

Batteries

A battery is a chemical power source created by assembling one or more electrochemical cells externally. It consists of two electrode terminals: the cathode (positive) and the anode (negative). Through an external circuit, electrons move from the negative terminal (anode) to the positive terminal (cathode). When linked to a load, a redox reaction occurs based on the reactants' capability to undergo chemical changes, resulting in the production of lower energy products. This chemical energy is converted into electrical energy and supplied to the load via an external circuit (see Figure 4). In addition to the anode and cathode, the electrolyte holds a pivotal role within the battery. It functions as an ion-conducting medium while insulating electrons and acts as a separator between the electrodes. While the electrolyte facilitates ion conduction, the external circuit provides a pathway for electron transport, effectively completing the electrochemical circuit. Batteries are broadly classified into two types: such as primary batteries and secondary batteries (refer to Figure 5), distinguished by their rechargeability. Primary batteries are non-rechargeable.
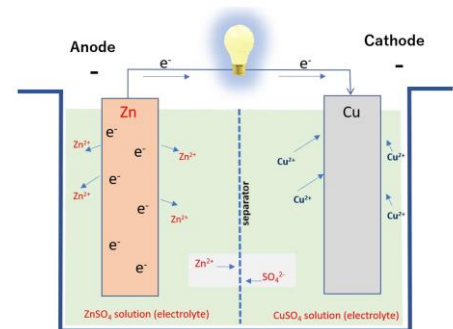
Figure 4 Schematic representation of the working principle of a Daniell battery

Primary batteries cannot be recharged. They are usually referred to as single-use or throwaway batteries since the chemical species undergo irreversible reaction after discharge. As a result, the ever-increasing
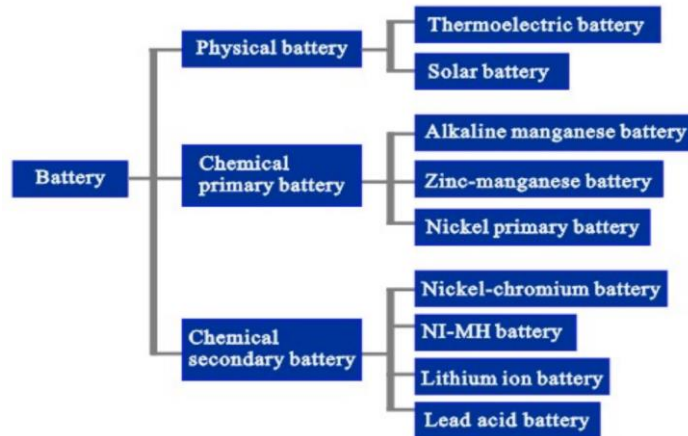
Figure 5 Classification of batteries

need for energy cannot be met by main batteries, which have a finite lifespan and no replenishing capability. This led to the development of secondary batteries, which are known as rechargeable batteries. In a secondary battery's charging phase, the cathode undergoes oxidation by losing electrons, while the negative electrode experiences reduction by accepting electrons. Conversely, during the discharging phase, the reverse process occurs. Throughout these cycles, the electrolyte remains unaffected, neither oxidized nor reduced. Therefore, rechargeable batteries can undergo numerous charge-discharge cycles before the battery components, such as electrodes and electrolytes, reach the end of their usable life. Consequently, they represent a more sustainable, environmentally friendly, and cost-effective option compared to traditional power sources. [4]

Nickel cadmium (NiCds) batteries

Nickel-cadmium (NiCd) batteries are appropriate for operating consistently at one stable potential and lower temperatures while boasting a notably extended shelf life. These batteries typically feature a cathode made of nickel hydroxide and an anode composed of cadmium hydroxide (refer to Figure 6). Aqueous KOH serves as the common electrolyte. The chemical reaction occurring during charge-discharge is represented by the equation below. During the charging phase, the nickel hydroxide ($Ni(OH)_2$) at the cathode transforms into nickel oxide hydroxide (NiOOH). Simultaneously, at the anode, cadmium hydroxide ($Cd(OH)_2$) oxidizes into cadmium (Cd). Conversely, during discharge, Cd reacts with NiOOH, yielding $Ni(OH)_2$ and $Cd(OH)_2$. However, NiCd batteries come with drawbacks: they tend to be expensive, and their energy density doesn't match up to choices like nickel-zinc (NiZn). Additionally, they undergo significant capacity loss when charged before completing the discharge cycle. [5]

$$Cd_{(s)} + 2NiO(OH)_{(s)} + 2H_2O_{(l)} \rightleftarrows Cd(OH)_{2(s)} + 2Ni(OH)_{2(s)} \tag{1}$$
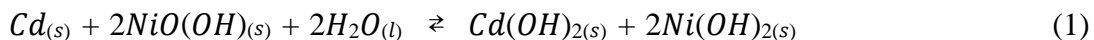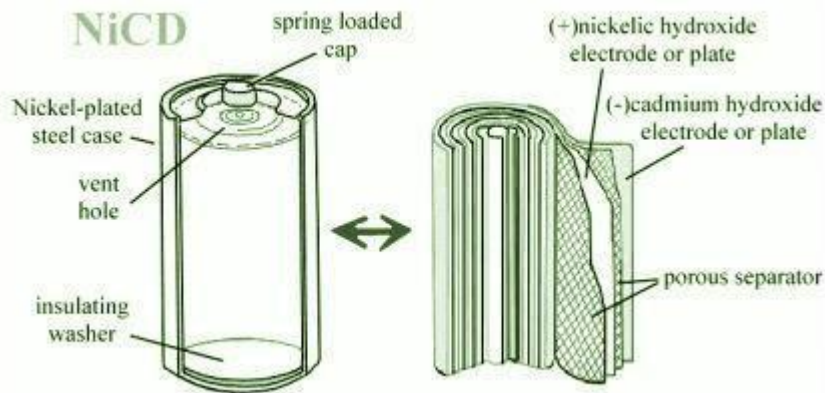
Figure 6 Schematic representation of a NiCd battery and its components

Lead acid batteries (LABs)

Lead acid batteries are one of the well-known rechargeable batteries, which were created in the nineteenth century. For almost a century, they have been widely utilized in the market. UPS, which is used for storing in backup power supplies in towers, automotive combustion, lights, high current demanding cases, off-grid household electricity, and conditions are a few of the areas where they are widely employed[6].
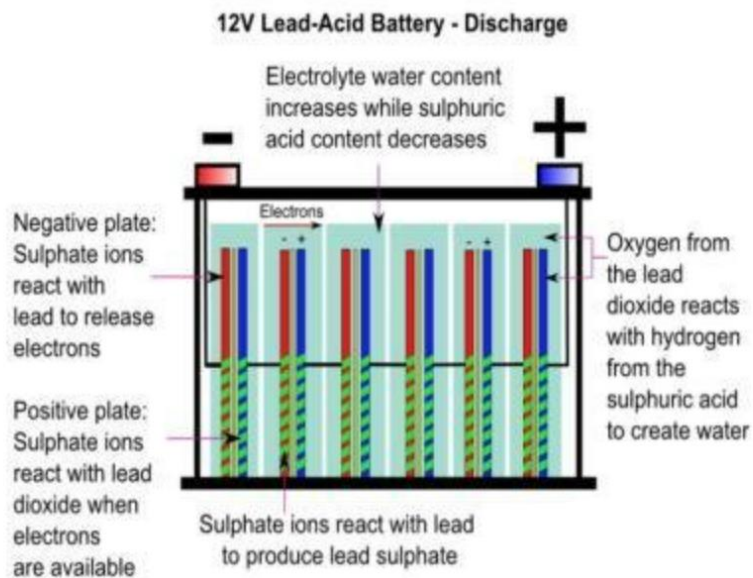
Figure-7 Schematic representation of LAB components and its working principle

Figure 7 depicts the design with numerous components and the operation of a general LAB. A LAB's discharge state has lead sulfate ($PbSO_4$) as both anode and cathode, but when it comes to electrolyte it is mostly aqueous due to H_2SO_4 breakdown. In a completely charged condition, the anode is Pb

and the cathode is lead dioxide, with a higher concentration of aq. H_2SO_4 in the electrolyte, as stated in equation below. The use of secondary batteries (rechargeable batteries) has created major environmental and health risks. Lead compounds are exceedingly dangerous, and the lack of recycling options is increasing the extent of lead concentration in landfills over time. As a result, "Getting Pb out" has become a catchphrase for several environmental / nature lovers and industry, driving research toward finding more greener alternatives[6].

$$Pb + PbO_2 + 2H_2SO_4 \leftrightarrows 2PbSO_4 + 2H_2O \qquad (2)$$
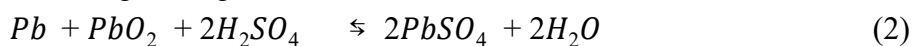
Lithium-ion batteries (LIBs)
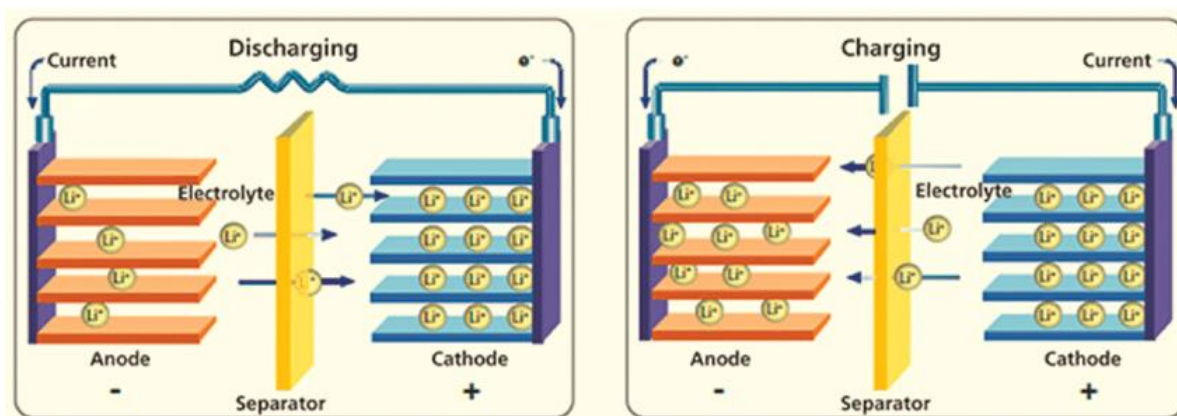
Figure 8 Schematic representation of the working principle of a Li ion battery

LIBs have emerged as a standout choice among secondary batteries for electrochemical energy storage, surpassing options like nickel-cadmium, lead-acid, nickel-zinc, and nickel-iron batteries. Their superiority is attributed to various factors, including a low reduction potential, rapid diffusion, easy compatibility of Li ions in different solid matrices, and high volumetric power density [7]. Illustrated in Figure 8, a standard LIB consists of an anode capable of lithium intercalation or alloying (e.g., graphite or silicon) and a cathode constructed from lithium-rich materials based on transition metal oxides like lithium cobalt oxide. Moreover, it incorporates a porous polymer separator and an organic electrolyte containing lithium salt. Unlike other secondary batteries that generate energy through reversible redox reaction of electrode materials, the fundamental mechanism of a typical LIB hinges on "intercalation" chemistry.
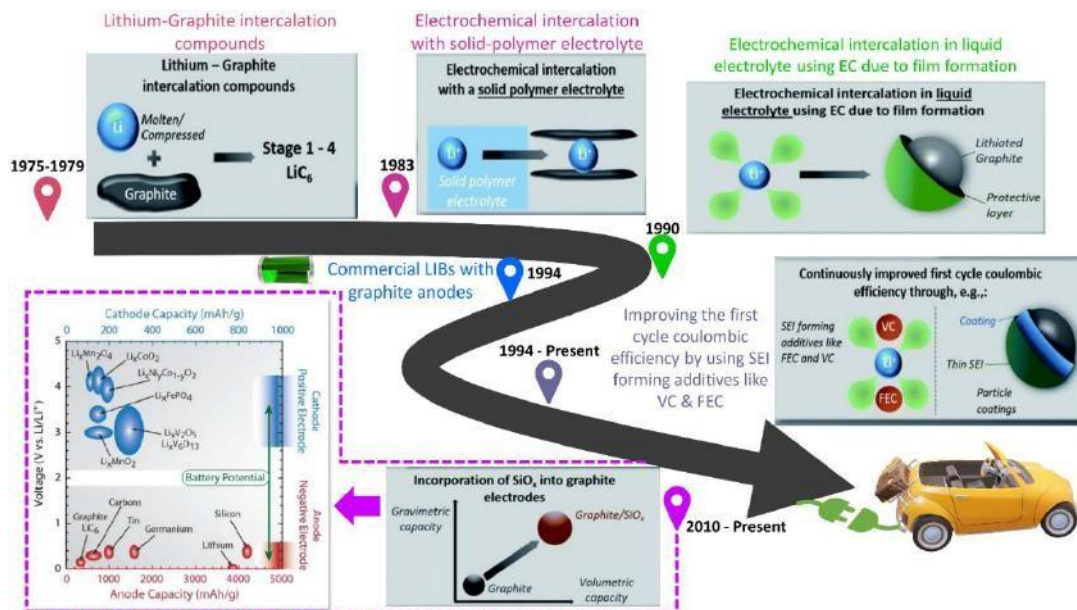
Figure 9 LIB technology - from its origin to the recent advancements

During the charge phase of a lithium-ion battery (LIB), the positive electrode experiences oxidation of lithium atoms, leading to the formation of lithium ions. These ions then traverse the electrolyte towards the anode, where they are incorporated by gaining an electron transferred from the cathode to the anode through an external circuit. Conversely, during the discharge phase, the intercalated lithium within the anode's structure migrates back to the cathode through the electrolyte. This reversible process facilitates the exchange of lithium ions between the electrodes, balanced by the electron flow in the external circuit[8]. Figure 9 presents a schematic delineating the developmental trajectory of LIB technology. Following an impressive 25-year endeavor, lithium-ion batteries were successfully introduced to the market, subsequently becoming an integral facet of our daily routines. Comprising four key components—cathode, anode, electrolyte, and separator—a lithium-ion battery mandates the presence and harmonious functioning of these elements for optimal operation.

Cathode

Table 1- List of some common cathode materials for LIBs[9]

| Active materials	Specific capacity mA h g^{-1}/mA h cm^{-3}	Potential (V vs. Li$^+$/Li)	Advantages	Disadvantages
LiFePO$_4$	170/612	3.4	Low cost, stable long cycle, commercialization	Low electronic conductivity, low specific capacity, low energy density
LiCoO$_2$	140/714	3.8	Long cycle, mature technology, high voltage, high energy density	High cost, low specific capacity, high toxicity, low thermal stability, irreversible phase change
High-voltage LiCoO$_2$	185/944	3.95		
LiNi$_{0.8}$Co$_{0.1}$Mn$_{0.1}$O$_2$	200/930	3.8		
LiNi$_{0.8}$Co$_{0.15}$Al$_{0.05}$O$_2$	220/979	3.6		
LiNi$_{0.5}$Mn$_{1.5}$O$_4$ (LNMO)	147/625	4.7	Super high voltage, high energy density	Low specific capacity, low thermal stability, irreversible phase change, electrolyte decomposition, poor cycle stability
LiNiPO$_4$ (LNP)	169/657	5.1		
LiCoPO$_4$ (LCP)	167/618	4.8		
CuF$_2$	528/2002	3.55	High specific capacity, low cost, high energy density	Large voltage hysteresis, poor cycle stability, low reversibility, poor rate capability, material dissolution, volume change
FeF$_3$	712/2196	2.74		
CoF$_2$	553/2038	2.80	High specific capacity, high energy density	
NiF$_2$	554/2040	2.96		
CuCl$_2$	399/1115	3.17	High specific capacity, low cost	Highly soluble in liquid
FeCl$_3$	496/1172	2.83		
S	1675/1937	2.28	Abundant, low toxicity, rather low cost, high specific capacity, high energy density	Dissolution and shuttle, low working potential, low electronic conductivity, large volume change
Li$_2$S	1166/1937	2.28		
O$_2$	1675/2698	2.96		Rather poor reaction kinetics
Li$_2$O$_2$	1168/2698	2.96		
Se	679/1659	2.07	High specific capacity, high electronic conductivity	High cost/high toxicity, dissolution and shuttle, low working potential
Li$_2$Se	578/1659	2.07		

The capacity and voltage of a lithium-ion battery are significantly influenced by its "cathode." In this type of battery, the chemical reactions involving lithium generate power, making lithium an essential

component introduced into the battery. The region reserved within the battery for lithium is referred to as the "cathode." However, due to lithium's instability, lithium oxide—a compound formed by lithium and oxygen—is used as a cathode material. In the context of a real battery's electrode reaction, the substance like lithium oxide that actively participates is termed the "active material." Thus, lithium oxide serves as the active material in the cathode of a Li-ion battery[10]. Table 1 provides a compilation of commonly utilized cathode materials along with their respective advantages and disadvantages. The cathode's composition, comprising active materials storing Li ions, a conductive additive like acetylene black/super P, and commonly PAA or PVDF as a binder, plays a crucial role in determining the battery's voltage.

Anode

Similar to the cathode, the anode substrate is also layered with active material. Within the anode, this active material facilitates the flow of electric current through the external circuit while enabling the reversible absorption and release of lithium ions generated by the cathode. During the battery's charging phase, the lithium ions are stored within the anode rather than the cathode. In the discharge state when the conducting wire links the cathode to the anode, the lithium ions naturally migrate back to the cathode via the electrolyte, while the separated electrons (e^-) travel through the wire, generating electricity.

In the case of the anode, stable graphite is employed as the primary material. The anode substrate is coated with active material, a conductive additive, and a binder, similar to the cathode structure.

Table 2- List of some common anode materials for LIBs[9]

Active materials	Specific capacity $mA\,h\,g^{-1}/mA\,h\,cm^{-3}$	Potential (V vs. Li^+/Li)	Advantages	Disadvantages
Graphite	372/735	0.17	Commercialization, long cycle stability	Low specific capacity, low energy density
Li	3861/2062	0	High specific capacity, low working potential, high energy density	Infinite volume change, Li dendrite formation, short circuit, high reactivity, consuming electrolytes
Si	3579/2190	0.4	High specific capacity, low working potential, high energy density, low cost	Large volume change, unstable interface, low first CE
P (red)	2596/2270	0.8	High specific capacity, high energy density, low cost	Large volume change, unstable interface, low first CE
Al	993/1386	0.38		
Sn	994/1991	0.38	High specific capacity, high energy density	Large volume change, unstable interface, low first CE, high cost
Ge	1384/2179	0.4		
$Li_4Ti_5O_{12}$ (LTO)	175/607	1.55	No volume change, long cycle stability, high rate capability	Low specific capacity, low energy density, high working potential, high cost
Fe_2O_3	1007/2741	1.2	High specific capacity	High working potential, high cost, low first CE, large volume change
NiS	591/1571	1.3		
TiF_3	767/2002	1.4		

Graphite and Silicon are regarded excellent for anode usage due to its optimum properties for instance structural integrity, lower electrochemical reactivity, conditions for storing a large amount of lithium ions, and inexpensive price. However, there are some drawbacks to these materials which will be discussed later in this thesis. A comprehensive overview of several anode-materials used today are shown in the Table 2.

Electrolytes

The electrolyte plays a pivotal role in enabling this essential function, serving as a pathway specifically for lithium ions to move from cathode to anode and vice versa. Typically, materials with high ionic conductivity are employed for the electrolyte, facilitating the swift movement of lithium ions in both directions. An electrolyte is composed of salts, solvents, and additives. Salts facilitate the migration of lithium ions, where salts, and additives are dissolved in solvents, added in small quantities, serve specialized purposes.
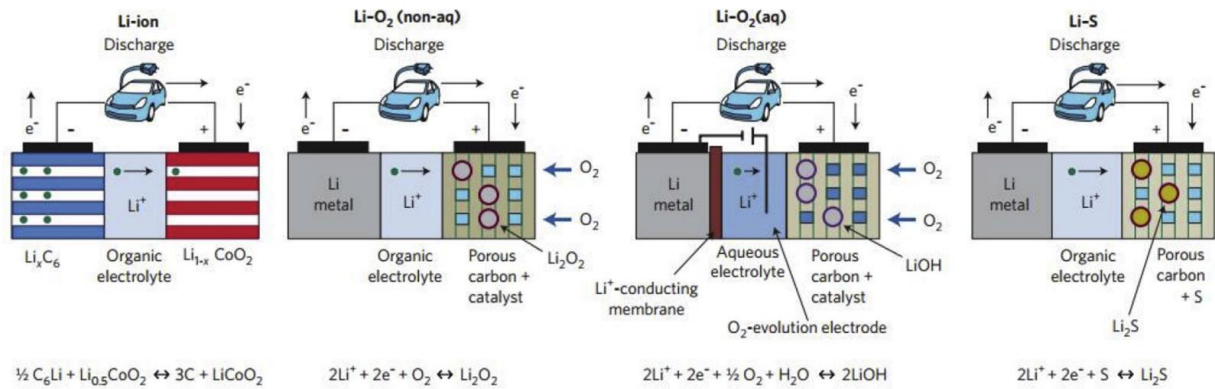
Li-ion
Discharge

e⁻

Li⁺

Li_xC_6 Organic $Li_{1-x}CoO_2$
electrolyte

$½ C_6Li + Li_{0.5}CoO_2 \leftrightarrow 3C + LiCoO_2$

Li-O₂ (non-aq)
Discharge

e⁻

Li
metal Li⁺

O₂
Li_2O_2
O₂

Organic Porous
electrolyte carbon +
catalyst

$2Li^+ + 2e^- + O_2 \leftrightarrow Li_2O_2$

Li-O₂ (aq)
Discharge

e⁻

Li
metal Li⁺

O₂
LiOH
O₂

Li⁺-conducting Aqueous Porous
membrane electrolyte carbon +
catalyst
O_2-evolution electrode

$2Li^+ + 2e^- + ½ O_2 + H_2O \leftrightarrow 2LiOH$

Li-S
Discharge

e⁻

Li
metal Li⁺

Organic Porous
electrolyte carbon
+ S
Li_2S

$2Li^+ + 2e^- + S \leftrightarrow Li_2S$

Figure 10. Different kinds of electrolytes for different Li based secondary batteries[95]

Table 3- Physio-chemical and electrochemical properties of some electrolytes[11].

Electrolyte/cell	Class/property	Conductivity at r.t. (Ω^{-1} cm^{-1})	Activation energy (eV)	Viscosity at r.t. (mPas.s)	Coulombic Efficiency (%)	Reversible cycles
1M $LiPF_6$ FEC/PC (1:1 v/v) (Li/Electrolyte/ KS15 graphite)	Liquid Self-extin-guishing	n.a.	n.a.	n.a.	100 (C/10)	200 (C/10)
Pyr_{14}TFSI-LiTFSI (Sn-C/Electrolyte/$LiFePO_4$)	Liquid Self-extin-guishing	2.5×10^{-3}	5.9×10^{-2}	~110	100 (~1C)	~2000 (~1C)
PVdF-HFP/Pyr_{12O1}TFSI-LiTFSI/SBA-15 (Li/Electrolyte/$LiFePO_4$)	Gel composite Self-ex-tinguishing	0.25×10^{-3}	8×10^{-2}	n.a.	100 (C/5)	200 (C/5)
DMMSA-LiSFI 4:1 (Li/Electrolyte/NMC 111)	Liquid Self-extin-guishing	3.1×10^{-3}	(VTF behaviour)	54	>95 (C/10)	~20 (C/10)
7M LiTFSI-DOL-DME (1:1 v/v) (Li/Electrolyte/S-C composite)	Liquid (concentrated)/ safety (SEI formation)	0.81×10^{-3}	(VTF behaviour)	72	100 (C/5)	100 (C/5)
3.3 NaFSA-TMP Graphite/Electrolyte/Li	Liquid (concentrated)/ safety (SEI formation)	2.2×10^{-3} (30 °C)	(VTF behaviour)	72 (30 °C)	100 (C/5)	1200 (C/5)
0.2 M $LiClO_4$ (PC)/SU-8 (amorphous-Si/ Electrolyte/Li)	Solid/high power density (patternable)	0.052×10^{-3}	0.16	n.a.	n.a.	10 (C/10)
PVDF-HFP/Pyr_{13}TFSI/LiTFSI/TiO_2 (5 wt%) (Li/Electrolyte/MnO_2)	Gel/high power density (patternable)	0.78×10^{-3}	n.a.	1–10 (120 °C, shear rate = 1 s^{-1})	<100 (C/10)	~100 (C/10)
MOF MIT-20 $LiBF_4$	Quasi-solid/not demon-strated in cell	4.8×10^{-4}	0.16	n.a.	n.a.	n.a.
1 M LiTFSI/EMIM-TFSI MOF (Li/Electrolyte/$LiFePO_4$)	Quasi-solid/high trans-port number	3.0×10^{-4}	~0.25	n.a.	>99 (C/10)	100 (C/10)
1M $LiPF_6$ EC/DMC—$OSiO_2$ (soggy sand) (Li/Electrolyte/graphite)	Quasi-solid/high trans-port number	~10^{-3}	n.a.	~400 (shear rate = 1 s^{-1})	n.a.	30 (~C/5)
1M LiTFSI DOL/DME—γ-Al_2O_3 (Li/Electrolyte/$LiFePO_4$)	Quasi-solid/dendrite control	4.0×10^{-3}	(VTF behaviour)	n.a.	100 (1C)	~100 (1C)
LiTFSI-NMAC SiO_2 ionogel (Li/Electrolyte/$LiFePO_4$)	Quasi-solid/dendrite control	1.4×10^{-3}	0.46	n.a.	100 (C/10)	60 (C/10)

This specific type of electrolyte exclusively facilitates the movement of ions towards the electrodes while impeding the flow of electrons. Within an electrolyte, only ions have the capability to travel. As discussed earlier regarding the cathode and anode, lithium ions traverse the electrolyte while electrons travel through the wire. Detailed schematics of various electrolytes used are presented in Figure 10, offering crucial insights into their configuration, which is essential for energy storage within a battery. The passage of ions through the electrolyte is pivotal for battery function; however, if ions were unable to move through the electrolyte, power utilization would be hindered, potentially posing safety risks.

Additionally, the velocity of lithium-ion movement is influenced by the type of electrolyte utilized. Consequently, only electrolytes meeting stringent criteria can be employed. Table 3 and Table 4 provide comprehensive information on the physio-chemical and electrochemical properties of commonly used electrolytes, as well as the advantages and drawbacks associated with various classes of emerging electrolytes, respectively.

Table 4 - Advantages and drawbacks of the different classes of emerging electrolytes[11].

Class	Pros	Cons	Main issues limiting industrial exploitation
Liquid/gel non-flammable and self-extinguishing	High conductivity; high thermal stability	Reduced stability towards reduction	—
Super-concentrated solutions	Dendrites suppression; good SEI formation	—	Cost of lithium salts
3-D patternable membranes	Ease of fabrication and scale-up; solid-state 3-D cells	Low conductivity	Inks development
MOFs/COFs	Tailoring structure/properties, e.g. transference number	Electrochemical stability towards reduction	Low Technology Readiness Level (TRL)
Soggy sands	High conductivity; high transference number	Complex surface chemistry; complex morphology control	Low TRL
Micro/mesoporous membranes	Dendrite suppression; high conductivity and transference number	Difficult fabrication in case of ceramics	Difficult impregnation; scale-up problems
Ionogels	High conductivity; high interfacial stability	Complex structure/properties tailoring	Low TRL
Thermo-responsive gel electrolytes	High safety	Non-reversible	High cost in terms of cell inactivation: reversible systems needed

Separator

The separation between the cathode and anode is maintained by a component known as the separator. While the cathode and anode contribute significantly to a battery's fundamental performance, the electrolyte and separator play a crucial role in ensuring its safety. The separator functions as a physical barrier between the cathode and anode, preventing direct electron transfer and permitting only the passage of ions through its minuscule pores. Consequently, the separator must meet specific physical and electrochemical criteria. Currently, widely used commercial separators are composed of synthetic resins such as polyethylene (PE) and polypropylene (PP).

Table 5- General requirements for separators used in Li-ion batteries[12].

Parameter	Requirement
Chemical and electrochemical stabilities	Stable for a long period of time
Wettability	Wet out quickly and completely
Mechanical property	>1000 kg·cm^{-1} (98.06 MPa)
Thickness	20–25 μm
Pore size	<1 μm
Porosity	40–60%
Permeability (Gurley)	<0.025 s·μm^{-1}
Dimensional stability	No curl up and lay flat
Thermal stability	<5% shrinkage after 60 min at 90 °C
Shutdown	Effectively shut down the battery at elevated temperatures

The essential characteristics of an ideal separator, including porosity, permeability, and wettability, are outlined in Table 5. Alongside monolayer separators, multilayer and microporous separators also exist, each serving as valuable and durable options tailored to specific battery types and mechanisms. These variations and their respective features are extensively detailed in the tables provided below (Tables 6, 7, and 8).

Table 6- Summarization of monolayer membranes[12]

Materials	Solvents	Processing method	Membrane thickness	Liquid electrolyte[a]	Electrolyte uptake	Ionic conductivity	Performance
PP, PE		Dry and wet processes	13–57 μm	LiPF$_6$–EC/DMC		0.4 × 10^{-3} to 2.1 × 10^{-3} S cm^{-1}	Thin thickness, high porosity, and large pore size
PP, PE		Dry and wet processes	25–50 μm	LiAsF$_6$–cyclic ester/ether			Preventing thermal runway
PP, PE			25 μm	LiPF$_6$–EC/PC/DEC			Low shutdown temperature
PP, PE		Dry and wet processes	20–25 μm	LiPF$_6$–EC/PC/DEC			
PE	Paraffin oil	Wet process	25 μm	LiPF$_6$–PC			High mechanical strength
PVDF	Acetone/butanol	Phase inversion		LiPF$_6$–PC/EC/DMC		3.7 × 10^{-3} S cm^{-1}	Regular discharging capacity and good rate capability
PVDF	Acetone/ethanol	Phase inversion	35–50 μm	LiPF$_6$–EC/DMC/DEC		3.0 × 10^{-3} to 5.0 × 10^{-3} S cm^{-1}	Stable discharge curves and low temperature performances
PVDF	DMF, TEP, NMP/water	Phase inversion	120–220 μm	LiPF$_6$–EC/DEC, LiPF$_6$–TEGDME	152–400%	2.0 × 10^{-3} S cm^{-1}	Sponge-like and finger-like structure
PVDF	NMP	Phase inversion	35–70 μm	LiPF$_6$–EC/DMC		0.7 × 10^{-3} to 2.1 × 10^{-3} S cm^{-1}	Good cycling ability and high capacity at high charge rate
PVDF	DBP, DEHP/Ethanol	Phase inversion	200 μm	LiPF$_6$–DMC/EMC/EC	185–230%	1.3 × 10^{-3} S cm^{-1}	Good reservation of liquid electrolyte and good electrochemical stability
PVDF	EC/PC	Casting method	100–200 μm	LiSO$_3$CF$_3$, LiN(SO$_2$CF$_3$)$_2$, LiPF$_6$–EC/DMC/PC		0.3 × 10^{-3} to 2.2 × 10^{-3} S cm^{-1}	Good Li/polymer electrolyte interfacial stability
PAN	DMF	Phase inversion	60–70 μm	LiClO$_4$–EC/DMC, LiPF$_6$–EC/DMC, and LiBF$_4$–EC/DMC		2.5 × 10^{-3} to 2.8 × 10^{-3} S cm^{-1}	Good electrochemical stability
PAN	EC/PC	Casting method		LiClO$_4$, LiN(SO$_2$CF$_3$)$_2$, or LiAsF$_6$–EC/PC or		2.0 × 10^{-3} to 6.1 × 10^{-3} S cm^{-1}	Good electrochemical stability and good lithium cyclability

Table 7- Summarization of multilayer membranes[12]

Materials	Substrate	Thickness	Liquid electrolyte[a]	Electrolyte uptake	Ionic conductivity	Electrochemical performance
PP	PE	254 μm				Enhanced thermal properties
PP	PE	12–38 μm				Enhanced puncture strength and thermal resistance
PP	PE	31 μm				Enhanced mechanical and thermal properties
PVDF	PET	33 μm	LiPF$_6$–EC/DEC/PC	290%	8.9 × 10^{-4} S cm^{-1}	Better capacity retention and good electrochemical stability
AN/MMA	PE	30–45 μm	LiClO$_4$–EC/DMC	85–91%	7.7 × 10^{-4} to 1.1 × 10^{-3} S cm^{-1}	Stable discharge capacity and excellent rate performance
PVDF	PE	37 μm	LiPF$_6$–EC/DEC/PC	302%	1.1 × 10^{-3} S cm^{-1}	High discharge capacity and better high rate performance
PVDF	PET	50 μm	LiBF$_4$–EC/PC		2.1 × 10^{-4} to 6.4 × 10^{-3} S cm^{-1}	Good electrochemical stability and good charge–discharge efficiency
PVDF–HFP	PET	75 μm	LiN(CF$_3$SO$_2$)$_2$–EC/PC		1.2 × 10^{-3} S cm^{-1}	Good capacity retention and stable coulombic efficiency
PVDF–HFP/PEGDMA blend	PE		LiClO$_4$–EC/DEC	180–280%	5.0 × 10^{-5}–4.0 × 10^{-4} S cm^{-1}	Enhanced electrical and thermal properties
PVDF–HFP/PEGDMA blend	PE		LiClO$_4$–EC/DEC	125%	3.8 × 10^{-4} S cm^{-1}	Improved ionic conductivity and thermal resistance
PVDF/PMMA/PEGDA blend	PET	100 μm	LiPF$_6$–EC/DMC/EMC	1000%	4.5 × 10^{-3} S cm^{-1}	Good cycle performance and high rate capacity
P3BT	PP	27 μm	LiPF$_6$–EC/PC			High rate charge–discharge capability and stable overcharge cycling performance
P3DT	PP/PE/PP	22 μm	LiPF$_6$–EC/DMC/EMC			Normal charge–discharge performance and good overcharging shutting capability

Table 8- Summarization of modified microporous membrane separators[12]

Substrate material	Modifying method	Induced materials	Membrane thickness	Liquid electrolyte[a]	Electrolyte uptake	Ionic conductivity	Performance
PE	Plasma	AN	23 μm	$LiPF_6$–DEC/EMC/EC		1.4×10^{-3} S cm^{-1}	Good wettability, stable columbic efficiency and better cycle performance
PP	Electron beam	AA, DEGDM	50 μm	$LiAsF_6$–PC/EC/DME		1.0×10^{-3} S cm^{-1}	Good mechanical and wettability
PE	Electron beam	GMA		$LiPF_6$–DMC/EC			Less electrolyte leakage and better cycle life
PE	Electron beam	MMA	28–42 μm	$LiPF_6$–DMC/EC	180–210%	0.9×10^{-3} to 1.0×10^{-3} S cm^{-1}	Stable cycle performance and excellent discharge capacity
PE	Electron beam	PEGBA	20 μm	$LiPF_6$–DMC/EC		4.1×10^{-4} to 6.2×10^{-4} S cm^{-1}	Enhanced electrochemical stability and better cycle performance
PE	Electron beam	Siloxane	20 μm	$LiPF_6$–DMC/EC	180–200%	7.0×10^{-4} S cm^{-1}	Enhanced electrochemical stability and stable cycling performance
PE	Gamma ray	None		$LiPF_6$–EMC/EC		9.0×10^{-4} S cm^{-1}	Improved thermal resistance and good capacity retention
PVDF	Gamma ray	AA and DMAM	80–100 μm	$LiPF_6$–PC/EC	25–38%		Good rate performance and stable cycle behavior
PVDF	UV	TPGDA	90 μm	$LiCF_3SO_3$–TEGDME		8.0×10^{-4} to 1.6×10^{-3} S cm^{-1}	Better mechanical stability and improved cycling performance
PVDF–HFP	UV	PEGDA	50 μm	$LiPF_6$–DMC/EC		4.0×10^{-3} S cm^{-1}	Higher liquid electrolyte retention and better cycling performance and

Anodes and Anodic Binders

Up to this point, we've covered the four fundamental components of a lithium-ion battery (LIB). Now, our focus shifts towards the anode and the crucial role played by anodic binders in LIBs. Each electrode within a battery comprises an active material, a conductive additive, and a binder. The binder holds together the anode material and the current collector, constituting a vital component of the electrode's structure. Presently, the predominant strategy for improving the energy and power density of LIBs involves extensive research and development concentrated on high-capacity anode materials and high-potential cathode materials. Notably, there's a concerted effort aimed at developing high-capacity anodes, which serve as a pivotal factor in determining the achievable capacity of lithium-ion batteries. In this context, this research focuses on stabilizing ultra-high capacity anode materials such as graphite and silicon to provide LIBs with increased capacity and fast charging for future applications. Several observations emerge from the comparison of various binders used in electrode materials for lithium-ion batteries. Cross-linking PAA-based binders with other polymers has notably enhanced Si anode performance, resulting in improved cycle life and capacity retention, surpassing conventional binders like CMC and PVDF. However, the SBR/CMC mixture, while exhibiting favorable characteristics such as improved wetting, reduced brittleness, and stronger adhesion to current collectors, displayed reduced cycling efficiency, especially in graphite electrodes with smaller particle sizes. Chitosan-based binders showcased higher capacity retention and cycling efficiency in both graphite and LiFePO4 electrodes compared to PVDF. Xanthan gum binders demonstrated stable cycle profiles and impressive capacity retention, particularly notable in LiFePO4 cathodes. PAN (polyacrylonitrile) binders, although possessing high polarity and electrochemical stability, were found to create rigid electrodes prone to cracking during manufacturing. Interestingly, aqueous-based binders exhibited promising potential in improving the electrochemical performance of electrode materials, particularly in Si anodes where factors such as volume change and mechanical strength are critical for sustained performance and cycle life enhancement. These findings highlight the significance of binder selection in optimizing the electrochemical properties of various active materials in lithium-ion batteries.

Table 8- different binders for electrodes in LIBs [13,14]

Active Material	Binder	Electrolyte	Measured temp °C	Weight %	Cycle number	Capacity retention %	CE %	Ref
Electrochemical performance of graphite anode								
Graphite	CMC	$LiPF_6$	Ambient	5	200	−98	NA	12
Graphite	CMC	$LiPF_6$	Ambient	4	30	98	−98	115
Graphite	SBR	$LiPF_6$	Ambient	5	800	−98	NA	12
Graphite	SBR/CMC 5:1	$LiPF_6$	Ambient	6	500	−95	NA	12
SiO	PAA	$LiPF_6$	Ambient	10	50	84	NA	64
Si	PAA	$LiPF_6$	Ambient	15	20	72	NA	164
Si	PAA	$LiPF_6$	Ambient	15	59	73	NA	166
Si	PAA	$LiPF_x$	Ambient	20	300	80	99	168
Graphite	PVDF	$LiPF_6$	55	4	290	80	NA	134
$LiNi_{0.4}Co_{0.2}Mn_{0.4}O_2$	PVDF	$LiPF_6$	60	5	100	84	NA	117
$LiMn_2O_4$	PVDF	$LiPF_6$	55	10	100	67.6	NA	158

There are several significant challenges associated with graphite anodes in lithium-ion batteries:(a) limited reversible capacity, which falls short in meeting the energy demands of advanced LIBs. (b) structural fracture of the graphitic framework during prolonged cycling, particularly at high current rates. (c) high irreversible capacity loss attributed to excessive electrolytic decomposition. (d) formation of a thick solid electrolyte interface (SEI) leading to high interfacial impedance, impacting battery performance[15]. Silicon (Si) has emerged as a promising alternative to graphite in battery anodes due to its favorable properties. However, Si anodes come with significant drawbacks that hinder their performance. These include rapid volume expansion by up to 300% during charge-discharge cycles, leading to pulverization, loss of electrical contact between Si particles and the current collector, inherent insulating properties, and the formation of a thick solid-electrolyte interface (SEI) due to repeated exposure of new Si surfaces [16–18]. These challenges result in notable issues such as capacity degradation, limited rate capability, and reduced cyclability of Si-based anodes. As previously mentioned, both graphite and silicon anode materials exhibit limitations that need addressing to enhance their stability and performance. Despite their individual drawbacks, they share a common disadvantage—the quality of the interphase formed between the electrodes, known as the solid-electrolyte interface (SEI) [19,20]. The development of SEI on these materials significantly influences their performance, as it involves a combination of active materials and electrolytes. Hence, comprehending and regulating the SEI formation is crucial in the endeavor to mitigate the drawbacks associated with these electrode materials. Table 8 provides a compilation of binders utilized in various typical electrodes.

SEI-solid-electrolyte interface

In basic terms, the solid-electrolyte interface (SEI) acts as a "protective layer" formed on the electrodes of lithium-ion batteries (LIBs) during their initial cycle through the breakdown of electrolytic components. This interface significantly impacts the battery's performance by directly or indirectly affecting factors such as irreversible capacity fade, cycling ability, internal resistance, the battery's amount of operation, lithium-ion movement, graphite behavior, silicon particle breakdown, and corrosion of cathode materials based on transition metals.
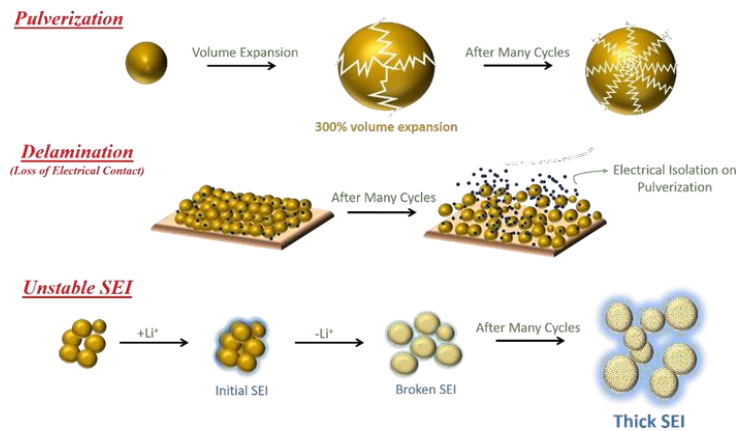
Figure 11 Schematic of pulverization of Si anodes and other issues in LIBs.

A thorough study of the SEI composition formed on anode surfaces has become critical for improving the performance of LIB anode materials. It would aid in the tuning of SEI production, which would limit the ongoing excessive breakdown of electrolyte on anode's surface. In essence, the SEI consists of deposits formed due to the degradation of salts, solvents, lithium ions, and contaminants present in the electrolyte. These components are unstable within the working potential range of the anode. SEI formation primarily occurs during the initial charging cycles and gradually expands until it reaches a mature state. An ideal SEI layer would be electrically insulating, exhibit good selectivity for lithium ions, allow permeation, and have low interfacial impedance. Once the SEI reaches maturity, electrons no longer pass through this layer, preventing further degradation of electrolyte components like salts and solvents. Consequently, the layer develops higher electrical resistance, leading to an increase in the anode's voltage. Consequently, the surface potential fluctuates within the stability range of the specified electrolyte.[19,21].

In practical application, the scenario differs slightly. With repeated cycling, the solid-electrolyte interface (SEI) layer thickens due to electron exposure to electrolyte components or the flow of bulk electrolyte to the electrode surface. Although this thickening isn't as drastic quantitatively as during the initial charge cycle, it gradually depletes active Li-ions, solvent species, and dissolved salts. Consequently, the resistance of the cell gradually increases over time. This process leads to the degradation of capacity and coulombic efficiency. Commonly used in lithium-ion batteries (LIBs), organic electrolytes primarily comprise carbonates such as ethylene carbonate, dimethyl carbonate, ethyl methyl carbonate, propylene carbonate, and similar compounds. Essentially, these electrolytes consist of aprotic salts with low molecular weight dissolved in organic solvents. These carbonates possess an oxidation potential of 4.7 V versus Li/Li^+, corresponding to their highest occupied molecular orbital (HOMO), and a reduction potential of 1.0 V vs Li/Li^+, corresponding to their lowest unoccupied molecular orbital (LUMO)[22].

This indicates that during the charging cycle or storage, reduction occurs on the negative electrode's surface below 1 V, while oxidation happens at the cathode surface beyond 4.7 V. Figure 12 provides a comparison of the energy levels of anode, electrolyte, and cathode in a redox pair within a battery system. In this representation, µA and µC signify the electrochemical potentials of the anode and cathode, respectively. The difference in energy between the lowest unoccupied molecular orbital (LUMO) and highest occupied molecular orbital (HOMO) establishes the stability window (depicted as Eg) of the electrolyte employed. Essentially, when the electrochemical potential (µA) surpasses the LUMO energy level, electrolyte reduction takes place, while if the electrochemical potential (µC) falls below the HOMO energy level, electrolyte oxidation occurs. Maximizing the energy gap between the cathode and anode contributes to enhancing the energy density of the redox pair.

Take graphite anodes as an example. The lithium-ion intercalation potential into graphite typically ranges between 0 V and 0.25 V concerning Li/Li+. This intercalation potential is notably lower than the reduction potential of most carbonate-based electrolytes. Consequently, during lithiation, the potential of graphite falls below the electrolyte's stability range, leading to its decomposition at the anode surface and contributing to the formation of the solid-electrolyte interface[21,23]. Given the extent of this research, the strategic design of SEI is critical for stabilizing the anodes based on graphite and silicon in LIBs. The H^+/H_2 reaction and the role of O_2/H_2O are integral considerations in the functioning and stability of batteries, specifically in relation to the electrolyte's HOMO-LUMO energy levels. During battery discharge, electrons departing from the anode release H^+ ions into the electrolyte. At the cathode, H^+ ions accepting electrons may potentially form H_2, a reaction aligned with the HOMO-LUMO energies. If the electrolyte's HOMO corresponds to the potential for H_2 formation, it could influence cathode and electrolyte stability, affecting battery performance. Additionally, O_2 and H_2O indirectly impact battery stability; O_2 interacts with cathode materials during charge/discharge cycles, while water, a product of side reactions or electrolyte decomposition, affects stability. Aligning the electrolyte's HOMO level with O_2 reduction potential or water decomposition potential may lead to undesired electrode reactions, compromising battery stability. Organic liquid electrolytes, notably carbonate-based solvents (e.g., PC, EC, DEC, DMC, EMC), serve as efficient Li+ ion solvents. They possess HOMO oxidation potentials around 4.7 volts and LUMO reduction potentials near 1.0 volt, enabling effective ion transport due to their low viscosity. Ethylene carbonate (EC) commonly included, forms a protective SEI layer on the carbon anode's surface, guarding against electrolyte decomposition and aiding stability after SEI formation. However, these solvents pose safety risks due to their high flammability (flash points below 30 °C). The preferred salt, LiPF6, might undergo autocatalytic decomposition, generating LiF and PF5. PF5 can react irreversibly with water or the carbonate electrolyte, causing battery degradation, particularly at temperatures exceeding 60 °C. Efforts to mitigate these challenges involve additives aimed at reducing LiPF6 decomposition by lowering operating temperatures, enhancing safety, and stability in carbonate-based electrolytes. In summary, while these organic liquid electrolytes exhibit favorable properties for ion transport and SEI formation, their flammability and potential salt decomposition require careful management, including additive usage, to ensure safety and stability in battery applications.
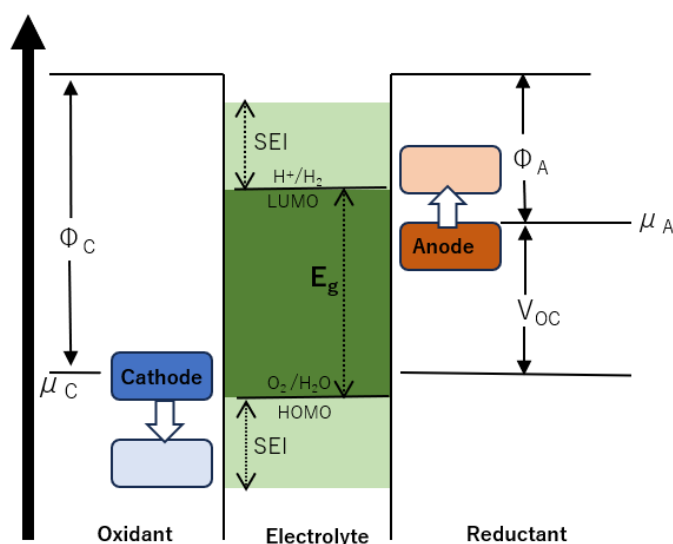

Figure 12 Energetics of the formation of SEI (or CEI) layer on anode/ cathode.

The electrical energy levels of graphite and silicon remain consistent, requiring an external mediator possessing an appropriate electrical energy level to customize the necessary solid-electrolyte interface (SEI) for stabilizing these anodes. While this external mediator cannot specifically define the capacity or energy density of lithium-ion battery (LIB) anodes, it serves as an inactive component within LIBs. Nevertheless, its inclusion proves beneficial as it aids in mitigating the inherent drawbacks and failure mechanisms associated with anodes and electrode-electrolyte interfaces. These inactive components, often referred to as interpreters, generally fall into two categories: (a) polymer binders, constituting part of the electrode composition with a low gravimetric weight, and (b) electrolyte additives, forming part of the electrolyte composition at low concentrations. These inert components are used in varied quantities and concentrations to stabilize LIB electrodes based on their mechanical and electrochemical properties. Positioned on either side of the SEI junction, polymer binders become part of the electrode laminate, while electrolyte additives are integrated into the electrolyte. Both components can directly influence the formation of the SEI on the electrode surface[13,14,16].

Hence, the primary objective of this study has been directed towards formulating, synthesizing, and systematically evaluating a new category of composite polymer binders. This effort aimed to stabilize both graphite and Si anodes by ensuring mechanical strength and regulating the formation of the solid-electrolyte interface (SEI) on these surfaces.

BIAN based robust binders for LIB electrodes

Compounds from the bis-iminoacenaphthene (BIAN) family have long been known as a class of suitable ligands for d-block metals in catalysis due to their ability to form complexes with practically all d-block metals. BIAN's ability to host such metal centers, as well as other diverse properties, stems from its structural significance. Due to the presence of diimine bonds, they have structural stiffness, the ability to produce a range of synthetic polymers depending on spacer substituents, and electron source-sink importance[24]. Furthermore, we also see in the previous research that the naphthalene moiety may be reduced to generate radical anions with alkali metals. Our group has been working on BIAN based molecules and polymers to investigate their electrochemical properties. To take this journey one step further, in this work we find some of the improvements to make them more robust as binder materials by adding a few other structural properties. This improvement led to an appreciable improvement in their binding ability and overall cell performance. Figure 13 gives a glimpse of our previous work on BIAN based polymers as binders in LIBs, Gourang et al. explored and use of bis-imino-acenaphthenequinone (BIAN)-fluorene as a binder for graphite-based anode[25]. The BIAN-fluorene copolymer leveraged three distinct properties (as depicted in Figure 13) to tailor the solid-electrolyte interface (SEI) formed on the graphite anode. Firstly, it employed the low-lying LUMO-driven n-doping mechanism to fine-tune the SEI on the graphite surface. Secondly, the polymer capitalized on its intrinsic electronic conductivity, facilitated by the extended conjugation within the polymer network. Lastly, it established a stable interaction with the graphite material, providing crucial mechanical stability. Consequently, the BIAN-fluorene binder not only offered essential mechanical reinforcement to the graphite framework but also played a significant role in crafting a desirable SEI characterized by low interfacial impedance.[24–27]. The researchers also employed BIAN-p-phenylene copolymer as a polymeric electrocatalyst for oxygen reduction reactions (ORR) and BIAN-based diamine (BIANODA) as an electrolyte additive to regulate the interface, aiming to stabilize MNC (metal nickel cobalt) cathodes in lithium-ion batteries (LIBs).
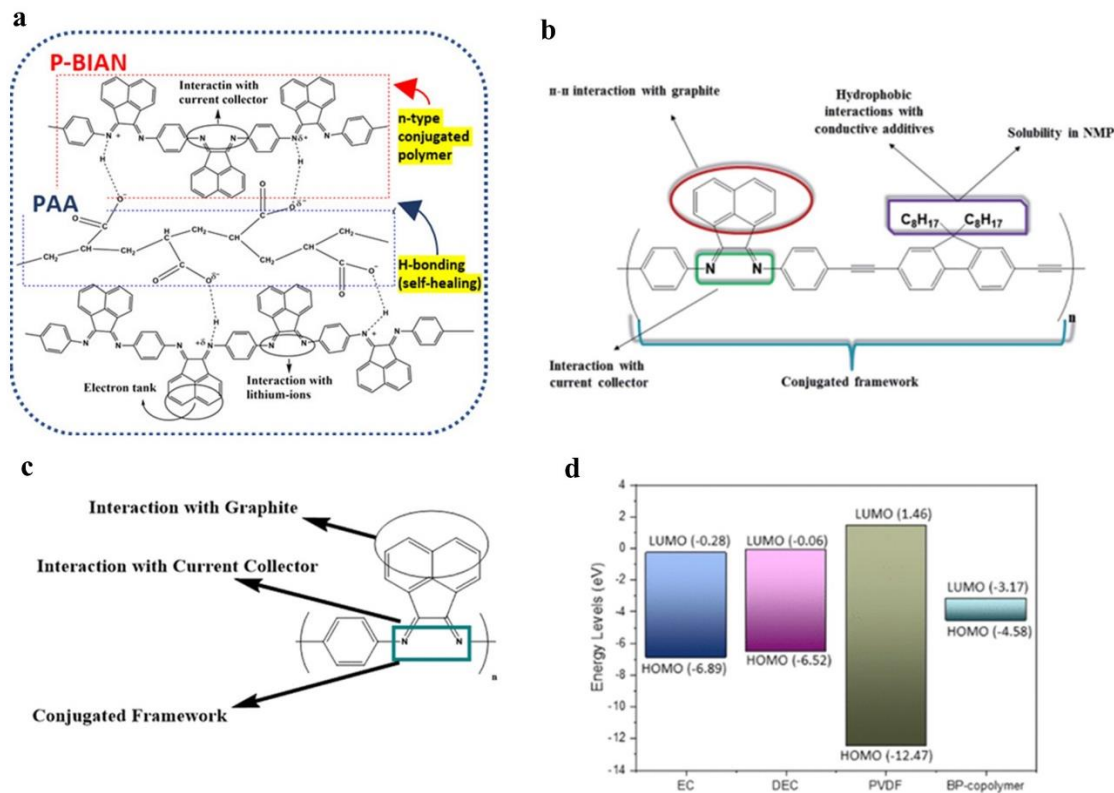
Figure 13 Previous works on BIAN by our group. a) BIAN-PAA for Si based anodes b) BIAN-based copolymer binder for graphite anodes c) polymerized-BIAN for Graphite anode   d) HOMO LUMO of polymerized -BIAN

Agman et al. documented the exceptional slong cycle performance of a graphite anode in LIBs by utilizing a BIAN-p-phenylene (BP) copolymer as a binder. Additionally, for silicon-based anodes, they capitalized on the structural properties of the BP-copolymer, establishing electrostatic hydrogen bonding between the carboxyl moiety of poly(acrylic acid) (PAA) and the electron-rich diimine present in the BP-copolymer.[27]. Due to its inherent self-healing capability, this design presented the required mechanical reinforcement. Moreover, it facilitated the creation of a thin solid-electrolyte interface characterized by reduced impedance. This was attributed to the composite polymer's lowered lowest unoccupied molecular orbital (LUMO) through the addition of poly(acrylic acid) (PAA) as dopant to the α-diimine structure. This adjustment enabled the composite polymer to undergo n-doping in the anodic environment, further enhancing its properties. However, the Li^+ ion diffusion, R_{ct} and activation energy can be improved further to enable XFC through additional binder design. This novel composite binder system has several key properties, including (a) intrinsic lithium ions that provide Li^+ ion diffusion sites that enhance Li^+ ion diffusion within the electrode matrix; (b) a low-lying LUMO that ensures its reduction before that of electrolytes to form a thinner SEI with higher ionic conductivity and low impedance; (c) a robust SEI that aids in Li^+ ion desolvation and diffusion across the SEI, and d) a robust BIAN moiety to interact with graphite layers and e) n-doping ability ensure reduced internal resistance. As shown in Figure 14, P-BIAN and Li PAA binder operate in concert to give great adhesion strength and outstanding mechanical properties, with the rigid LiPAA chain and an abundance of carboxylate groups serving as the framework and Li^+ ion reservoir as well as Li^+ ion diffusion facilitator[28,29].
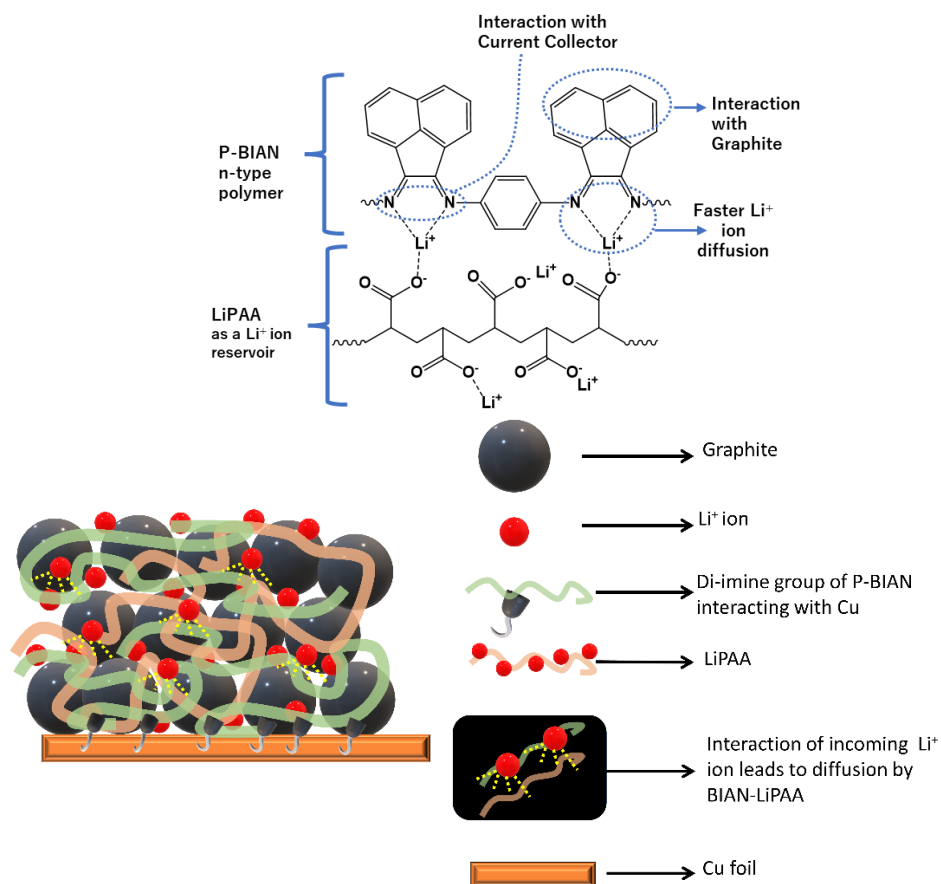
ssss

Figure 14 Structure and designing concept of BIAN-LiPAA for Graphite based anodes and schematics of binding mechanism.

Outline of this thesis

The primary objective of this thesis is to explore and exploit the advantageous structural and chemical characteristics of polymers belonging to the bis(imino)acenaphthene (BIAN) family. The aim is to systematically develop, fabricate, and apply innovative BIAN-based durable and versatile polymers as binders to support high-capacity anodes in lithium-ion batteries (LIBs). Chapter 1 serves as a general introduction, outlining the scope and context of the research. In Chapter 2, the focus is on elucidating a BIAN-LiPAA composite polymer designed specifically for graphite-based anodes. This section discusses how strategic minor modifications in the composite polymer facilitated the achievement of Extremely Fast Charging (XFC) capabilities. Building on the success observed in Chapter 2, Chapter 3 delves into the synthesis and detailed exploration of another BIAN-based composite polymer engineered to stabilize silicon-based anodes. Chapter 4 serves as a comprehensive summary, consolidating the outcomes and insights obtained from these research endeavors, culminating in a general conclusion.

Chapter 2
Enabling Ultrafast Charging in Graphite Anodes Using BIAN-Based Conjugated Polymer/ Poly(lithium acrylate) as a Binder

ABSTRACT

The facile diffusion of Li^+ ions through the solid electrolyte interface (SEI) is crucial to realize extremely fast–charging (XFC) batteries. Graphite is a promising candidate for electric vehicles and other battery applications. However, it exhibits a poor delithiation capacity due to exfoliation under high current rates. Therefore, herein, a composite polymer binder, named BIAN-LiPAA, with intrinsic Li^+ ions was prepared to achieve fast charging and better ion diffusion. The remarkably low-lying energy level of the lower unoccupied molecular orbital of the BIAN-LiPAA binder makes it an n-doped composite binder in an anodic environment, which leads to the reduction of the binder before electrolyte degradation to form a thin and conducting SEI. The proposed composite binder exhibits a considerably low SEI, charge transfer resistance, and an activation energy of 21.00 kJ/mol with improved Li^+ diffusion in the graphite matrix (2.86×10^{-10} cm^2 s^{-1}). Anodic half-cells fabricated using the BIAN-LiPAA binder exhibit discharge capacities of 276, 114.5, and 62.1 mAh/g at 1, 5, and 10 C, respectively, considerably higher than those of the PVDF-, LiPAA-, P-BIAN- based cells. Under XFC conditions, BIAN-LiPAA exhibits high-capacity retentions of 94.2% and 83.5% at 10 and 5 C, respectively, after 2000 charge-discharge cycles.

Introduction

Despite the recent advancements in Li-ion batteries (LIBs), the commercialization of electric vehicles (EVs) has been hindered by the undesirable charging speeds of LIBs.[15,30] One of the main factors that can enable the commercialization of EVs is the realization of extremely fast charging (XFC) in high-energy LIBs. However, two main issues must be solved to realize XFC in batteries: the charge transfer resistance (R_{ct}) and activation energy (E_a) of lithiation inside electrodes must be improved.[31,32]

Binders, as an important component of electrodes, decide the quality of the solid electrolyte interface (SEI) and mechanical and electrochemical connectivity of an electrode. Quick charging often weakens the anode matrix because the binder fails to hold the electrode intact. Therefore, an improved binder that can hold the anode matrix and current collector together is needed. Furthermore, many multifunctional polymer binder materials can be designed by systematically studying the fundamentals and structure–activity relationship of the novel polymer binders. A good binder should possess the following necessary structural and functional features to exhibit good binding abilities to improve cell performance: (a) a conjugated framework, (b) self-healing properties, (c) a low lowest unoccupied molecular orbital (LUMO), and (d) good mechanical strength.[24,33] This study reports our attempt at mitigating the above discussed issues with the graphite based electrodes by combining these four factors and systematically designing a multifunctional binder system. Herein, a composite binder system that is a mixture of a bis-imino-acenapthene quinone (BIAN)-type conjugated polymer and lithium polyacrylate (LiPAA) is proposed. The idea is to improve the Li$^+$ ion diffusion coefficient, activation energy, and internal resistance of the graphite based anodic half cells, which will then improve the overall cell performance and support XFC.[23,34]

Our previous studies have reported the robustness of BIAN-type conjugated polymer binders in graphite and Si-based anodes.[24,35–37] Structural highlights of the BIAN-type conjugated polymer binder are as follows: (a) the fused-planar naphthalene moiety of the polymer forms a π–π stacking interaction with the graphite skeleton, (b) the copper current collector clings to the diamine component of the polymer, allowing the binder to hold the electrode laminate intact on the current collector, and (c) the conjugated network of the polymer is provided by the BIAN-phenylene moiety as a component of the polymeric backbone, ensuring better electronic conductivity across the electrode matrix.[24,36] However, the Li$^+$ ion diffusion, R_{ct}, and activation energy of lithiation of the anode can be further improved to enable XFC through additional binder design.

The addition of LiPAA to bis-imino-acenapthene quinone-phenylene co-polymer (P-BIAN) makes the reported composite binder more robust because LiPAA introduces a Li$^+$ ion reservoir that greatly promotes Li$^+$ ion diffusion and improves the activation energy of lithiation of the anode.[36] Komaba and Yabuuchi et al. reported that, when LiPAA is used as a binder, after the electrode fabrication, a thin layer of LiPAA uniformly covers the surface of the active material particles, serving as an artificial SEI. This artificial SEI decreases the direct contact between the active material and electrolyte because the binder is subsequently reduced in the first cycle.[38] Additionally, the drawback of using an acidic binder, such as polyacrylic acid (PAA), is that carboxylic acid groups are electrochemically reduced and converted to lithium carboxylates. The protons released during the reduction can accelerate the decomposition of LiPF$_6$.[39]

Furthermore, PAA has carboxylic acid groups that can be reduced to carboxylate groups at the anode, forming LiPAA and releasing H$_2$ gas as a byproduct. This process of formation of LiPAA consumes many Li$^+$ ions and decreases the overall Li$^+$ ion count. The water content in the LiPAA based cell decreases

because LiPAA does not follow the same decomposition process as PAA.[28] LiPAA as a binder also exhibits a few drawbacks. For example, PAA films exhibit superior mechanical flexibility to LiPAA films.[23] To compensate for this lack of mechanical stability of LiPAA, P-BIAN was used along with LiPAA to form the composite binder BIAN-LiPAA. As reported in our previous work polymerized-BIAN exhibited a tensile strength of 34 MPa, Young's modulus of 1.1 GPa, and a strain of 4.4%, better than the tensile strength (22 MPa), Young's modulus (0.35 GPa) and strain (2.4%) of poly(vinylidene fluoride) (PVDF), respectively. Therefore, the polymerized-BIAN copolymer is mechanically stronger than conventional binders.[24] Lowering the interfacial charge transfer–related overpotential is one of the crucial factors that can help realize XFC, which can be achieved by improving diffusion, impedance, and activation energy.[40]
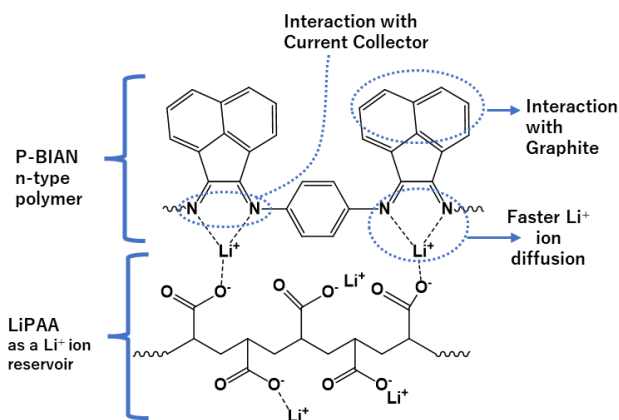

Figure 1. Structure and designing concept of the BIAN-LiPAA polymer.

P-BIAN and LiPAA binders operate in concert to afford great adhesion strength and outstanding mechanical properties, with the rigid LiPAA chain and an abundance of carboxylate groups serving as the framework, Li^+ ion reservoir, and Li^+ ion diffusion facilitator.[17]

As shown in Figure 1, this novel composite binder system has the following key properties: (a) the presence of intrinsic Li^+ ions that provide Li^+ ion diffusion sites to improve Li^+ ion diffusion within the electrode matrix, (b) a low LUMO level that ensures its reduction before that of the electrolyte to form a thinner SEI with higher ionic conductivity and low impedance, (c) a robust SEI that promotes Li^+ ion desolvation and diffusion across the SEI, (d) a robust BIAN moiety that interacts with graphite layers, and (e) n-doping ability that ensures reduced internal resistance.

Materials and Methods

Materials

1,4-Phenylenediamine, acenaphthenequinone, acrylic acid, n-methylpyrrolidone (NMP), and acetic acid were purchased from Tokyo Chemical Industry Co., Ltd. LiOH was purchased from Sigma Aldrich. MeOH was purchased from Wako Chemicals Ltd. Super dehydrated acetonitrile was purchased from Wako Pure Chemical Industries, Ltd. Battery-grade graphite and PVDF were procured from Sigma Aldrich. A 1.0 M $LiPF_6$ ethylene carbonate/diethyl carbonate (EC/DEC = 1:1) electrolyte was purchased from Sigma Aldrich. Battery-grade acetylene black, was purchased from Denka Japan Private Co. Ltd. Copper foils with a thickness of 20 m were purchased from Nilaco Co. All the materials were used without any further purification.

Synthesis

The synthesis of the P-BIAN was performed using the procedure reported by Matsumi et al.[24,25,35–37] The synthesis process of BIAN-LiPAA is shown in Figure 2. The synthesized polymer was successfully

characterized via ^{1}H NMR and Fourier transform infrared (FT-IR) spectroscopy. Because the reactants (i.e., acenaphthene quinone and 1,4-phenylenediamine) are harmful, dangerous, and carcinogenic (upon sustained exposure) and can cause eye and skin irritation and allergic reactions, rigid safety rules were implemented during their handling. Proper safety measures must be performed when handling these compounds. LiPAA was synthesized via a two-step procedure.
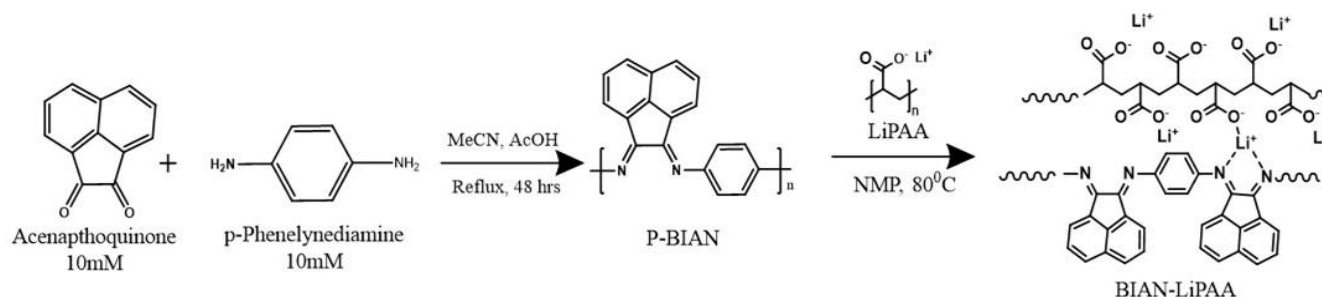

Figure 2. Synthesis of BIAN-LiPAA polymer composite

First, lithium acrylate (AALi) was synthesized by reacting acrylic acid with LiOH monohydrate in methanol (mole ratio 1:1). Second, the obtained AALi was polymerized using azobis(isobutyronitrile) (AIBN) as an initiator and methanol as the solvent. The obtained LiPAA was filtered, rinsed with MeOH, and dried at 50 °C before use. The obtained polymer was characterized by ^{7}Li NMR, and its pH was tested using a pH meter.

Result and discussion

^{1}H NMR spectra were recorded using a Bruker AVANCE II 400 MHz spectrometer. ^{7}Li NMR spectra were recorded using a Bruker AVANCE II 500 MHz spectrometer. In the spectra, the respective chemical shifts were measured in parts per million according to the protons of the deuterated solvent used as an internal standard. The FT-IR spectra were recorded using a Perkin Elmer 100 FT-IR spectrometer. In the attenuated total reflection mode, the spectra were averaged across 100 scans with a resolution of 2 cm^{-1}. Scanning electron microscopy (SEM) images of the corresponding anodes before and after fabrication at a voltage of 1.0 kV were obtained using a Hitachi S-4500 field-emission scanning electron microscope. A Fisons instruments S-probe TM 2803 was used to perform X-ray photoelectron spectroscopy (XPS). A peel test of the electrodes was performed at a speed of 3 mm/min at room temperature (26 °C) using a tensile testing machine (3365-L5, INSTRON) with a load cell (10 kN).

As shown in Figure 3 a and Table 1, in the FT-IR spectrum of BIAN-LiPAA, the peaks at 1656, 1165, and 1115 cm^{-1} are attributed to the C=N stretching vibration of imine in P-BIAN, C–O stretching vibration of C–O–Li$^+$, and C–N$^+$ stretching vibration of quaternary N due to electrostatic interaction between N and Li$^+$, respectively. In the XPS spectrum, as shown in Figure 3c-d, the peak at 399.5 eV is attributed to the typical α-diimine (C=N) nitrogen of BIAN and that at 401.0 eV is attributed to the quaternary diimine nitrogen[24] atoms, and the presence of this peak indicates its participation in the electrostatic interaction with LiPAA. Figure 3b also shows that all the acid groups in PAA chain have been lithiated and the pH is neutral.
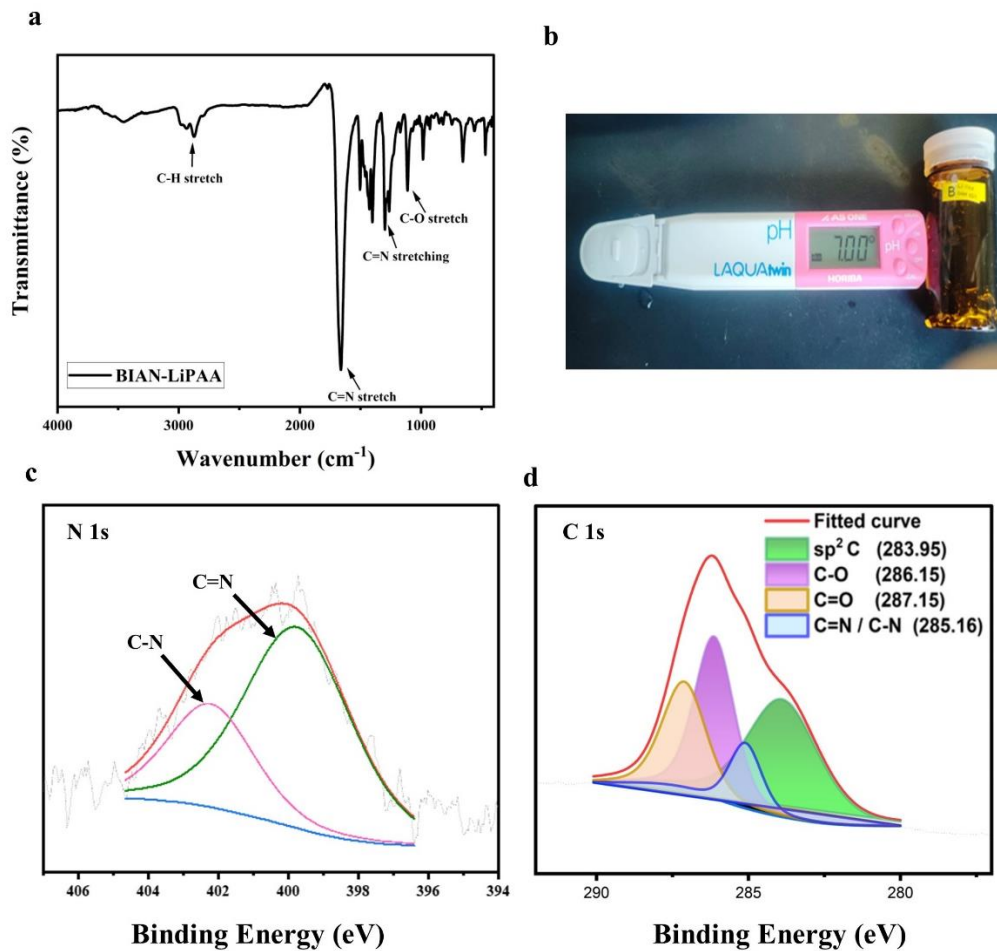
Figure 3. (a) IR spectra of BIAN-LiPAA, (b) pH test of LiPAA (c) N 1s XPS spectrum of BIAN-LiPAA, (d) C 1s XPS spectrum of BIAN-LiPAA .

Table 1. IR characterization of BIAN-LiPAA.

Absorption (cm^{-1})	Appearance	Group	Comments
1656	Medium-strong	C=N stretching	Imine in P-BIAN
1256	Medium	C-N stretching	In P-BIAN
760	Strong	C-N wagging	
1722	Strong	C=O stretch	Carboxylic, C=O PAA
1165	Strong	C-O stretch	C-O$^-$ Li$^+$
1115	Medium	C-N $^{\delta+}$ stretch	C-N $^{\delta+}$ stretch Quaternary N- atom, decreased due to the electro-static interaction of N and Li$^+$

Computational studies

Computational analysis is crucial in designing binders for Li-ion battery anodes as it predicts critical parameters like HOMO-LUMO levels, charge density, and Gibbs free energy. These calculations offer insights into electronic and structural properties, aiding in material selection and performance optimization. Understanding energy transfer processes and stability at a molecular level guides the

development of efficient and stable anode binders. It allows for the fine-tuning of molecular structures to enhance conductivity, stability, and overall battery performance, ultimately accelerating advancements in Li-ion battery technology.

Dmo3, or density functional theory with the M06-2X functional, is important in these calculations for several reasons. It provides an accurate and efficient approach to calculate electronic properties, energetics (like HOMO-LUMO levels), and charge density of materials relevant to Li-ion battery anodes. The M06-2X functional, a specific formulation within Dmo3, is known for accurately predicting molecular geometries and energetics. By utilizing Dmo3, we can better understand the behavior of anode materials at the molecular level, aiding in the design and optimization of binders for enhanced Li-ion battery performance.

HOMO-LUMO Calculation

Because the LUMO level of the binder plays a crucial role in SEI formation and minimizing electrolyte degradation,[35] density functional theory (DFT) calculations of BIAN-LiPAA were performed on Materials Studio using Dmol 3 software with the optimization parameters, DND basis set, generalized gradient approximation (GGA) (pW91) density functional, and unrestricted spin polarization by maintaining the charge neutrality. The DFT-optimized structure of the BIAN-LiPAA binder is shown in Figure 4a.
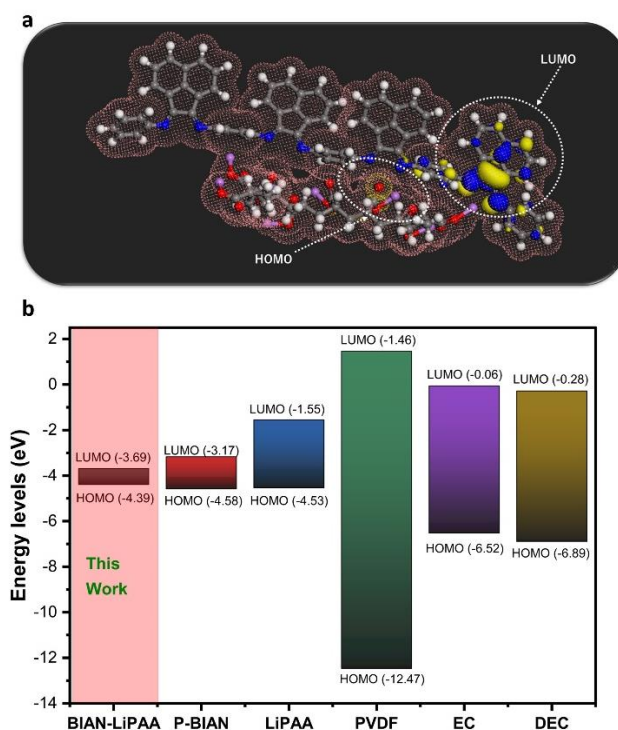

Figure 4. Computational studies. (a) DFT-optimized structure of BIAN-LiPAA (b) Calculated HOMO–LUMO energy levels of BIAN-LiPAA compared with those of other materials.

The low-lying LUMO ($E_{LUMO} = -3.69$ eV) is located on and around the nitrogen atom of the BIAN moiety, and the highest occupied molecular orbital (HOMO) is located around C–O–Li. As shown in Figure 4b, according to the DFT calculations, the bandgap of BIAN-LiPAA is considerably lower than that of the electrolyte components (EC, DEC) and other counterparts taken as reference binder materials in this work, that are P-BIAN, LiPAA and PVDF. The appearance of such a low LUMO level is due to a) the presence of the extended conjugation, b) delocalized lone pair of electrons on the nitrogen atoms, and c) intermolecular electrostatic interaction between N (from the P-BIAN framework) and Li$^+$ ions (from the

LiPAA chain). In an anodic environment, n-type doping is easier and better in BIAN-LiPAA than P-BIAN, LiPAA, PVDF, and so forth. This is because the reduction of BIAN-LiPAA prevents the excessive decomposition of the electrolyte and leads to the formation of a thinner SEI with lower interfacial impedance.[24,27]

Charge density calculation

Table 2. Charge on each nitrogen atom in P-BIAN and BIAN-LiPAA

Nitrogen atoms	Charge on nitrogen atoms in P-BIAN	Charge on nitrogen atoms in BIAN-LiPAA (Significant decrease)
N 1	-0.1315	-0.1113
N 2	-0.1314	-0.1139
N 3	-0.1299	-0.1284
N 4	-0.1320	-0.1217
N 5	-0.1327	-0.1130
N 6	-0.1337	-0.1064
N 7	-0.1305	-0.0970
N 8	-0.1359	-0.0.1071

Table 3. Charge on each lithium atom in LiPAA and BIAN-LiPAA

Nitrogen atoms	Charge on lithium atoms in LiPAA	Charge on lithium atoms in BIAN-LiPAA (Significantly decreased)
Li 1	0.3118	0.2862
Li 2	0.3743	0.3423
Li 3	0.3813	0.3299
Li 4	0.3365	0.3393
Li 5	0.2804	0.4238
Li 6	0.3710	0.3632
Li 7	0.3502	0.2765
Li 8	0.5288	0.3786

When the charges on N and Li atoms are carefully examined using the same parameters as that of HOMO-LUMO calculations, it is observed that the negative charge values on all N atoms of BIAN-LiPAA are

lower than those on the N atoms of P-BIAN Li atoms of BIAN-LiPAA show a lower charge value than the Li atoms of LiPAA. The detailed values are mentioned in Table 2 and Table 3. During the calculation we considered 4 units of polymerized BIAN (P-BIAN) and 8 units of LiPAA. That means the system under study had 8 nitrogen atoms and 8 lithium atoms.

This indicates that N and Li atoms interact, further lowering the energy of the LUMO. The Gibbs free energy change (ΔG) was calculated to determine the energy required for this process to occur to achieve a stable lithiated state.[26]

The energy of the reactants and product are $E_{P\text{-BIAN}} = -3434.75$ Ha, $E_{LiPAA} = -2232.4244$ Ha, and $E_{BIAN\text{-}LiPAA} = -5667.30$ Ha. Hence, $\Delta G = E_{BIAN\text{-}LiPAA} - (E_{P\text{-BIAN}} + E_{LiPAA}) = -0.1256$ Ha $= -78.81$ kcal/mol. Because the ΔG value is negative, interaction of N atoms of P-BIAN moiety with Li^+ ions of LiPAA is a thermodynamically spontaneous process, and BIAN-LiPAA is more thermodynamically stable than P-BIAN and LiPAA.

Electrode preparation

The electrode slurry was prepared by heating a mixture of the 1:1 P-BIAN/LiPAA binder (10%), acetylene black (10%), and graphite (80%) in slight excess of NMP as the solvent. The mixture was heated at 80 °C overnight to ensure effective mixing of the materials. A slight heating opens the polymer strands, hence improves the solubility of the P-BIAN. Then, the excess solvent was removed under reduced pressure using a rotary evaporator. The slurry was coated on a copper foil via the doctor blade method, with a coating thickness of 0.100 mm. After drying the electrode under vacuum at 70 °C for 8 h, it was roll pressed to a thickness of 0.06 mm at 80 °C. The resultant electrode was used to make anodic half-cells for further electrochemical study. To collect reference data, electrodes with the PVDF binder were fabricated via a similar method.

Electrochemical studies

A graphite anode, a polypropylene separator (Celgard 2500), a 1.0 M $LiPF_6$ (50:50) EC/DEC electrolyte, and Li metals (as the counter and reference electrodes) were used to fabricate 2025-type coin cells. Anodic half-cells were fabricated in an argon-filled glovebox (UNICO UN-650), with H_2O, and O_2 levels less than 0.05 ppm. At 25 °C, charge–discharge analysis was sperformed using a battery cycler (Electrofield-EFT-001). Electrochemical characterizations were performed using a BioLogic VMP electrochemical workstation equipped with a frequency response analyzer. Cyclic voltammetry (CV) was performed using anodic half-cells at 25 °C between 0.01 and 2.1 V versus Li/Li^+ at a scan rate of 0.1 mVs^{-1}. Electrochemical impedance spectroscopy (EIS) and dynamic EIS (DEIS) experiments were performed with a sinus amplitude of 10 mV and a frequency range from 10 MHz to 0.1 Hz.

Cyclic Voltammetry

Cyclic voltammetry (CV) is a vital electrochemical technique widely employed in battery research, especially for assessing novel anodic binders in Li-ion batteries. This method involves sweeping the electrode potential in a linear manner while recording the resulting current response. By analyzing the peaks and troughs in the current-voltage curve,
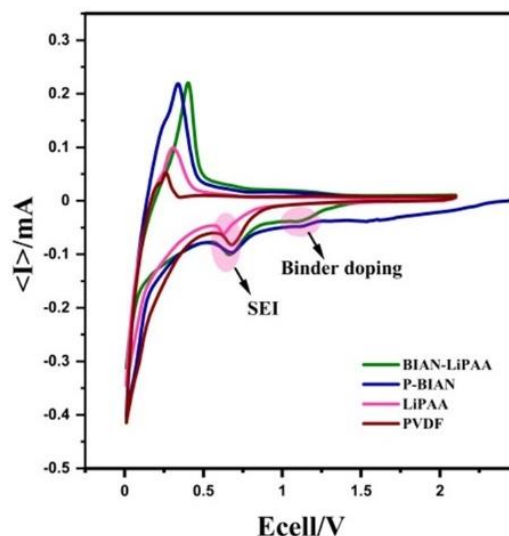
Figure 5. Comparison of CV curves at 0.1 mV/s.

CV offers crucial insights into the redox behavior of the anodic binder, shedding light on oxidation and reduction processes and hence the charge storage mechanisms. Moreover, it provides essential data on the electrochemical stability and kinetic properties of the binder, enabling researchers to design electrodes with enhanced charge-discharge rates and prolonged cycling life. CV helps determine the electrochemical window within which the binder remains stable, aiding in optimizing the battery's safety and performance. Comparative analyses of different binders using CV facilitate the selection of the most effective binder material. By studying various binder compositions through CV, researchers can fine-tune the formulation to achieve desired electrochemical attributes, such as improved stability and increased capacity. Additionally, CV assists in understanding degradation mechanisms, enabling strategies to mitigate binder degradation for prolonged battery longevity and enhanced efficiency. In essence, CV plays a pivotal role in unraveling the electrochemical intricacies of anodic binders, shaping the landscape of modern Li-ion battery development.

Therefore, to evaluate the doping potential of the binder, CV was performed. As shown in Figure 5, in the cyclic voltammogram of P-BIAN and BIAN-LiPAA the characteristic peaks at 1.1 V versus Li/Li$^+$, corresponding to P-BIAN binder doping, were observed.
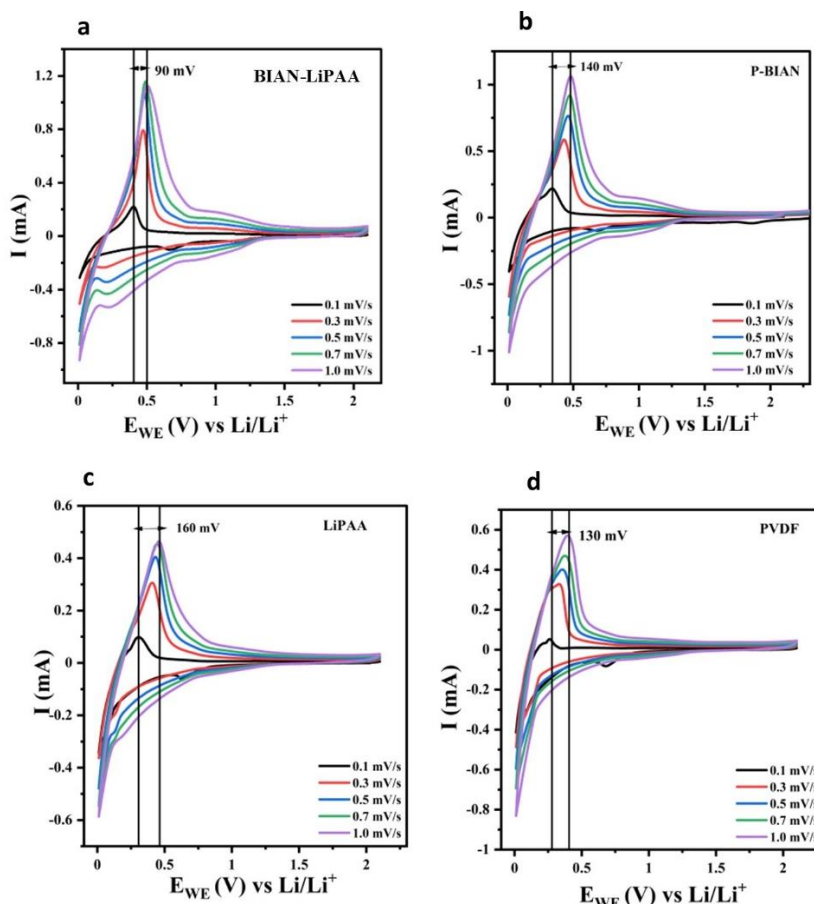
Figure 6. Overpotential under CV scan rates for (a) BIAN-LiPAA, (b) P-BIAN, (c) LiPAA, (d) PVDF

Prior degradation of binder saves electrolyte which also helps in formation thinner and robust SEI. A thinner and robust SEI in Li-ion batteries improves efficiency by lowering impedance at the electrode-electrolyte interface. This enhancement stabilizes the battery by reducing electrolyte decomposition and minimizing side reactions, leading to a longer cycle life and reduced capacity fade over time. Additionally, a well-formed, thin SEI layer mitigates dendrite growth, enhancing battery safety and longevity. It also optimizes energy density and rate capability by allowing for efficient ion transport and maximizing the active surface area of the electrode. Overall, a thin, durable SEI contributes to a more reliable and efficient Li-ion battery. This indicates that binder doping affects SEI formation on the BIAN-LiPAA binder-based anode. As shown in Figure 5, the first peak is observed in the potential window of 0.95–1.2 V versus Li/Li$^+$, which corresponds to binder doping. The second peak at ~0.65 V versus Li/Li$^+$ corresponds to regular electrolyte (EC) decomposition.[24] BIAN-LiPAA exhibits the lowest delithiation overpotential of 90 mV when the scan rate increases from 0.1 to 1.0 mV/s (Figures 6), which is attributed to the synergistic effect of the thinner SEI and Li$^+$ ion conducting anode domain.[31] However, P-BIAN, LiPAA, and PVDF exhibit overpotentials of 140, 160, and 130 mV, respectively. BIAN-LiPAA exhibits much lowered overpotential compared to other reference binder materials.

Charge–Discharge Study

Charge-discharge studies are essential for evaluating the performance of a battery system. They provide valuable insights into the battery's energy storage capabilities, charge and discharge rates, efficiency, and overall stability.
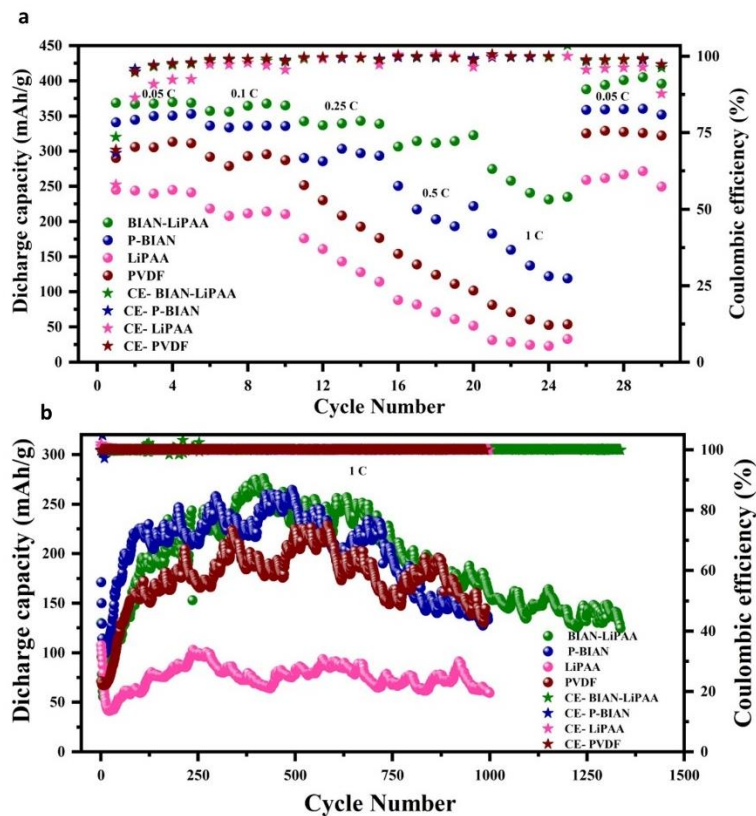
Figure 7. Comparison of Charge discharge study (a) Rate Study, (b) Long Cycling.

By monitoring the voltage and current profiles during these cycles, we can understand the battery's behavior under varying conditions and assess how well it retains its capacity over time. This analysis aids in optimizing charging protocols, determining the battery's cycle life, identifying potential degradation mechanisms, and ultimately advancing battery technology to meet the demands of various applications.

Therefore, charge–discharge tests were performed to compare the discharge capacity, stability, and cyclability of the BIAN-LiPAA binder-based anode to those of PVDF–, P-BIAN–, and LiPAA–based anodes. This study showed how efficiently Li^+ ions intercalated and deintercalated in the graphite matrices. The cycling profiles of anodic half-cells fabricated using BIAN-LiPAA and PVDF binders at various current rates in the potential window from 0.01 to 2.1 V vs. Li/Li^+ are shown in Figure 7a. The initial discharge capacity at the onset of a cycle test shows an escalating trend with an increasing number of cycles, primarily due to the dynamic transformations occurring within the graphite electrodes of lithium-ion batteries. Through cycling, graphite experiences an enlargement in d-spacing, facilitating heightened lithium ion insertion and extraction rates. Concurrently, the graphite's morphological changes, particularly the tendency to exfoliate into nanosheets during prolonged cycling or in cells with substantial Depth of Discharge (DOD), significantly augment the surface area exposed to the electrolyte. This morphological shift increases the quantity of Li-intercalatable graphite, amplifying the storage capacity for lithium ions. Moreover, the potential reduction of the graphite side enlarges the electrochemical window, optimizing active material utilization. Cumulatively, these processes foster enhanced lithium-ion intercalation, offer a greater number of active sites, and expand the electrochemical window, collectively contributing to the observable rise in initial discharge capacity as the number of cycles progresses.

The cell with the BIAN-LiPAA binder exhibits a considerably higher discharge capacity at all current rates, with improved an initial Coulombic efficiency (CE) of 73%, and which subsequently reached and

stabilized itself at 99%, than the cell with the reference binder systems. This shows that very few Li^+ ions are lost during SEI formation in the BIAN-LiPAA-based cell. The discharge capacity of the LiPAA- and PVDF-based anodes exhibits poor stability. The continuous decrease in the capacity of LiPAA- and PVDF-based anodes is due to the poor binding ability of the binder.

Long-cycle charge–discharge analysis at a rate of 1 C (372 mA/g) was performed to assess the cyclability and specific discharge capacity of the cells with P-BIAN/LiPAA polymer and the reference binder materials. Figure 7b compares the long-cycle discharge results of different binder systems in the potential window from 0.01 to 2.1 V vs Li/Li^+. The BIAN-LiPAA binder–based anodic half-cell underwent 1336 cycles at a rate of 1 C and exhibited appreciable capacity retention, exhibiting a maximum discharge capacity of 276 mAh/g. However, the PVDF binder–based anode underwent 1000 cycles and exhibited a maximum reversible capacity of 228 mAh/g with poor capacity retention due to its inability to provide mechanical robustness and maintain conductivity. A thin and conducting SEI plays an important role in maintaining the good health of the electrode.

Extremely fast-charging study

The need for an extremely fast-charging battery arises from the growing demand for quick and convenient energy replenishment in modern society. Fast-charging batteries can significantly reduce charging times, enhancing user experience, and facilitating the widespread adoption of electric vehicles and portable electronics. An anodic binder plays a crucial role in achieving this goal by enabling efficient charge and discharge rates. It helps maintain the structural integrity of the anode during rapid charging, ensuring that the active materials remain intact and accessible. A well-designed anodic binder optimizes conductivity and promotes homogeneous electron/ion transport within the electrode, enhancing the overall efficiency and speed of the charging process. Therefore, anodic half-cells were fabricated in similar ways to study in the same voltage range to evaluate the XFC performance of the BIAN-LiPAA binder– and PVDF binder–based anodic half-cells at 5 C (Figure 8a) and 10 C (Figure 8b) current rates.

The BIAN-LiPAA binder–based anodic half-cell exhibits higher capacity and cycling stability than the PVDF counterpart. The BIAN-LiPAA binder–based half-cells exhibit capacities of 62.1 and 114.5 mAh/g at 10 and 5 C, respectively, which are 4.77 and 2.03 times higher than those of the PVDF counterparts, respectively, at the same current rate.
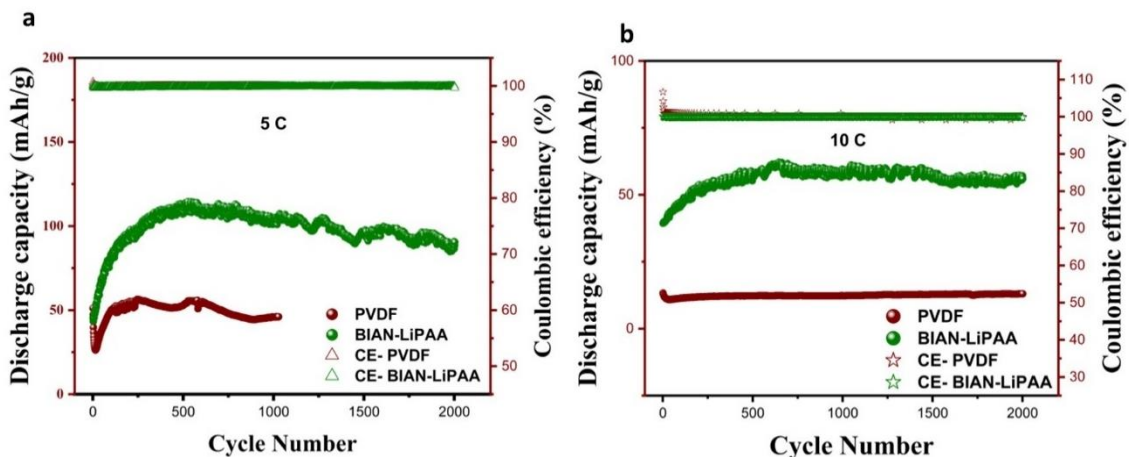

Figure 8. Comparison of charge discharge study at faster current rate (a) 5C, (b) 10C

Electrochemical impedance spectroscopy (EIS)

As we know, the performance of a cell is significantly influenced by its internal resistance. Internal resistance in a battery is like a bottleneck that hinders the smooth flow of electrons and ions during charge

and discharge cycles. This resistance leads to energy losses in the form of heat, reducing the overall efficiency and power output of the battery.
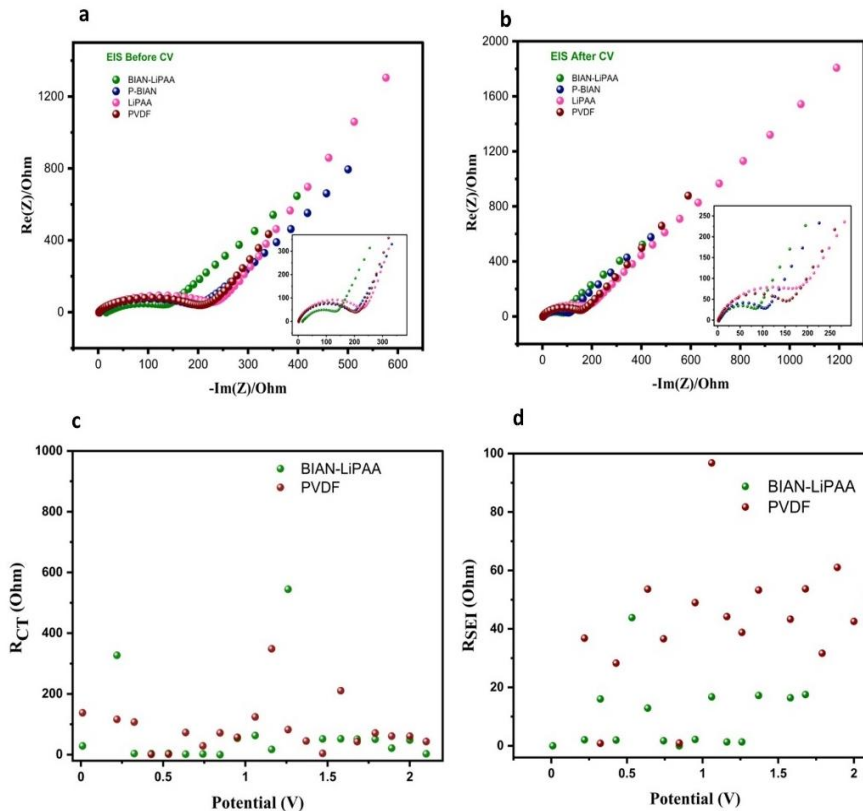

Figure 9 (a) Comparison of EIS spectra before CV. (b) Comparison of EIS spectra after CV. (c) R_{CT} comparison plot. (d) R_{SEI} comparison plot.

High internal resistance can cause voltage to drop under load, limiting the battery's ability to deliver power when needed. It can also contribute to reduced cycle life and affect the battery's capacity retention over time.

Electrochemical Impedance Spectroscopy (EIS) plays a key role in analyzing a battery's internal resistance and understanding its impact on performance. EIS is a powerful tool that allows researchers to study the complex electrical properties of batteries by measuring impedance at different frequencies. By analyzing impedance data, EIS provides valuable insights into the various resistance components within the battery, including the internal resistance. Understanding and quantifying internal resistance through EIS helps in optimizing battery designs, identifying degradation mechanisms, and devising strategies to mitigate resistance-related issues. Ultimately, EIS enables a deeper understanding of how internal resistance influences a battery's performance and aids in the development of more efficient and reliable energy storage systems. Therefore, to measure the internal resistance of the cells with different binder systems, potentiostatic electrochemical impedance spectroscopy (PEIS) was performed. BIAN-LiPAA shows the lowest impedance than the other counterparts in the PEIS spectra, which were recorded before and after one CV cycling at 0.1 mV/s, respectively. Figure 9a and 9b show that the diffusion of Li$^+$ significantly improves and a better Li$^+$ ion–conducting SEI is formed.

Binder doping has led to very low interfacial impedance in the case of BIAN-LiPAA binder–based cells. In the case of PEIS, the cell resistance was recorded without any direct current. It does state about the internal cell resistance, but we cannot get the individual resistance components such as R_{SEI}, $R_{CT,}$ and R_{PC}.
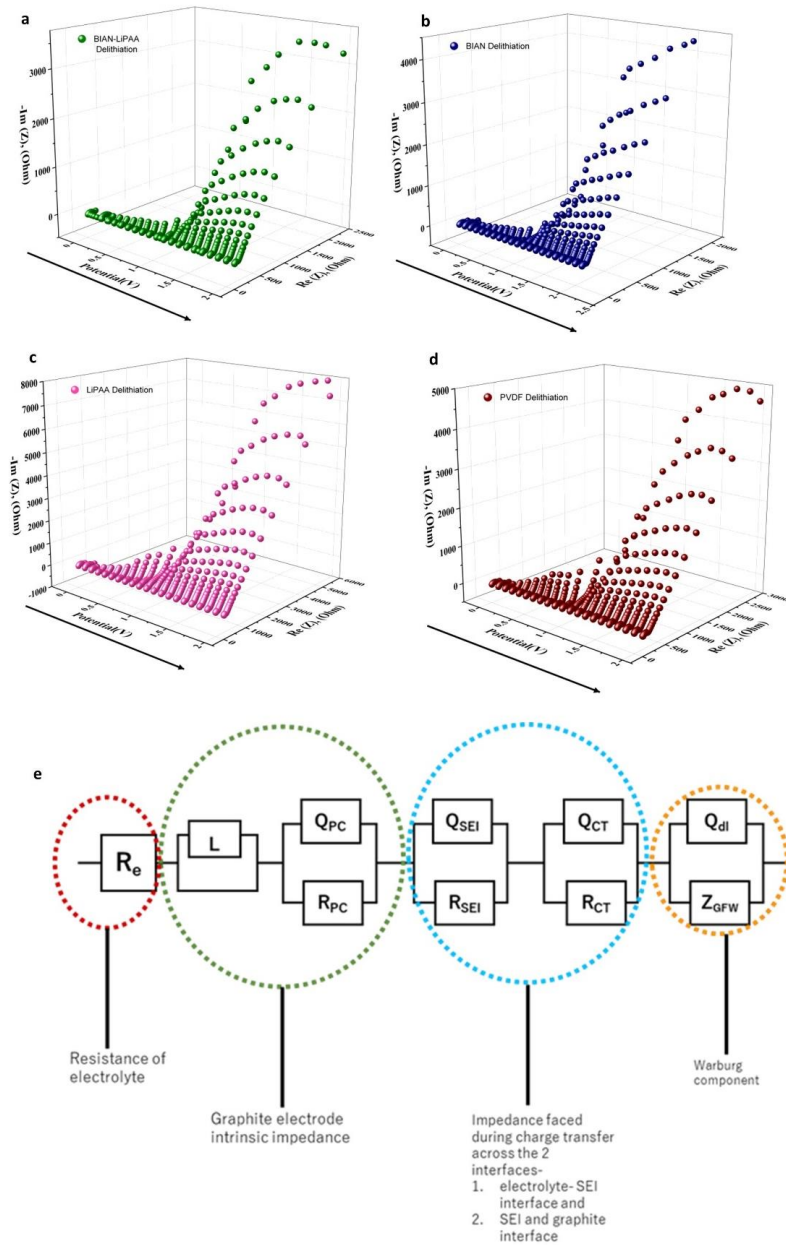
Figure 12. DEIS Nyquist plots at different potentials of (a) BIAN-LiPAA, (b) P-BIAN, (c) LiPAA, (c) PVDF, (e) EECM model used for fitting the Nyquist plots.

Differential Electrochemical Impedance Spectroscopy (DEIS) and PEIS are both valuable techniques used in battery research to analyze the electrochemical behavior of batteries, but they differ in their approach and the insights they provide. PEIS involves applying a constant potential to the battery and measuring the resulting current, allowing for the study of the impedance of the system at that specific potential. On the other hand, DEIS involves applying a small-amplitude sinusoidal potential perturbation superimposed on a constant potential bias, resulting in a periodic potential waveform. DEIS measures the response of the system to this periodic potential, providing information on impedance changes with respect to the perturbation frequency.

DEIS involves the application of small perturbations on top of a steady-state condition. It measures the differential response of the system to these perturbations, allowing researchers to obtain more detailed information about changes in the system's impedance.

DEIS is particularly useful for investigating subtle changes in the battery's impedance caused by various factors like aging, state of charge, temperature variations, or structural modifications. It provides high-resolution insights into the dynamic behavior of batteries under different operating conditions. This is particularly useful in identifying and analyzing multiple processes such as charge transfer, diffusion, and surface phenomena that may not be easily distinguishable using PEIS.

Therefore, to further understand PEIS data, DEIS was performed to measure impedance during the charge and discharge cycles, and the variable frequency response against the potential was recorded corresponding to an AC signal. As shown in Figure 10 a-d, the Nyquist plots at various potentials of BIAN-LiPAA exhibit a lower impedance compared to the same of PVDF.

Circuit fitting was done for complete quantitative understanding. The data obtained from DEIS were fitted to the appropriate equivalent electric circuit models (EECMs). The EECM was decided by referring to a previous report published by our group[24] (Figures 10 e).

After fitting the data, it is clearly observed in Figure 9c that the BIAN-LiPAA binder–based cell exhibits lower impedance than the PVDF counterpart, which clearly indicates that the SEI formed in the BIAN-LiPAA binder–based cell is superior to that in PVDF-based cells. The obtained data in Figure 9d show that the charge transfer resistance (R_{ct}) values of the BIAN-LiPAA binder–based cell are considerably lower than those of the PVDF-based anodic half cells. After DEIS, circuit fitting was done to segregate the different resistance components, which were analyzed to obtain a qualitative understanding.

Different resistance components of BIAN-LiPAA-base anodic half-cells have been plotted and compared with the same in the case of PVDF cells. The R_{pc}, R_{SEI}, and R_{ct} values of the BIAN-LiPAA binder–based cell are significantly lower than those of the PVDF binder–based cell. This further proves the robust SEI formation in the BIAN-LiPAA binder–based cell. The R_{pc} is the resistance experienced by Li^+ ions in the graphite matrix, R_{SEI} is the resistance experienced by Li^+ ions while moving through the SEI, and R_{ct} is the charge transfer resistance. As shown in schematic representation in Figure 11a, a thin and conducting SEI always facilitates better Li^+ ion diffusion. To further study the quality of the SEI formed, the Li^+ ion diffusion coefficient values were calculated. Using the DEIS data in the Warburg region, the Li ion diffusion coefficient can be calculated using the following formula[41] mentioned bellow:

$$D_{Li^+} = \frac{R^2 T^2}{2A^2 n^4 F^4 C^2 \sigma\,2}$$

where R is the gas constant, T is the absolute temperature, A is the area of the electrode, n is the charge number of the electroactive species (n = 1), F is the Faraday constant, C is the concentration of lithium ions, and σ is the Warburg factor. The Warburg factor was obtained from the slope of the plots of Z' vs ω 1/2, (ω is the angular frequency) in the Warburg region. The diffusion coefficient obtained from the BIAN-LiPAA binder–based anodic half-cell is 2.86 E−10, considerably higher than those of PVDF and other reference binder-based cells. This is attributed to the robust SEI formed and improved impedance in the presence of high concentrations of Li^+ ions. Li^+ ion diffusion in the host material is one of the rate-determining processes. Therefore, the temperature-dependent EIS study can be used to calculate the activation energy (E_a) for Li ion diffusion using the Arrhenius equation, $1/R_{CT} = Ae^{-\left(\frac{Ea}{RT}\right)}$, for more details see Figure 11b and Table 4.[31,42] Arrhenius equation for calculation of the activation energy is as follows,

$$\ln 1/R_{CT} = lnA + ((-Ea)/R)(1/T)$$

For example-

If slope = -1.07389 ± 0.33, then $-E_a$= 2.303 x Slope x R. Therefore, E_a=21.00 kJ/mol

As shown in Figure 11b, the Ea value of the BIAN-LiPAA binder–based cell is 21.0kJ/mol, considerably

lower than those of the PVDF-, P-BIAN-, and LiPAA-based cells, which are 39.63, 45.37, and 31.56 kJ/mol, respectively.

Table 4. Activation energy of different binder systems.

Binder	Activation energy of Lithiation (kJ/mol)
BIAN-LiPAA	21.00 (slope= -1.07)
LiPAA	31.56 (slope= -1.64)
P-BIAN	45.37 (slope= -2.31)
PVDF	39.63 (slope= -2.07)

Therefore, the considerable improvement in E_a is attributed to the low R_{ct} values and robust SEI formation. This shows the clear advantage of using a Li-surplus anode.[28,43,44] As shown in Figure 11e, a tensile testing machine (3365-L5, INSTRON) with a load cell (5 kN) was used to perform a peel test at a crosshead speed of 3 mm/min at room temperature to study the mechanical properties of different binders. BIAN-LiPAA shows an appreciable adhesion with a 99.45% weight retention. However, P-BIAN, LiPAA, and PVDF show 89.78%, 74.59%, and 75.50% retentions, respectively (Figure 12 and Table 5). This study also confirms that the BIAN-LiPAA composite polymer binder exhibits improved electrochemical stability and mechanical properties. Then, as part of the postmortem study, XPS was performed to further understand the electrode composition, SEI thickness, and electrode health after long cycling. The clear peaks with good intensity in the XPS spectrum show that the SEI is thinner than 10 nm; hence, it offers lower interfacial resistance.[31] As shown in Figure 11c, 11d, the C=N and C–N peaks are observed at 284.8 and 285.4 eV in the XPS spectrum, respectively.

Postmortem Study

As shown in Figure 6d, the peak at 399.3 eV in the XPS spectrum is attributed to the quaternary nitrogen and the C=N peak is observed at 398.86 eV.[24,26] The formation of a thinner SEI is attributed to the low-lying LUMO of the composite binder. Because the binder decomposes before the electrolyte, it stops the irreversible decomposition of electrolytes and prevents the accumulation of salt at the SEI, which ensures the SEI does not become thicker and nonconductive.[19,22,23,45] After the completion of the long-cycling study at 1 C, the cells were decrimped in an argon-filled glove box. The electrode was removed from the superfluous cell components and rinsed several times with the dehydrated EC/DEC solvent before drying in a high vacuum for 16 h. As shown in Figures 11f, 11g and 11h, the SEM images clearly show that, compared to the BIAN-LiPAA based pristine electrode, huge cracks are present in PVDF electrodes after 1000 cycles, but only tiny cracks are observed in the BIAN-LiPAA binder–based electrodes after 1336 cycles.
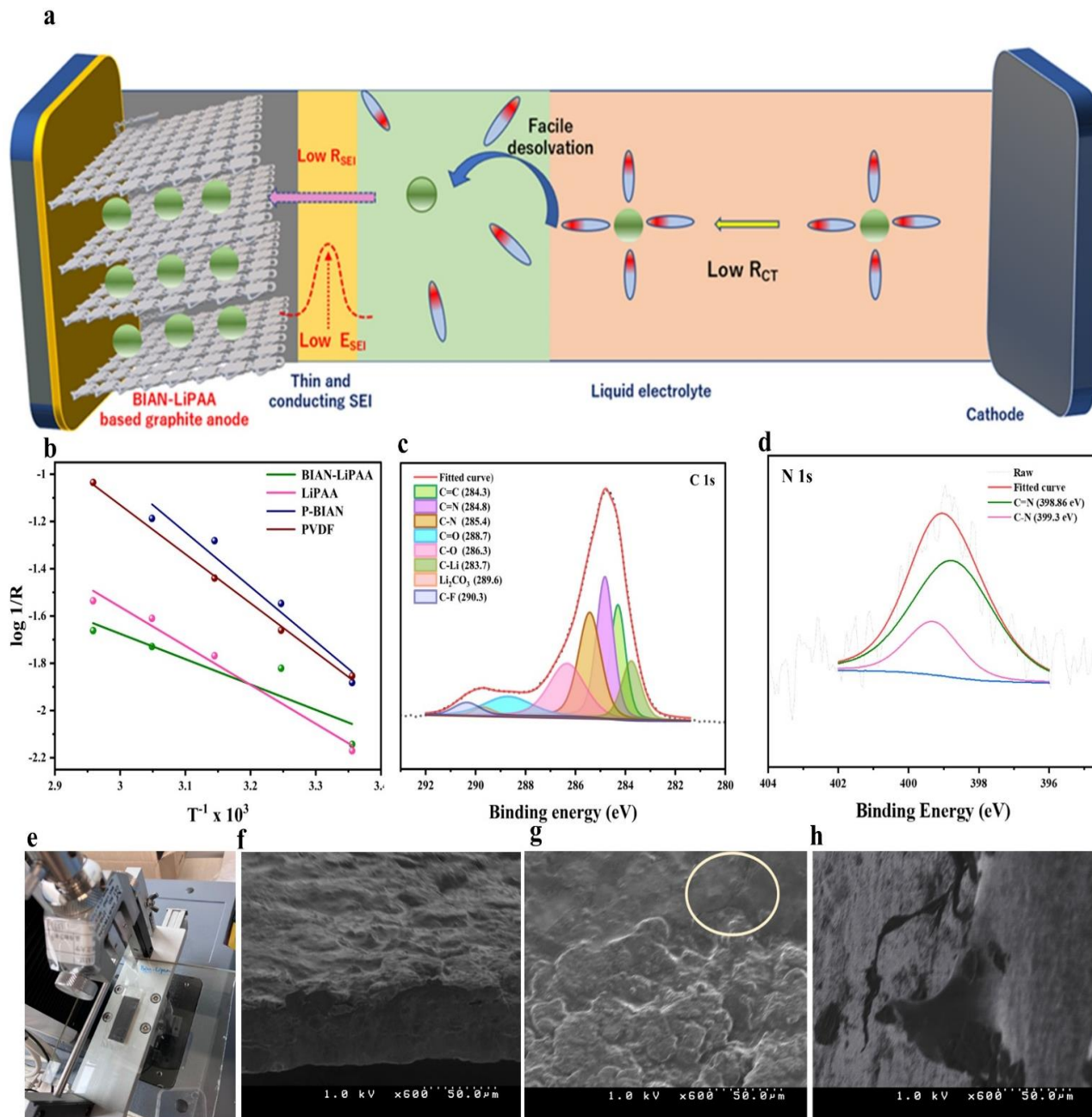
Figure 11. (a) Schematic representation of the kinetics of BIAN-LiPAA binder–based half-cells. (b) Temperature dependent Arrhenius plot for lithiation in graphite-based anodes with different binders at 0.2 V (c) C 1s XPS spectrum of BIAN-LiPAA and (d) N 1s XPS spectrum of BIAN-LiPAA. (e) Peel test of BIAN-LiPAA. (f) Cross-sectional SEM images of pristine BIAN-LiPAA binder–based electrode. (g)SEM image of BIAN-LiPAA based electrode (h) SEM image of PVDF based electrode.
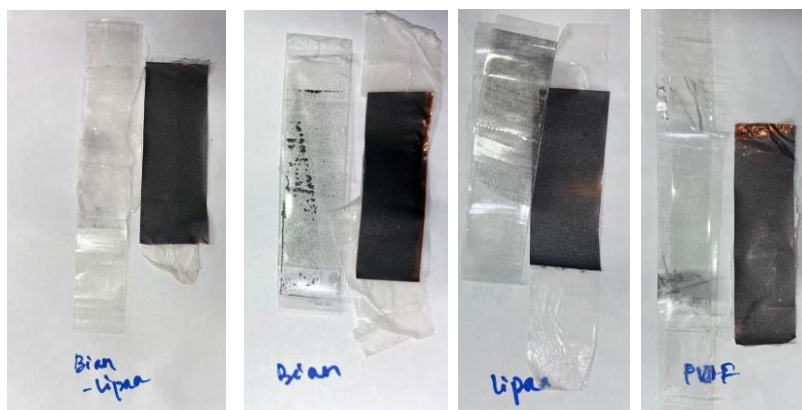
Figure 12. Pictures of electrodes with different binder materials after the peel test.

Table 5. Peel test details of all the electrodes with different binder materials

Binder material	Weight of electrode before peeling	Weight of electrode after peeling	Percent of weight retained
BIAN-LiPAA	0.1296	0.1289	99.45 %
P-BIAN	0.09122	0.0819	89.78 %
LiPAA	0.12143	0.09058	74.59 %
PVDF	0.1625	0.1227	75.50 %

This difference is attributed to the excellent adhesion of the novel composite polymer binder system. Table 6 compares the performance of the BIAN-LiPAA binder with other reported binders used to fabricate graphite-based anodes such as CMC-Na, Acryl S020, xanthan gum (XG), styrene-butadiene rubber (SBR), poly(N-vinylformamide), PVDF, BIAN-fluorene copolymer, P-BIAN, poly (acrylamide-co-diallyldimethylammonium chloride) (AMAC), and allylimidazolium-based poly (ionic liquid).

Conclusions

This lithium surplus anode fabricated using the BIAN-LiPAA binder exhibited a considerably improved Li$^+$ ion diffusion coefficient, a low overpotential, and the lowest activation energy for Li intercalation in the anode domain. The low R$_{ct}$ values and easy diffusion led to the fast-charging ability and showed good stability even at a higher current rate such as 10 and 5 C. The low energy level of the LUMO of the binder system decreased electrolyte decomposition, hence forming a thinner and more robust SEI, which was also confirmed via XPS. BIAN-LiPAA exhibits a higher CE, and low (charge transfer, diffusion, and SEI) resistance probably due to the formation of an improved SEI. As shown in Table 1, our BIAN-LiPAA composite polymer binder is a superior alternative to PVDF and moreover, deeper studies on the synergistic effects in the Li$^+$-rich composite polymer binder systems are currently underway.

Table **6** Comparison of the performances of the BIAN-LiPAA binder and other reported binders for the graphite anodes.

Binders	Peak discharge capacity	Current rate	References
PVDF	~200 mAh/g ~56 mAh/g ~12 mAh/g	1 C 5 C 10 C	[46–48] and this work
CMC-Na	~200 mAh/g	1 C	[49–51]
Acryl S020	~166 mAh/g	1 C	[51,52]
AMAC	~210 mAh/g	1 C	[47]
LiPAA	102 mAh/g	1 C	This work
XG	~350 mAh/g	1 C	[50,51]
SBR	~340 mAh/g	1 C	[53,54]
SBR-PVDF	~260 mAh/g	1 C	[55,56]
BIAN-fluorene polymer	~270 mAh/g	1 C	[46]
Allylimidazolium-based poly(ionic liquid)	~210 mAh/g	1 C	[48,57]
P-BIAN	~260 mAh/g	1 C	[24] and this work
BIAN-LiPAA	~276 mAh/g ~ 114 mAh/g ~ 62 mAh/g	1 C 5 C 10 C	This work

Chapter 3
Stabilization of Si-based Anode for LIB Using BIAN Type Conjugated Polymer/Poly(lithium acrylate) Composite Binder

ABSTARCT

The pressing demand for high-energy-density lithium-ion batteries (LIBs) has drawn significant attention to silicon (Si) as a material with remarkable specific capacity. However, practical use of Si in batteries is stymied by its substantial volume expansion during the charge-discharge cycles. To address this challenge, the development of innovative binders tailored for Si anodes has emerged as an effective approach to enhance their electrochemical performance and cycle life. In this work, a robust polymer composite binder, poly(iminoacenapthylene-1,1'-biphenylyl-3,3'-diol)/poly(lithium acrylate) (BIAN-DHBDN/LiPAA), is proposed. This binder was applied to composite anodes containing 25% silicon and 25% graphite (Si-Gr), exhibiting several interesting properties such as a higher mechanical strength, optimum electrical conductivity, facilitated formation of a thin solid electrolyte interphase (SEI) layer. Consequently, the anodic half cells demonstrated remarkable stability over 800 charge-discharge cycles, retaining a high reversible capacity of approximately 1200 mAh g^{-1}, with an efficient Li^{+} ion diffusion characterized by a diffusion coefficient of 2.86×10^{-10} cm^2 s^{-1} and a significantly higher initial coulombic efficiency of 87%. Notably, the batteries exhibited 95% capacity retention and 99% coulombic efficiency during the long cycling charge-discharge study. The advantageous effects, including suppressed electrolyte decomposition, mechanical stability, low overpotential (25 mV), and enhanced Li^{+} ion diffusion, were supported through techniques such as cyclic voltammetry (CV), electrochemical impedance spectroscopy (EIS), and dQ/dV plot analysis. Furthermore, postmortem analysis of the anode was conducted using X-ray photoelectron spectroscopy (XPS) and scanning electron microscopy (SEM).

Introduction-

Lithium-ion batteries have become the cornerstone of modern energy storage, powering a wide range of applications, from smartphones to electric vehicles. [58] The continuous pursuit of higher energy density and longer cycle life has driven extensive research into novel materials and innovative designs for battery components. [59] Among these components, the binder system plays a pivotal role in ensuring the structural stability and overall performance of electrodes. [60,61] In the context of silicon (Si) anodes, the demand for improved binder materials has never been more pressing, given the immense potential of Si to revolutionize lithium-ion battery technology. [62,63] Silicon has long tantalized researchers with its high theoretical capacity, making it a promising candidate to replace conventional graphite anodes. [62–64] However, the practical utilization of silicon has been hampered by its dramatic volume expansion (up to 300%) during lithiation. This leads to pulverization, delamination[61,65], and continuous SEI regeneration[58].

Uncontrolled SEI formation involves irreversible consumption of lithium ions and electrolytes, impairing Coulombic efficiency[66] and depleting Li^+ ions[60]. Strategic solutions to these issues include nano structuring Si, carbon composites, material coatings, and innovative binders to enhance performance and stability. [62] In this regard, conventional polymeric binders, such as PAA, poly(vinylidene fluoride) (PVDF) or carboxymethyl cellulose (CMC), [60,61] have proven inadequate in effectively mitigating these challenges, prompting the urgent need for innovative binder systems tailored to the unique demands of silicon anodes. Herein, a N- atom and Li^+ rich composite polymer binder system named BIAN-DHBDN/LiPAA is proposed, which offers a multifaceted approach to tackle the complexities associated with silicon anodes. [67,68] As shown in Figure 1 this multifunctional composite binder designed through the synergistic integration of several efficiency-enhancing elements offers following strategic advantages:

1) The inclusion of imine group N-atoms facilitates superior adhesion by coordinating with the current collector (Cu foil)[67,68].

2) Incorporation of -OH moieties enhance mechanical stability by forming hydrogen bonds with Si-particles. [62,69]

3) Its low LUMO level ensures binder degradation before electrolyte, reducing electrolyte degradation. [67,70]

4) The binder's ability to form a thinner SEI, results in lower internal resistance and activation energy.

5) It contains a lithium surplus component to compensate for Li^+ ion loss during the SEI formation in the first cycle as well as in the subsequent cycles.

6) The presence of COO^- moieties promotes faster Li^+ ion diffusion.

7) Lithium ions within poly (lithium acrylate) enhance ionic conductivity, leading to improved battery performance, charge, and discharge rates.

8) Nitrogen atom interactions with Li^+ ions reinforce the binder's structural integrity.

9) The absence of acidic hydrogen in the LiPAA unit prevents HF formation and H_2 gas evolution within the cell.
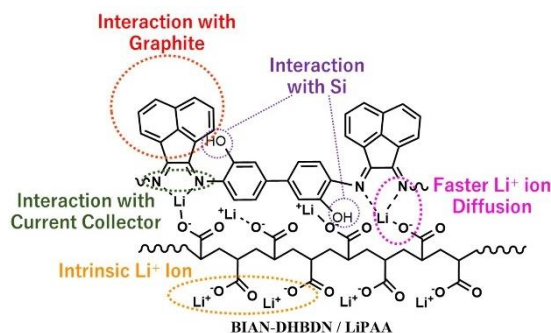
Figure 1 Structure and designing concept of BIAN-DHBDN / LiPAA polymer composite binder.

Additionally, this study sheds light on designing structurally tailored binders to achieve a harmonious balance between mechanical integrity and electrode flexibility, thus prolonging the cycle life of Si anodes.

MATERIALS AND METHODS

3,3'-Dihydroxybenzidine, acenaphthenequinone, acrylic acid, N-methylpyrrolidone (NMP), and acetic acid were purchased from Tokyo Chemical Industry Co., Ltd. LiOH was purchased from Sigma Aldrich. MeOH was purchased from Wako Chemicals Ltd. Highly dehydrated acetonitrile was purchased from Wako Pure Chemical Industries, Ltd. Battery-grade graphite and PVDF were purchased from Sigma Aldrich. A 1.0 M LiPF$_6$ ethylene carbonate/diethyl carbonate (EC/DEC = 1:1) electrolyte was purchased from Sigma Aldrich. Battery-grade acetylene black was purchased from Denka Japan Private Co. Ltd. Copper foils with a thickness of 20 μm were purchased from Nilaco Co. All the materials were utilized as received without any additional purification.

Synthesis and Characterization

The reported polymer was successfully prepared by an acid catalyzed Schiff base reaction as reported by Matsumi et al. [67,68,71–74] (Figure 2). The reported polymer was successfully characterized by mass spectroscopy (MS) followed by nuclear magnetic resonance (NMR), infrared spectroscopy (IR), and X-ray photoelectron spectroscopy (XPS). Because the reactants (i.e., acenaphthoquinone and 3,3'-dihydroxybenzidine) are harmful, dangerous, and carcinogenic (upon sustained exposure) and can cause eye and skin irritation and allergic reactions, rigid safety rules were implemented during their handling. Proper safety measures must be performed when handling these compounds.

Figure 2 Synthesis of BIAN-DHBDN/LiPAA polymer composite

Electrode Preparation

The electrode slurry was made by combining a 1:1 mixture of BIAN-DHBDN/LiPAA binder (25%), acetylene black (25%), graphite (25%), and 100 nm silicon nano particle (25%) in NMP solvent. This mixture was mixed well for 2 hours using a Planetary Centrifugal Mixer SK-350TII to ensure thorough

blending of the components. The slurry was applied to a copper foil using the doctor blade technique, resulting in a coating thickness of 0.100 mm. After vacuum drying the electrodes at 70 °C for 8 hours, they were roll pressed at 80 °C to achieve a thickness of 0.06 mm.[65,75] The resulting electrode was utilized to make anodic half-cells for further electrochemical investigation. For comparison purposes, electrodes with a PAA binder were prepared using a similar procedure.

Electrochemical Studies

A Si-Gr composite anode, along with a polypropylene separator (Celgard 2500), a 1.0 M $LiPF_6$ (50:50) EC/DEC electrolyte, and Li metals (used as counter and reference electrodes) were used in the fabrication of 2025-type coin cells. The anodic half-cells were prepared within an argon-filled glovebox (UNICO UN-650) maintaining H_2O and O_2 levels below 0.05 ppm. Charge-discharge analyses were conducted at 25°C using a battery cycler (Electrofield-EFT-001). Electrochemical characterizations were carried out using a BioLogic VMP electrochemical workstation equipped with a frequency response analyzer. Cyclic voltammetry (CV) was executed on the anodic half-cells at 25°C within the voltage range of 0.01 to 2.1 V versus Li/Li$^+$ at a scan rate of 0.1 mVs−1.[76,77] Electrochemical impedance spectroscopy (EIS) and dynamic EIS (DEIS) experiments were performed with a sinusoidal amplitude of 10 mV and a frequency range from 10 MHz to 0.1 Hz.[78]
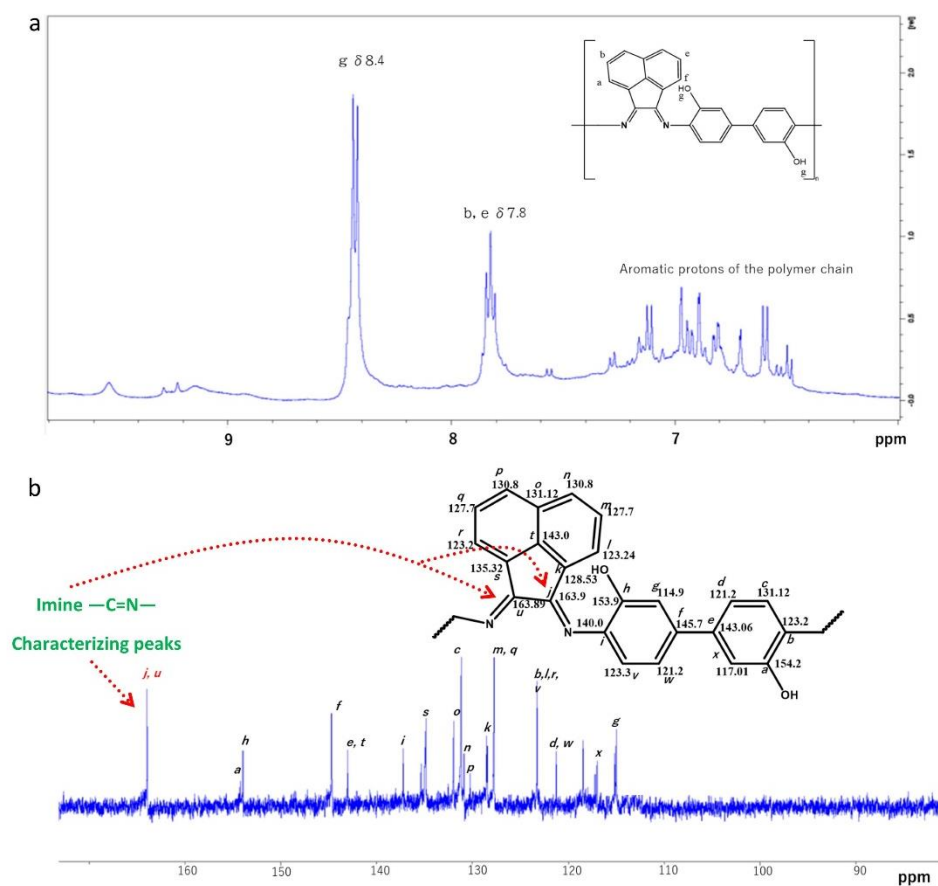
Results and Discussion

Figure 3 (a) ^{1}H NMR spectrum (b) ^{13}C NMR spectrum of BIAN-DHBDN polymer

As shown in Figure 3a in the ^{1}H NMR spectrum the disappearance of NH$_2$ proton peaks at δ4.5 ppm was observed in comparison with ^{1}H NMR spectrum of the starting material (DHBDN), provided strong evidence for the completion of the polymerization reaction. Additionally, the upfield shift of the alcoholic OH proton peak from δ9.1 ppm to δ8.5 ppm, attributed to extended conjugation, further supported the structural alterations in the polymer. The ^{13}C NMR spectra (Figure 3b) exhibited distinct chemical shift values for different carbon atoms. Notably, the anticipated C=O peak at 190 ppm was absent, replaced by a C=N imine carbon peak at 160 ppm. Additionally, the C-N carbon peak shifted from 136 ppm in the diamine monomer to 140 ppm in the imine-based polymer. This shift suggests an alteration in the electron density surrounding the imine carbon due to resonance effects or neighboring groups' electronic influence. Further, the absence of the ketone carbon peak near 187.0 ppm, present in the monomer diketone, confirmed successful polymerization.

Additionally, in Figure 4, the IR spectrum revealed distinctive peaks associated with functional groups within the polymer. A peak at 1283 cm^{-1} was attributed to the C-N stretching vibration, signifying the presence of C-N bonds. The peak at 1659 cm^{-1} corresponded to the imine C=N stretching vibration within the BIAN-DHBDN imine.
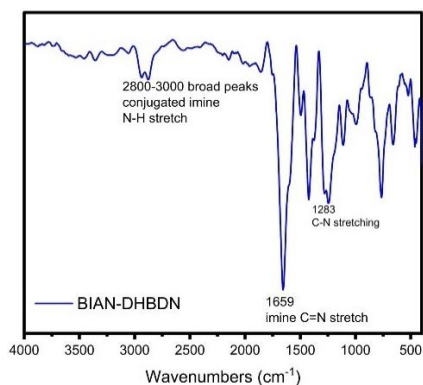

Figure 4 IR spectrum of BIAN-DHBDN polymer

Broad peaks observed in the range of 2800-3000 cm^{-1} were attributed to the conjugated imine N-H stretch. Complementing the IR spectra, in the XPS spectrum, the peak at 399.7 eV was attributed to the characteristic diimine (C=N) nitrogen within BIAN-DHBDN. Additionally, as shown in Figure 5, the C 1s XPS spectrum displayed a peak at 286 eV, confirming the presence of C=N bonds. The N 1s XPS spectra of BIAN-DHBDN / LiPAA exhibited a peak at 400 eV, suggesting the coordination nitrogen atoms to Li$^+$ ions of LiPAA.

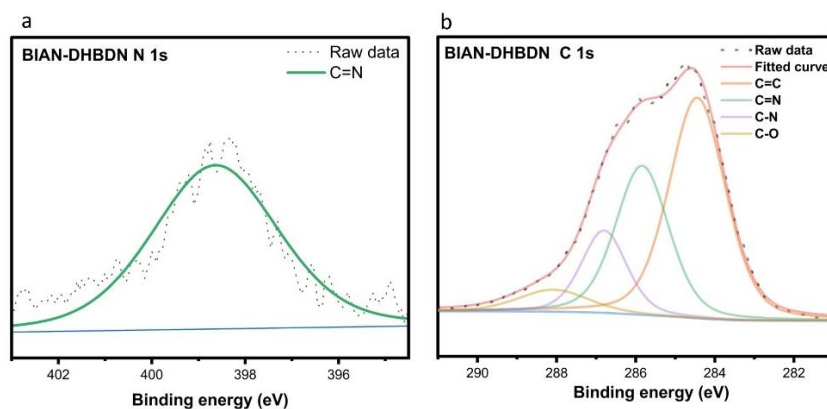Figure 5 (a) N 1s, (b) C 1s XPS spectra of BIAN-LiPAA

Collectively, this multi-spectroscopic approach provides a detailed and systematic characterization of the polymer, elucidating its structural and compositional features. Further analyses and investigations are warranted to comprehensively understand its chemical and physical properties.

HOMO-LUMO Study

Because the LUMO level of the binder plays a crucial role in SEI formation and minimizing electrolyte degradation, density functional theory (DFT) calculations of BIAN-LiPAA were performed on Materials Studio using Dmol 3 software with the optimization parameters, DND basis set, generalized gradient approximation (GGA) (pW91) density functional, and unrestricted spin polarization by maintaining the charge neutrality.[67,71,74] As shown in Figure 6, the remarkably low-lying energy level of the lower unoccupied molecular orbital of the BIAN-DHBDN/LiPAA binder makes it an n-doped composite binder in an anodic environment, which leads to the reduction of the binder before electrolyte degradation to form a thin and conducting SEI. The proposed composite binder exhibits a considerably low SEI resistance, and an activation energy with an improved Li^+ diffusion in the anode matrix. BIAN-DHBDN/LiPAA binder with a low LUMO level could offer wide range of advantages related to improved electron transport, enhanced redox reactions, optimized electrode-electrolyte interface, reduced voltage losses, and the potential for innovative binder designs. These advantages collectively contribute to the overall performance and longevity of lithium-ion batteries with silicon-based anodes.
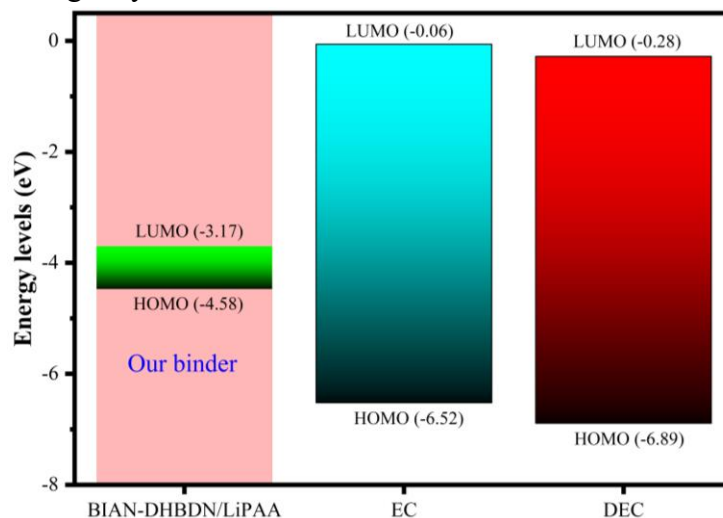

Figure 6 HOMO-LUMO comparison of BIAN-DHBDN/LiPAA, EC and DEC

Peel Test

The adhesion capability of the binder material is a crucial parameter for assessing its effectiveness in restricting the rapid and vigorous volume expansion of SiNPs. Binders with suboptimal adhesion tend to lead to delamination of anodes.[79] Therefore, an ideal binder should exhibit strong adhesion properties.[80] This study focuses on evaluating the force-displacement curves during a 180° peeling test for Si electrodes with different binders: BIAN-DHBDN/LiPAA and PAA as depicted in Figure 7a-c. The average adhesion forces for PAA electrodes are determined to be 7.87 N. In contrast, the BIAN-DHBDN/LiPAA electrode exhibits a significantly higher adhesion force, of 9.45 N. This high adhesion force of our binder is 1.58 N higher than that of the PAA electrode (Figure 7d and 7e). Additionally, the BIAN-DHBDN/LiPAA electrode displays minimal shedding of electrode material when subjected to peeling, illustrating its superior adhesion compared to PAA, where the Si electrode is exposed to the copper (Cu) foil.
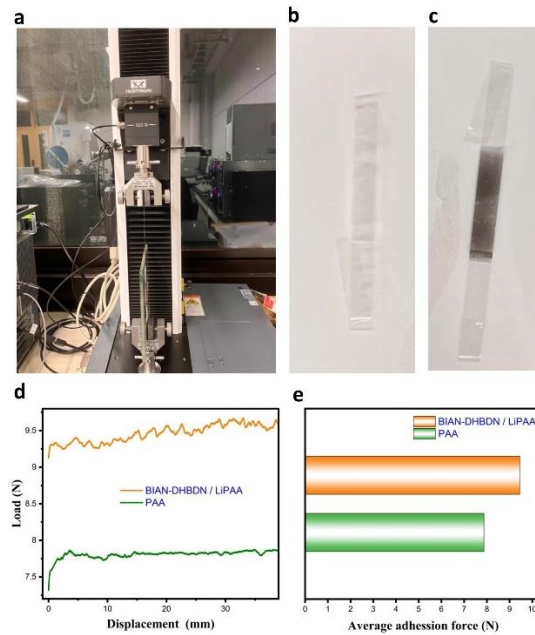
Figure 7 (a) Peel test setup, amount of shedding of electrode material when (b) BIAN-DHBDN/LiPAA (c) PAA are subjected to peel test, (d) comparison of peel strength of electrodes (e) average adhesion forces of electrodes.

This enhanced adhesion in BIAN-DHBDN/LiPAA is attributed to both hydrogen bonding and ionic coordination present in the BIAN-DHBDN/LiPAA binder. Consequently, the active material remains firmly adhered to the Cu foil. Furthermore, the swelling ratio of the binder in the electrolyte plays a pivotal role in influencing the morphology and electrochemical performance of the electrode. This significant difference highlights the critical role of BIAN-DHBDN/LiPAA in maintaining the stability and structural integrity of the anode.[81,82]

Cyclic voltammetry

In the initial cathodic sweep, a broad reduction peak ranging from 0.5 to 0.9 V was observed, corresponding to the electrolyte's decomposition, and contributing to the formation of the solid electrolyte interface (SEI) film. This broad peak vanished in subsequent cycles, suggesting the successful formation of a relatively stable SEI on the active material's surface during the initial cycle.[67,68,72]
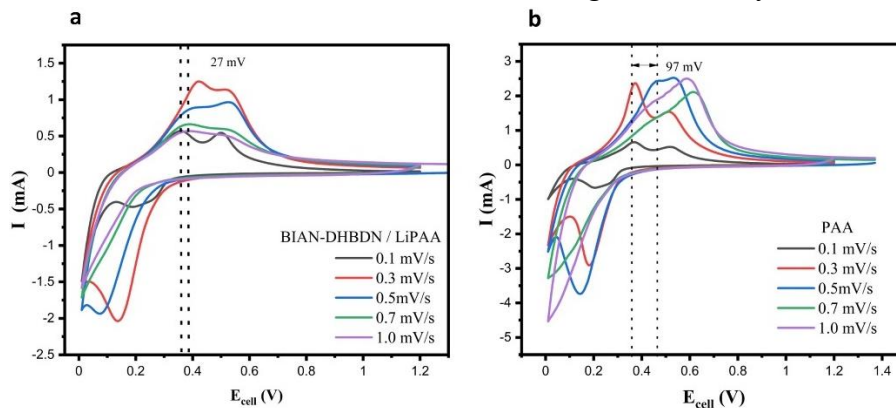

Figure 8 Comparison study of cyclic voltammetry scan rate study and overpotential of a) BIAN-DHBDN/LiPAA b) PAA

The cyclic voltammograms (CV) depicted in Figure 8a showcase the cycles of the BIAN-DHBDN/LiPAA

electrode at different scan rate. A sharp reduction peak below 0.3 V was observed, which was attributed to the lithiation process involving the transformation from silicon crystal to Li−Si alloys. This aligns with the extended discharge plateau observed in Figure 9. On the anodic sweep, peaks at around 0.3 and 0.5 V were noted, indicating the Li$^+$ extraction from Li−Si alloys leading to the formation of amorphous Si. In the subsequent lithiation cycles, the amorphous Si primarily engaged in the lithiation reaction, as opposed to the initial crystalline Si. Following the first cycle, a broad reduction peak emerged at around 0.2 V, corresponding to the lithiation of amorphous silicon. Notably, the CV profiles of the BIAN-DHBDN/LiPAA electrode (Figure 8a) shows a very low overpotential of 27 mV compared to that of the PAA based electrode with an overpotential of 97 mV (Figure 8b). This suggests favorable interfacial characteristics of the electrode, improved kinetics of electrode reactions, and a more even distribution between active material and Super P within the BIAN-DHBDN/LiPAA electrode.[58,59,61] The quality of the solid electrolyte interface (SEI) will affect the cell impedance and charge-discharge studies which will be further understood by the ex-situ SEM observation.[59,60,83]

Electrochemical Impedance Spectroscopy

In Figure 10, the impedance is demonstrated through Nyquist plots for both the BIAN-DHBDN/LiPAA electrode and the PAA electrode. All impedance assessments were conducted at 2s5 °C. The impedance spectra primarily comprise different components such as the electrolyte resistance R_E, solid interfacial resistance (R_{SEI}) and charge transfer resistance (R_{CT}), respectively. In the low-frequency region, a straight line is observed, representing Li$^+$ diffusion within the electrode bulk. The corresponding resistance values from the fitting are presented in Table 1. Before initiating cycling, the BIAN-DHBDN/LiPAA electrode displayed smaller R_{CT} and R_{SEI} values compared to the CMC systems. This indicates a positive interfacial attribute of the electrode, improved kinetics of electrode reactions, and a more consistent distribution between SiNP and Super P within the BIAN-DHBDN-LiPAA electrode. This suggests that introducing the BIAN-DHBDN/LiPAA binder effectively reduced the generation of new SEI and enhanced the conductivity of the contact network, which are crucial for accommodating volume changes during cycling. These improvements significantly contributed to the enhanced capacity and stability of the BIAN-DHBDN/LiPAA anode.[84]
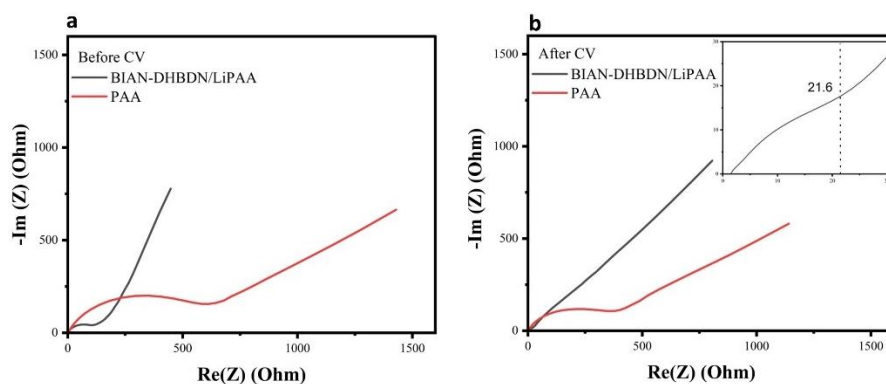
Figure 9 PEIS comparison data of BIAN-DHBDN/LiPAA and PAA (a) before CV (b) and after CV.

A thin and conducting SEI always facilitates better Li ion diffusion.[85] To further study the quality of the SEI formed, the Li ion diffusion coefficient values were calculated. Using the impedance and frequency data in the Warburg region, the Li ion diffusion coefficient can be calculated using the following formula:

$$D_{Li}^+ = \frac{R^2 T^2}{2A^2 n^4 F^4 C^2 \sigma^2}$$

Table 1. Charge transfer resistance values of BIAN-DHBDN/LiPAA and PAA

	R_{CT} Before CV	R_{CT} After CV	D_{Li}^+
BIAN-DHBD/LIPAA	30.04	13.07	1.93402E-09
PAA	498.2	313.9	8.60858E-10

Charge-discharge study

Rate study

To assess the rate capability and its impact on battery performance, varied charging and discharging current rate tests were conducted on the anodic binder. This comprehensive evaluation revealed the binder's effectiveness in managing rapid charge and discharge cycles, which is critical for optimizing overall battery efficiency.

Figure 10a demonstrates a consistent capacity stability of BIAN-DHBDN/LiPAA as current rate escalates from 30 mA/g to 400 mA/g and maintains this capacity even beyond 400 mA/g. Conversely, the PAA-based electrode displays a substantial and abrupt capacity reduction with varying current rates. Furthermore, it fails to restore its initial capacity upon reducing the current rate.

Notably, the initial coulombic efficiency stands at 87% for BIAN-DHBDN/LiPAA, contrasting with PAA's significantly lower 46%. This discrepancy suggests a considerable irreversible consumption of Li ions during the formation of a thick SEI for PAA. Conversely, BIAN-DHBDN/LiPAA's higher initial coulombic efficiency can be attributed to 1) surplus inherent Li^+ ions in the binder compensating for Li^+ ion loss during SEI formation and 2) a thinner SEI due to absence of uncontrolled SEI growth, which limits new surface exposure for SEI formation.
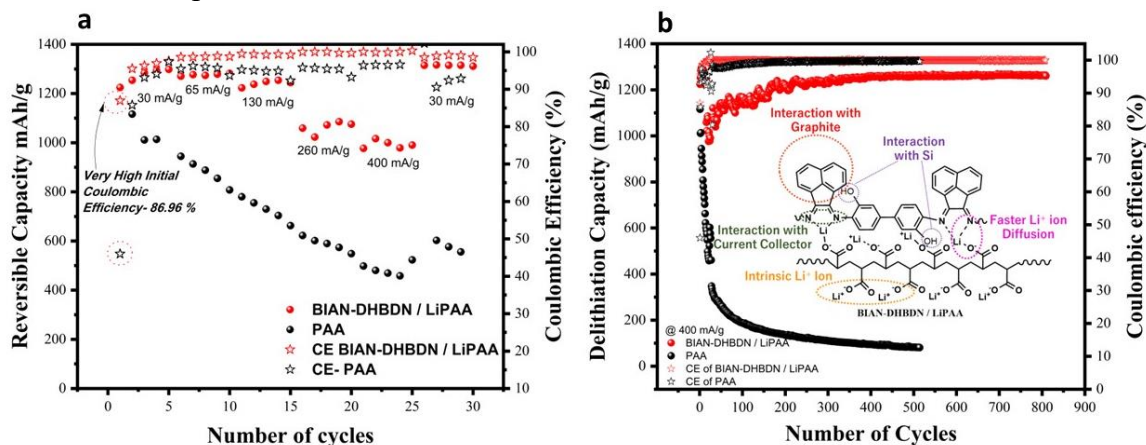
Figure 10 Comparison of charge-discharge study (a) at different current rates (b) at 400 mA/g current rate.

Long cycling

As observed from the rate study, the Si-based anodes experience considerable stress under high current rates. Consequently, conducting a prolonged cycling study at a high current rate becomes imperative to ascertain the binder's ability to sustain structural integrity and performance during extended periods of intense utilization.

In this context, electrodes employing BIAN-DHBDN/LiPAA and PAA were subjected to a long cycling study at a current rate of 400 mA/g. Figure 10b displays the resulting dataset, revealing notable

distinctions. BIAN-DHBDN/LiPAA demonstrated a sustained capacity of 1260 mAh/g over more than 800 cycles, underscoring its remarkable stability. Conversely, the electrode with PAA as the binder exhibited a sharp decline in capacity, stabilizing at a significantly lower range of around 200 mAh/g. This contrasting behavior underscores the efficacy of the BIAN-DHBDN/LiPAA binder in mitigating volume expansion and stabilizing the Si anode over extended cycling. The observed trend in the PAA electrode could likely be attributed to uncontrolled SEI formation and a subsequent drastic reduction in Li$^+$ ions due to the thickening of the SEI.[82,86] Further analysis is warranted to conclusively determine the precise mechanisms driving this behavior.

Potential profile analysis
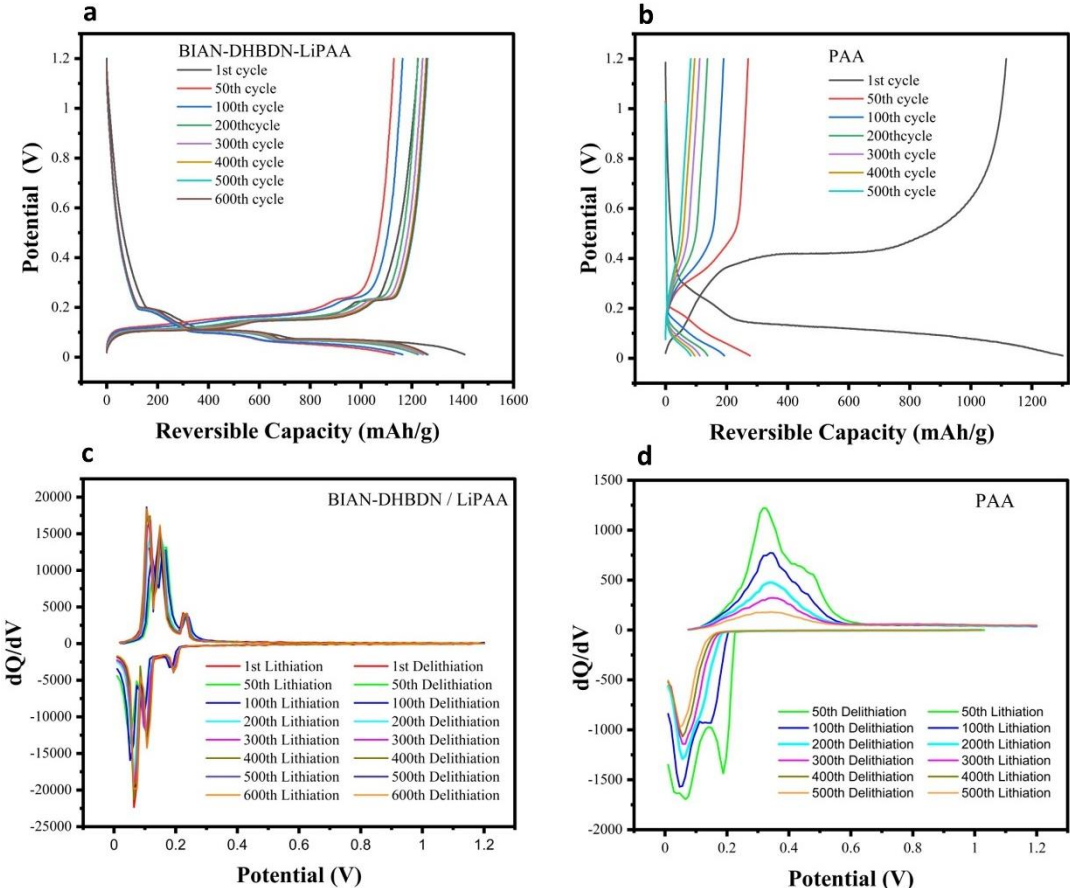
Figure 11 Comparison of potential vs capacity profiles of different charge-discharge cycles of (a) BIAN-DHBDN/LiPAA, (b) PAA, comparison of differential capacity curves of different charge-discharge cycles of (c)BIAN-DHBDN/LiPAA, (d)PAA binder based cells

A comprehensive analysis of the potential profile significantly complements the in-depth exploration of extended cycling charge-discharge studies, offering valuable insights into the observed behavior. As depicted in Figure 11a and 11b in the case of BIAN-DHBDN/LiPAA, the initial lithiation profile exhibits a marginal irreversible capacity loss attributed to SEI formation. In contrast, PAA manifests a substantial irreversible capacity loss, suggesting a thicker SEI formation. This observation corroborates the favorable outcomes noted in the rate study, long cycling, and higher coulombic efficiency. Crucially, in comparison to PAA, BIAN-DHBDN/LiPAA showcases exceptional coherence and alignment in the lithiation and delithiation profiles, persisting from the 1st cycle up to the 600th cycle. This remarkable consistency

underscores the stability of the anode and strongly implies the absence of any undesirable side reactions within the specified electrochemical environment. Such comprehensive insights into electrochemical behavior, as elucidated through potential profile analysis, are pivotal for advancing anodic binder design and formulation, ultimately optimizing performance for silicon-based anode applications.[59,87,88]

Differential capacity profile analysis

Differential Capacity Analysis (DCA) curves, depicted as dQ/dV vs. V, elucidate structural alterations during charge/discharge, offering valuable insights.[89–91] Analyzing the shifts in peak position and height provides a window into distinct degradation mechanisms. To imbue a structural perspective into the comprehensive electrochemical analysis, DCA was performed (Figure 11c and 11d). Notably, in the case of PAA, cycling induces peak shifts towards voltages, indicating conductivity loss and binder decomposition. Concurrently, diminished peak heights and voltage shifts suggest lithium inventory loss, likely due to excessive electrolyte decomposition, a thicker solid electrolyte interface (SEI), and Li ion depletion. Moreover, a decline in peak height at a relatively constant voltage implies active material loss or decomposition. Conversely, BIAN-DHBDN/LiPAA exhibits a consistent and coherent peak evolution, manifesting structural integrity and absence of lithium-ion loss over an extensive 800-cycle range. This implies that BIAN-DHBDN/LiPAA is more robust compared to the conventional binder PAA.

Activation energy

Temperature-dependent Arrhenius plots are instrumental in determining the activation energy, representing the energy barrier for lithium ions to traverse within the battery. This insight sheds light on Li^+ ion diffusion, charge transfer resistance, and their influence on the battery's efficiency and power output, particularly at varying temperatures.

In this study, impedance measurements were meticulously recorded at temperatures of 25, 35, 45, 55, and 65°C. Subsequently, the Arrhenius equation (Equation 2) was employed,

$$1/R_{CT} = Ae^{-\left(\frac{Ea}{RT}\right)}$$

incorporating the recorded R_{CT} values to calculate the activation energy (Ea) for each condition. The resulting activation energy values were determined as 28.5 kJ/mol for the BIAN-DHBDN/LiPAA-based electrode and 35.2 kJ/mol for the PAA-based electrode. The significantly higher Ea in the case of PAA strongly indicates the formation of a thicker solid electrolyte interface (SEI), leading to increased impedance in Li ion diffusion through the SEI and the electrode bulk.

Having substantiated and rationalized the findings observed in the charge-discharge study, the next step involves a physical examination of the electrode morphology and structural integrity post extensive cycling at a higher current rate. To achieve this, a disassembly of the cells was meticulously planned, facilitating a direct observation of the electrode's physical attributes.

Postmortem study

Following a series of experiments aimed at substantiating the favorable characteristics of BIAN-DHBDN/LiPAA in stabilizing Si anodes compared to the inadequate performance of PAA, a postmortem analysis was conducted utilizing X-ray Photoelectron Spectroscopy (XPS) and Scanning Electron Microscopy (SEM). Coin cells were carefully disassembled within an Ar environment in a glove box, after which the electrodes were subjected to a 10-hour vacuum drying to ensure complete dryness of the electrode surface.

In Figure 12, the XPS spectrum provided insight into the elemental composition and SEI thickness.
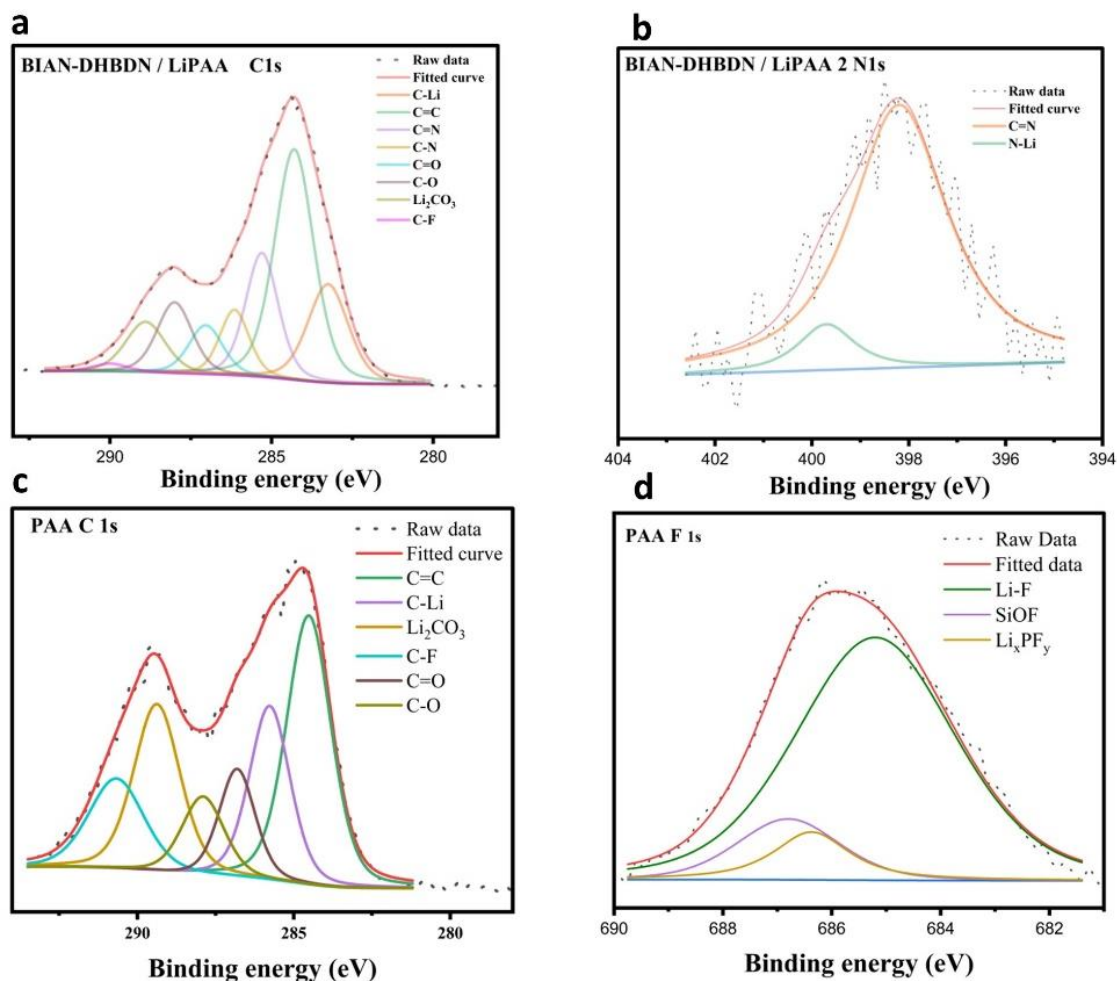
Figure 12. Postmortem XPS spectra of cycled BIAN-DHBDN/LiPAA electrode.

In the N 1s spectrum of the BIAN-DHBDN/LiPAA-based electrode, a prominent peak at 398.5 eV attributed to the C=N bond,[73] along with another peak at approximately 400 eV representing coordinating nitrogen, possibly due to N--Li$^+$ interaction, were observed (Figure 12b). The high intensity of the XPS spectra indicated that the SEI thickness was less than 5 nm.[92–94] Analysis of the C 1s spectrum (Figure 12a) revealed a relatively low fluoride content and minimal deposition of excess salts on the anode surface. Conversely, PAA exhibited an abundance of salts and a thicker SEI, aligning with our earlier inferences regarding its performance (Figure 12c, 12d). In Figure 13, SEM images captured at a 50μm scale revealed noticeable cracks and volume expansion in the cycled electrodes compared to pristine ones, particularly due to SiNP's volume expansion. The BIAN-DHBDN/LiPAA-based electrode displayed smaller cracks, while the PAA-based electrode exhibited major cracks and pores. Cross-sectional SEM images revealed a volume expansion of 1.2 times the original thickness for BIAN-DHBDN/LiPAA and 1.7 times for PAA, highlighting the superior binding ability of BIAN-DHBDN/LiPAA in stabilizing Si-based anodes.

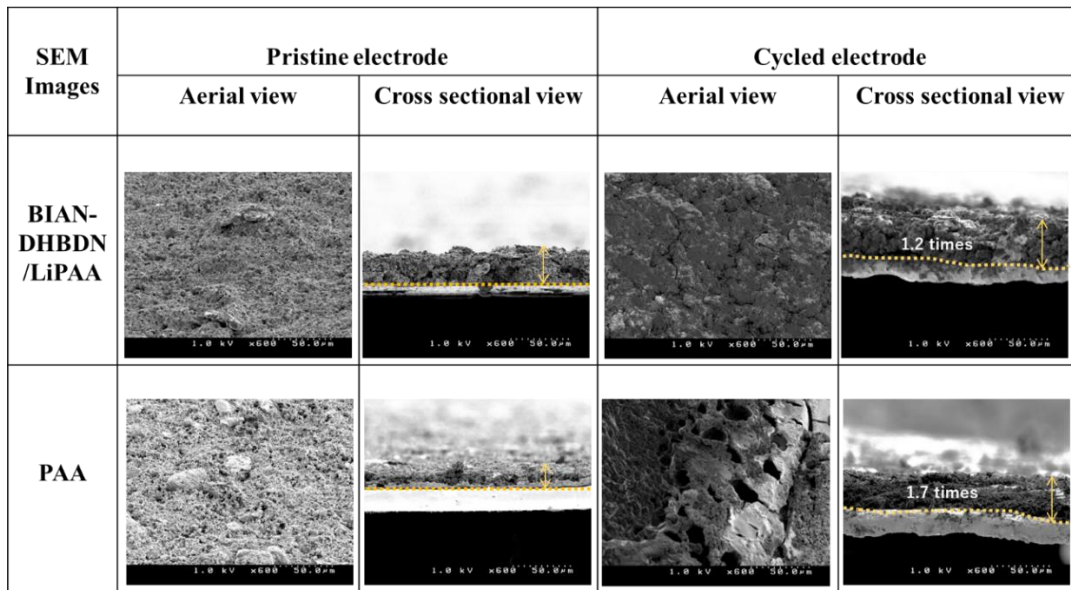| SEM Images	Pristine electrode		Cycled electrode	
	Aerial view	Cross sectional view	Aerial view	Cross sectional view
BIAN-DHBDN /LiPAA				1.2 times
PAA				1.7 times

Figure 13 SEM images of the cycled electrodes compared to the pristine ones to check the surface morphology and volume expansion after long cycling study.

Therefore, these findings validate our initial speculations and affirm the inferences drawn from previous experiments, providing crucial insights into the superior performance of BIAN-DHBDN/LiPAA in stabilizing Si-based anodes compared to PAA.

Conclusions

In conclusion, this study presents a comprehensive exploration of a novel BIAN-DHBDN/LiPAA composite binder for silicon (Si) anodes in lithium-ion batteries (LIBs). The pressing need for high-energy-density LIBs has fueled the quest for efficient Si anodes, but Si's substantial volume expansion during charge-discharge cycles poses a challenge. The proposed BIAN-DHBDN/LiPAA binder, tailored to accommodate Si's volume changes, exhibited remarkable properties, including mechanical strength, maintained electrical conductivity, and facilitated the formation of a thin solid electrolyte interphase (SEI) layer. Utilizing various characterization techniques, the study highlighted the binder's synergistic advantages, such as suppressed electrolyte decomposition, low overpotential, and enhanced Li^+ ion diffusion. The computational analysis provided valuable insights into the binder's energy levels and activation energy, further affirming its potential. Experimental results demonstrated the outstanding stability and performance of the Si anode with BIAN-DHBDN/LiPAA over 800 charge-discharge cycles, maintaining a high reversible capacity and coulombic efficiency. The binder's effectiveness was evident in rate capability tests and long cycling studies, showcasing its ability to mitigate volume expansion and stabilize Si anodes. Postmortem analysis further validated the binder's role in reducing cracks and volume expansion. Overall, the BIAN-DHBDN/LiPAA composite binder emerges as a promising solution for Si anode stabilization, offering a pathway to significantly enhance the electrochemical performance and cycle life of Si-based LIBs, thus contributing to the advancement of high-energy-density battery technology.

Chapter 4
General Conclusion

The journey through this exploration has shed light on the remarkable progress made in the realm of energy storage, specifically within the domain of lithium-ion batteries (LIBs). The pressing demand for high-energy-density LIBs, driven by the growing need for efficient and sustainable energy storage solutions, has led to significant research efforts and innovative developments. Graphite and Silicon (Si) anodes, with their remarkable specific capacity, have emerged as a promising avenue for enhancing the performance of LIBs. However, Si's substantial volume expansion during charge-discharge cycles posed a formidable challenge. The solution to this challenge lay in the development of innovative binders tailored specifically for Graphite and Si anodes.

Throughout this journey, the reported α-diimine type conjugated polymers and LiPAA composite binder has emerged as a promising and effective solution to address the limitations associated with Graphite and Si anodes. The binder's unique characteristics, including mechanical strength, maintained electrical conductivity, and its ability to facilitate the formation of a thin and efficient solid electrolyte interphase (SEI) layer, have significantly contributed to improving anode performance. Furthermore, the conjugated polymer and LiPAA binder's intrinsic lithium ions played a pivotal role in enhancing the diffusion of Li^+ ions, which is a crucial aspect of battery performance. This chapter aims to summarize the thesis, giving an adequate introduction and summarizing all our research work.

Summary of chapter 1

Why We Need Energy Storage Devices?

In today's world, energy plays a crucial role in our daily lives, from powering our smartphones to fueling our vehicles and providing electricity for our homes and industries. However, energy sources are not always readily available, and their generation often fluctuates. This intermittency is a significant challenge for renewable energy sources such as wind and solar, which rely on weather conditions. To bridge the gap between energy production and consumption, we need energy storage devices. These devices store excess energy when it's available and release it when needed, making energy supply more reliable, resilient, and efficient.

Promising Energy Storage Devices

Several energy storage technologies are being developed and improved to address our growing energy storage needs. Some of the most promising ones include:

1. Batteries: Batteries are one of the most widely used energy storage devices due to their versatility, efficiency, and ability to store electricity for various applications

2. Pumped Hydro Storage: This technology involves pumping water from a lower reservoir to an upper reservoir when excess electricity is available and releasing it through turbines to generate electricity when needed.

3. Flywheels: Flywheel energy storage systems store energy as rotational kinetic energy, which can be converted back into electricity when required

4. Supercapacitors: Supercapacitors store energy electrostatically and can provide rapid bursts of power. They are often used in conjunction with batteries for peak power demands.

5. Thermal Energy Storage: This approach stores energy in the form of heat and uses it for heating, cooling, or electricity generation when necessary.

The Significance of Batteries

Batteries are a remarkable energy storage technology that has a profound impact on our daily lives. They have become an integral part of countless applications, including portable electronics, electric vehicles, and renewable energy systems. The history of batteries dates back centuries, with each development contributing to their modern-day significance.

A Brief History of Batteries

The concept of the battery can be traced back to the work of Italian physicist Alessandro Volta in the late 18th century. Volta invented the first chemical battery, known as the Voltaic Pile, which generated a continuous electric current. This marked the birth of electrochemistry and paved the way for further battery innovations. Over the years, various types of batteries were developed, including the lead-acid battery by Gaston Planté in 1859 and the alkaline battery by Lewis Urry in the 1950s. These developments made batteries more practical and efficient, leading to their widespread use in various applications.

Types of Batteries

Batteries come in various types, each with their own advantages and disadvantages. The choice of battery type depends on the specific application and requirements. Some common types of batteries include:

1. Lead-Acid Batteries- Lead-acid batteries are known for their reliability and are widely used in automotive applications. They are inexpensive but have limited energy density and a relatively short lifespan.

2. Nickel-Cadmium (Ni-Cd) Batteries- Ni-Cd batteries have been popular for decades but are now less common due to the toxicity of cadmium and the emergence of newer battery technologies.

3. Nickel-Metal Hydride (NiMH) Batteries- NiMH batteries are an improvement over Ni-Cd batteries, offering higher energy density and less environmental impact.

4. Lithium-Ion (Li-ion) Batteries- Li-ion batteries have gained significant prominence in recent years due to their high energy density, lightweight design, and suitability for various applications, from smartphones to electric vehicles.

Why Li-ion Batteries are Promising Candidates?

Lithium-ion batteries have emerged as one of the most promising candidates for energy storage due to several key advantages:

1. High Energy Density: Li-ion batteries offer a high energy-to-weight ratio, making them ideal for portable devices and electric vehicles, where weight is a crucial factor.

2. Long Cycle Life: They can endure hundreds of charge and discharge cycles, making them durable and cost-effective over time.

3. Low Self-Discharge: Li-ion batteries have a relatively low self-discharge rate, allowing them to hold their charge for extended periods without significant loss

4. Quick Recharge: Li-ion batteries can be recharged relatively quickly compared to other battery types.

5. Versatility: They come in various forms, including cylindrical, prismatic, and pouch cells, enabling flexibility in design and application.

Components of Li-ion Batteries

Li-ion batteries are composed of several key components, each playing a crucial role in their operation. The main components of a Li-ion battery include:

1. Anode- The anode is typically made of graphite and is responsible for the storage of lithium ions during charging.

2. Cathode- The cathode, usually made of lithium cobalt oxide or other lithium transition metal oxides, accepts the lithium ions during discharge.

3. Separator- A porous separator prevents direct contact between the anode and cathode, allowing the flow of lithium ions while preventing short-circuits.

4. Electrolyte- The electrolyte is a conductive solution that facilitates the movement of lithium ions between the anode and cathode.

Graphite and Silicon Anodes- Promising Anode Materials

Both graphite and silicon have been explored as anode materials in Li-ion batteries, and each has its set of advantages and disadvantages.

Graphite Anodes

Advantages: Graphite anodes are stable and have a long cycle life, making them a reliable choice for conventional Li-ion batteries. They are also lightweight and cost-effective.

Disadvantages: Their energy storage capacity is limited, which may not meet the increasing demands of high-energy applications such as electric vehicles.

Silicon Anodes

Advantages: Silicon anodes have a much higher theoretical energy storage capacity compared to graphite, making them ideal for high-capacity applications. They can significantly increase the energy density of Li-ion batteries.

Disadvantages: Silicon anodes suffer from a significant volume expansion during lithium insertion, leading to mechanical stress and reduced cycle life. This expansion issue has been a major challenge in their practical implementation.

The Role of Binders

Importance of Binder- Binders are essential components of Li-ion batteries, both for graphite and silicon anodes. They play a crucial role in electrode manufacturing and battery performance.

For Graphite Anodes- Binders help maintain the structural integrity of the electrode by holding the active material (graphite) and conductive additives together. Without binders, the electrode materials could separate and lose electrical connectivity, affecting the battery's performance.

For Silicon Anodes- In the case of silicon anodes, binders are even more critical. The significant volume expansion and contraction of silicon during charge and discharge cycles can cause the electrode to disintegrate. Binders help mitigate these issues by securing the silicon particles and maintaining electrode integrity.

The Need for Exploration- The Role of Scientists

Scientists and researchers play a vital role in advancing energy storage technologies, including Li-ion batteries. There are several compelling reasons to explore this field:

1.Energy Transition: As the world transitions to cleaner and more sustainable energy sources, the demand for efficient energy storage technologies, like Li-ion batteries, is on the rise.

2. Environmental Concerns: Developing more sustainable and environmentally friendly battery technologies is critical to reduce the environmental impact of energy storage.

3. Global Energy Security: Reliable and efficient energy storage is essential for enhancing energy security and ensuring a stable energy supply.

4. Technological Advancements: Ongoing research can lead to breakthroughs in battery technology, making energy storage more cost-effective and efficient.

The Potential of Conjugated Polymers as binders

Conjugated polymers have emerged as promising candidates for binders in Li-ion batteries for several reasons:

Flexibility and Versatility: Conjugated polymers can be tailored for various battery electrode materials, providing versatility in design.

Improved Adhesion: They offer better adhesion to electrode materials, enhancing electrode integrity and performance.

Conductivity: Some conjugated polymers have semiconducting properties, improving the electrical conductivity of the electrode.

Stability: Conjugated polymers can be engineered for stability in the battery's operating conditions.

In conclusion, the need for energy storage devices is evident in our modern world, with batteries being a significant player in this field. Lithium-ion batteries have risen to prominence due to their high energy density, long cycle life, and versatility. The choice of anode material, such as graphite or silicon, has its own set of advantages and disadvantages, while binders are crucial for maintaining electrode integrity. Continuous exploration and research in this field are essential to meet the increasing demand for efficient, sustainable, and cost-effective energy storage solutions. Conjugated polymers show promise as binders, offering improved performance and versatility for the next generation of Li-ion batteries.

Enabling Ultrafast Charging in Graphite Anodes Using BIAN-Based Conjugated Polymer/Lithium polyacrylate as a Binder

Summary of chapter 2

The development of lithium-ion batteries (Li-ion batteries) has played a pivotal role in modern technology, serving as the power source for a wide range of applications, from smartphones to electric vehicles. A key aspect of fast-charging batteries is the ability of Li^+ ions to easily traverse the solid electrolyte interface (SEI), enabling quick and efficient charge and discharge cycles. Graphite is a promising candidate for anode materials in Li-ion batteries, but it faces challenges, particularly concerning delithiation capacity when subjected to high current rates. To overcome these limitations and achieve extremely fast-charging (XFC) capabilities, researchers have explored the use of composite polymer binders. One such innovative binder is named BIAN-LiPAA, which has intrinsic Li+ ions and unique electronic properties, making it a promising candidate for improving Li-ion battery performance. BIAN-LiPAA, the composite polymer binder, offers several distinct advantages in enhancing Li-ion battery performance. It features a low-lying energy level of the lower unoccupied molecular orbital (LUMO), making it an n-doped composite binder within an anodic environment. This unique property allows BIAN-LiPAA to be reduced before electrolyte degradation, forming a thin and conducting SEI. The low R_{SEI}, R_{CT}, and Ea are indicative of the promising characteristics of this composite binder. Additionally, BIAN-LiPAA significantly improves Li^+ ion diffusion within the graphite anode matrix, contributing to faster charge and discharge rates.

Anodic half-cells constructed with the BIAN-LiPAA binder showcased impressive performance metrics. At various current rates (1 C, 5 C, and 10 C), the discharge capacities demonstrated by these cells exceeded those of counterparts using PVDF, LiPAA, and P-BIAN based binders. These findings highlight BIAN-LIPAA's potential in facilitating fast-charging capabilities while maintaining excellent energy storage and delivery performance.

Under the demanding conditions of extremely fast-charging (XFC), the BIAN-LIPAA binder exhibited high-capacity retention rates of 94.2% and 83.5% at 10 C and 5 C, respectively, after 2000 charge-discharge cycles. This remarkable stability under XFC conditions is a testament to the binder's robustnes. The success of BIAN-LiPAA in enhancing Li-ion battery performance is attributed to several key factors. The low energy level of its LUMO decreases electrolyte decomposition, thus forming a thinner and more resilient SEI, as evidenced by X-ray photoelectron spectroscopy (XPS) analysis. Furthermore, BIAN-LiPAA demonstrates a higher Coulombic efficiency (CE) and lower resistance components, including charge transfer resistance, diffusion resistance, and SEI resistance. This suggests that BIAN-LIPAA not only facilitates fast charging but also contributes to overall battery stability and efficiency.

In summary, the BIAN-LiPAA composite polymer binder holds great promise in the realm of Li-ion battery technology. It has shown significant enhancements in Li+ ion diffusion, low overpotential, and reduced activation energy for Li intercalation, all of which are critical factors for achieving extremely fast-charging capabilities. Its unique electronic properties make it an effective n-doped composite binder, contributing to a thinner and more robust SEI. BIAN-LiPAA has the potential to replace traditional binders like PVDF, and ongoing research is exploring the synergistic effects within Li+-rich composite polymer binder systems. As the demand for fast-charging and high-performance Li-ion batteries continues to grow, innovative solutions like the BIAN-LiPAA binder represent a significant step forward in meeting these requirements.

Stabilization of Si-based Anode for LIB Using BIAN Type Conjugated Polymer/Poly(lithium acrylate) Composite Binder

Summary of chapter 3

The demand for high-energy-density lithium-ion batteries (LIBs) has become increasingly pressing in today's energy-driven world. Silicon (Si) has emerged as a material of particular interest due to its remarkable specific capacity, which holds promise for enhancing the energy density of LIBs. However, the practical utilization of Si in batteries is hindered by a significant challenge - its substantial volume expansion during the charge-discharge cycles. To address this challenge, researchers have explored innovative binders tailored for Si anodes as an effective approach to enhance their electrochemical performance and cycle life.

In this study, a robust polymer composite binder, BIAN-DHBDN/LiPAA, is proposed and applied to composite anodes containing 25% silicon and graphite (Si-Gr). sBIAN-DHBDN/LiPAA exhibits several interesting properties, including enhanced mechanical strength to accommodate Si's volume expansion, maintained electrical conductivity within the electrode structure, and facilitating the formation of a thin and effective solid electrolyte interphase (SEI) layer. Moreover, the intrinsic lithium ions within the BIAN-DHBDN/LiPAA binder contribute to improved diffusion of Li^+ ions. Consequently, anodic half-cells incorporating the BIAN-DHBDN/LiPAA binder demonstrate remarkable stability over 800 charge-discharge cycles, retaining a high reversible capacity of approximately 1200 mAh g^{-1}. The efficiency of Li^+ ion diffusion is characterized by a diffusion coefficient of $2.86 \times 10{-10}$ cm^2 s^{-1}, along with a significantly higher initial coulombic efficiency of 87%. Notably, the batteries exhibit impressive performance, with 95% capacity retention and 99% coulombic efficiency during long cycling charge-discharge studies. This success can be attributed to the synergistic effects of the binder, which include suppressing electrolyte decomposition, enhancing mechanical stability, reducing overpotential (25 mV), and improving Li^+ ion diffusion.

These effects are supported through various characterization techniques, such as cyclic voltammetry (CV), electrochemical impedance spectroscopy (EIS), and dQ/dV plot analysis. Furthermore, the study conducts postmortem analysis of the anode using advanced techniques such as X-ray photoelectron spectroscopy (XPS) and scanning electron microscopy (SEM) to validate the binder's role in reducing cracks and mitigating volume expansion. In conclusion, this study represents a comprehensive exploration of a novel BIAN-DHBDN/LiPAA composite binder tailored for silicon (Si) anodes in lithium-ion batteries (LIBs). The critical demand for high-energy-density LIBs has led to the quest for efficient Si anodes, but Si's substantial volume expansion during charge-discharge cycles poses a significant challenge. The proposed BIAN-DHBDN/LiPAA binder, designed to accommodate Si's volume changes, exhibits remarkable properties, including mechanical strength, maintained electrical conductivity, and facilitating the formation of a thin solid electrolyte interphase (SEI) layer. Utilizing various characterization techniques, this study highlights the binder's synergistic advantages, such as efficient Li^+ ion diffusion, suppressed electrolyte decomposition, low overpotential, and enhanced Li^+ ion conductivity. Computational analysis provides valuable insights into the binder's energy levels and activation energy, further affirming its potential. Experimental results demonstrate the outstanding stability and performance of the Si anode with BIAN-DHBDN/LiPAA over 800 charge-discharge cycles, maintaining a high reversible capacity and coulombic efficiency. The binder's effectiveness is evident in rate capability tests and long cycling studies, showcasing its ability to mitigate volume expansion and stabilize Si anodes.

In essence, the BIAN-DHBDN/LIPAA composite binder emerges as a promising solution for Si anode stabilization, offering a pathway to significantly enhance the electrochemical performance and cycle life of Si-based LIBs. This development contributes to the advancement of high-energy-density battery technology, which is of critical importance for various applications in our energy-driven world.

Prospects

In this dissertation I have tried to explore the practical use of novel polymers BIAN based α-diimine polymer and LiPAA composite in the context of binders. I have investigated these polymers' extensive redox capabilities, their significance in electrochemistry, and the relationship between their structure and properties, all with the aim of enhancing the stability of anodes in high-performance lithium-ion batteries (LIBs). We have adopted a structured approach to enhance the stability of both graphite and silicon anodes in LIBs by crafting BIAN-based polymers that can address the key issues associated with these electrodes. This work has plenty of future scope such as their application on micron silicon for LIBs and a variety of hard carbons for Na ion batteries. Such conjugated polymer composite binders offer solutions to challenges in LIBs with micron-sized silicon anodes and hard carbon-based anodes in Na-ion batteries. These polymers enhance mechanical stability by accommodating volume changes and improving electrode adhesion. They also boost electronic conductivity, providing better charge/discharge rates. Moreover, conjugated polymer binders create more stable SEI, enhancing cycling performance. Their tunable properties, compatibility with electrolytes, and sustainability make them promising choices to address these anode-related issues in advanced energy storage systems.
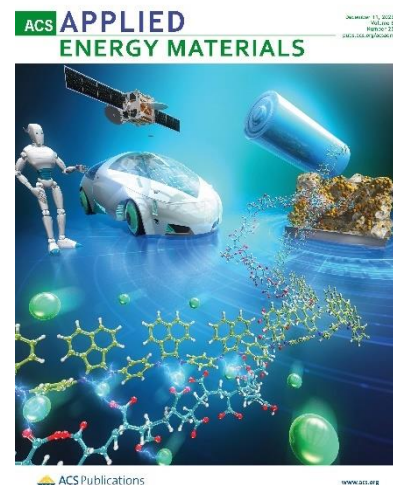
Publications and Conferences

Publications

1. "**Enabling Ultrafast Charging in Graphite Anodes Using BIAN-Based Conjugated Polymer/Lithium polyacrylate as a Binder.**"

<u>Sameer Nirupam Mishra</u>, Saibrata Punyasloka, Bharat Srimitra Mantripragada, Anusha Pradhan and Noriyoshi Matsumi

ACS Appl. Energy Materials

Selected for cover page artwork.

2. Manuscript ready- **Stabilization of Si-based Anode for LIB Using BIAN Type Conjugated Polymer/Poly(lithium acrylate) Composite Binder**

Conferences

1. **Stabilization of Si Based Anode for Lib Using Bian Type Conjugated Polymer/Poly(Lithium Acrylate) Binder**

第72回高分子学会年次大会

会期：2023年5月24日（水）～26日（金）

会場：Ｇメッセ群馬

2. **Stabilization of Si-based Anode for LIB Using BIAN Type Conjugated Polymer/Poly (lithium acrylate) Composite Binder**

第72回高分子討論会

会期：2023年9月26日（火）～28日（木）

会場：香川大学 幸町キャンパス

Poster number- 3Pd060

Received Excellent Poster Award

Oral presentation-

3. **Stabilization of Various Anodes For Lib Using Bian-Type Conjugated Polymer/Poly(Lithium Acrylate) Binders**

The 64th Battery Symposium in Japan, November 28th to 30th, 2023

Osaka International Convention Center, Osaka, Japan

Program No: 3C10

Reference

(1)   Koyama, K. The Role and Future of Fossil Fuel. IEEJ energy Journal Special Issue October 2017, https://eneken.ieej.or.jp/data/7647.pdf

(2)   Winter, M.; Brodd, R. J. What Are Batteries, Fuel Cells, and Supercapacitors? *Chem Rev* **2004**, *104* (10), 4245–4269. https://doi.org/10.1021/cr020730k.

(3)   Ding, J.; Hu, W.; Paek, E.; Mitlin, D. Review of Hybrid Ion Capacitors: From Aqueous to Lithium to Sodium. *Chemical Reviews*. American Chemical Society July 25, 2018, pp 6457–6498. https://doi.org/10.1021/acs.chemrev.8b00116.

(4)   Goodenough, J. B.; Park, K. S. The Li-Ion Rechargeable Battery: A Perspective. *Journal of the American Chemical Society*. January 30, 2013, pp 1167–1176. https://doi.org/10.1021/ja3091438.

(5)   Jeyaseelan, C.; Jain, A.; Khurana, P.; Kumar, D.; Thatai, S. *9 Ni-Cd Batteries*; 2020.

(6)   May, G. J.; Davidson, A.; Monahov, B. Lead Batteries for Utility Energy Storage: A Review. *Journal of Energy Storage*. Elsevier Ltd February 1, 2018, pp 145–157. https://doi.org/10.1016/j.est.2017.11.008.

(7)   Tomaszewska, A.; Chu, Z.; Feng, X.; O'Kane, S.; Liu, X.; Chen, J.; Ji, C.; Endler, E.; Li, R.; Liu, L.; Li, Y.; Zheng, S.; Vetterlein, S.; Gao, M.; Du, J.; Parkes, M.; Ouyang, M.; Marinescu, M.; Offer, G.; Wu, B. Lithium-Ion Battery Fast Charging: A Review. *eTransportation*. Elsevier B.V. August 1, 2019. https://doi.org/10.1016/j.etran.2019.100011.

(8)   Chen, Y.; Kang, Y.; Zhao, Y.; Wang, L.; Liu, J.; Li, Y.; Liang, Z.; He, X.; Li, X.; Tavajohi, N.; Li, B. A Review of Lithium-Ion Battery Safety Concerns: The Issues, Strategies, and Testing Standards. *Journal of Energy Chemistry*. Elsevier B.V. August 1, 2021, pp 83–99. https://doi.org/10.1016/j.jechem.2020.10.017.

(9)   Wu, F.; Maier, J.; Yu, Y. Guidelines and Trends for Next-Generation Rechargeable Lithium and Lithium-Ion Batteries. *Chemical Society Reviews*. Royal Society of Chemistry March 7, 2020, pp 1569–1614. https://doi.org/10.1039/c7cs00863e.

(10) Manthiram, A. A Reflection on Lithium-Ion Battery Cathode Chemistry. *Nature Communications*. Nature Research December 1, 2020. https://doi.org/10.1038/s41467-020-15355-0.

(11) Quartarone, E.; Mustarelli, P. Review—Emerging Trends in the Design of Electrolytes for Lithium and Post-Lithium Batteries. *J Electrochem Soc* **2020**, *167* (5), 050508. https://doi.org/10.1149/1945-7111/ab63c4.

(12) Lee, H.; Yanilmaz, M.; Toprakci, O.; Fu, K.; Zhang, X. A Review of Recent Developments in Membrane Separators for Rechargeable Lithium-Ion Batteries. *Energy and Environmental Science*. Royal Society of Chemistry December 1, 2014, pp 3857–3886. https://doi.org/10.1039/c4ee01432d.

(13) Lingappan, N.; Kong, L.; Pecht, M. The Significance of Aqueous Binders in Lithium-Ion Batteries. *Renewable and Sustainable Energy Reviews*. Elsevier Ltd September 1, 2021. https://doi.org/10.1016/j.rser.2021.111227.

(14) Zou, F.; Manthiram, A. A Review of the Design of Advanced Binders for High-Performance Batteries. *Advanced Energy Materials*. Wiley-VCH Verlag December 1, 2020. https://doi.org/10.1002/aenm.202002508.

(15) Zhang, H.; Yang, Y.; Ren, D.; Wang, L.; He, X. Graphite as Anode Materials: Fundamental Mechanism, Recent Progress and Advances. *Energy Storage Materials*. Elsevier B.V. April 1, 2021,

pp 147–170. https://doi.org/10.1016/j.ensm.2020.12.027.

(16) Deng, L.; Zheng, Y.; Zheng, X.; Or, T.; Ma, Q.; Qian, L.; Deng, Y.; Yu, A.; Li, J.; Chen, Z. Design Criteria for Silicon-Based Anode Binders in Half and Full Cells. *Advanced Energy Materials*. John Wiley and Sons Inc August 1, 2022. https://doi.org/10.1002/aenm.202200850.

(17) Li, Z.; Zhang, Y.; Liu, T.; Gao, X.; Li, S.; Ling, M.; Liang, C.; Zheng, J.; Lin, Z. Silicon Anode with High Initial Coulombic Efficiency by Modulated Trifunctional Binder for High-Areal-Capacity Lithium-Ion Batteries. *Adv Energy Mater* **2020**, *10* (20). https://doi.org/10.1002/aenm.201903110.

(18) Asenbauer, J.; Eisenmann, T.; Kuenzel, M.; Kazzazi, A.; Chen, Z.; Bresser, D. The Success Story of Graphite as a Lithium-Ion Anode Material-Fundamentals, Remaining Challenges, and Recent Developments Including Silicon (Oxide) Composites. *Sustainable Energy and Fuels*. Royal Society of Chemistry November 1, 2020, pp 5387–5416. https://doi.org/10.1039/d0se00175a.

(19) Agubra, V. A.; Fergus, J. W. The Formation and Stability of the Solid Electrolyte Interface on the Graphite Anode. *Journal of Power Sources*. Elsevier December 15, 2014, pp 153–162. https://doi.org/10.1016/j.jpowsour.2014.06.024.

(20) Wang, Q.; Yao, Z.; Zhao, C.; Verhallen, T.; Tabor, D. P.; Liu, M.; Ooms, F.; Kang, F.; Aspuru-Guzik, A.; Hu, Y. S.; Wagemaker, M.; Li, B. Interface Chemistry of an Amide Electrolyte for Highly Reversible Lithium Metal Batteries. *Nat Commun* **2020**, *11* (1). https://doi.org/10.1038/s41467-020-17976-x.

(21) Yamada, Y.; Usui, K.; Chiang, C. H.; Kikuchi, K.; Furukawa, K.; Yamada, A. General Observation of Lithium Intercalation into Graphite in Ethylene-Carbonate-Free Superconcentrated Electrolytes. *ACS Applied Materials and Interfaces*. American Chemical Society July 23, 2014, pp 10892–10899. https://doi.org/10.1021/am5001163.

(22) Peljo, P.; Girault, H. H. Electrochemical Potential Window of Battery Electrolytes: The HOMO-LUMO Misconception. *Energy Environ Sci* **2018**, *11* (9), 2306–2309. https://doi.org/10.1039/c8ee01286e.

(23) Shi, Q.; Heng, S.; Qu, Q.; Gao, T.; Liu, W.; Hang, L.; Zheng, H. Constructing an Elastic Solid Electrolyte Interphase on Graphite: A Novel Strategy Suppressing Lithium Inventory Loss in Lithium-Ion Batteries. *J Mater Chem A Mater* **2017**, *5* (22), 10885–10894. https://doi.org/10.1039/c7ta02706k.

(24) Gupta, A.; Badam, R.; Nag, A.; Kaneko, T.; Matsumi, N. Bis-Imino-Acenaphthenequinone-Paraphenylene-Type Condensation Copolymer Binder for Ultralong Cyclable Lithium-Ion Rechargeable Batteries. *ACS Appl Energy Mater* **2021**, *4* (3), 2231–2240. https://doi.org/10.1021/acsaem.0c02742.

(25) Patnaik, S. G.; Vedarajan, R.; Matsumi, N. BIAN Based Electroactive Polymer with Defined Active Centers as Metal-Free Electrocatalysts for Oxygen Reduction Reaction (ORR) in Aqueous and Nonaqueous Media. *ACS Appl Energy Mater* **2018**, *1* (3), 1183–1190. https://doi.org/10.1021/acsaem.7b00293.

(26) Mantripragada, B. S.; Badam, R.; Matsumi, N. BIAN-Based Porous Organic Polymer as a High-Performance Anode for Lithium-Ion Batteries. *ACS Appl Energy Mater* **2022**, *5* (6), 6903–6912. https://doi.org/10.1021/acsaem.2c00530.

(27) Gupta, A.; Badam, R.; Matsumi, N. Heavy-Duty Performance from Silicon Anodes Using

Poly(BIAN)/Poly(Acrylic Acid)-Based Self-Healing Composite Binder in Lithium-Ion Secondary Batteries. *ACS Appl Energy Mater* **2022**, *5* (7), 7977–7987. https://doi.org/10.1021/acsaem.2c00278.

(28) Hays, K. A.; Ruther, R. E.; Kukay, A. J.; Cao, P.; Saito, T.; Wood, D. L.; Li, J. What Makes Lithium Substituted Polyacrylic Acid a Better Binder than Polyacrylic Acid for Silicon-Graphite Composite Anodes? *J Power Sources* **2018**, *384*, 136–144. https://doi.org/10.1016/j.jpowsour.2018.02.085.

(29) Han, B.; Piernas-Muñoz, M. J.; Dogan, F.; Kubal, J.; Trask, S. E.; Bloom, I. D.; Vaughey, J. T.; Key, B. Probing the Reaction between PVDF and LiPAA vs Li 7 Si 3 : Investigation of Binder Stability for Si Anodes . *J Electrochem Soc* **2019**, *166* (12), A2396–A2402. https://doi.org/10.1149/2.0241912jes.

(30) Mahmud, S.; Rahman, M.; Kamruzzaman, M.; Ali, M. O.; Emon, M. S. A.; Khatun, H.; Ali, M. R. Recent Advances in Lithium-Ion Battery Materials for Improved Electrochemical Performance: A Review. *Results in Engineering* **2022**, *15*. https://doi.org/10.1016/j.rineng.2022.100472.

(31) Pradhan, A.; Badam, R.; Miyairi, R.; Takamori, N.; Matsumi, N. Extreme Fast Charging Capability in Graphite Anode via a Lithium Borate Type Biobased Polymer as Aqueous Polyelectrolyte Binder. *ACS Mater Lett* **2023**, *5* (2), 413–420. https://doi.org/10.1021/acsmaterialslett.2c00999.

(32) Yao, Y. X.; Chen, X.; Yao, N.; Gao, J. H.; Xu, G.; Ding, J. F.; Song, C. L.; Cai, W. L.; Yan, C.; Zhang, Q. Unlocking Charge Transfer Limitations for Extreme Fast Charging of Li-Ion Batteries. *Angewandte Chemie - International Edition* **2023**, *62* (4). https://doi.org/10.1002/anie.202214828.

(33) Wang, Y.; Zhang, L.; Qu, Q.; Zhang, J.; Zheng, H. Tailoring the Interplay between Ternary Composite Binder and Graphite Anodes toward High-Rate and Long-Life Li-Ion Batteries. *Electrochim Acta* **2016**, *191*, 70–80. https://doi.org/10.1016/j.electacta.2016.01.025.

(34) Patnaik, K. S.; Badam, R.; Peng, Y.; Higashimine, K.; Kaneko, T.; Matsumi, N. Extremely Fast Charging Lithium-Ion Battery Using Bio-Based Polymer-Derived Heavily Nitrogen Doped Carbon. *Chemical Communications* **2021**, *57* (100), 13704–13707. https://doi.org/10.1039/d1cc04931c.

(35) Patnaik, S. G.; Vedarajan, R.; Matsumi, N. BIAN Based Electroactive Polymer with Defined Active Centers as Metal-Free Electrocatalysts for Oxygen Reduction Reaction (ORR) in Aqueous and Nonaqueous Media. *ACS Appl Energy Mater* **2018**, *1* (3), 1183–1190. https://doi.org/10.1021/acsaem.7b00293.

(36) Gupta, A.; Badam, R.; Matsumi, N. Heavy-Duty Performance from Silicon Anodes Using Poly(BIAN)/Poly(Acrylic Acid)-Based Self-Healing Composite Binder in Lithium-Ion Secondary Batteries. *ACS Appl Energy Mater* **2022**, *5* (7), 7977–7987. https://doi.org/10.1021/acsaem.2c00278.

(37) Badam, R.; Shibuya, M.; Mantripragada, B. S.; Ohira, M.; Zhou, L.; Matsumi, N. BIAN-Based Durable Polymer Metal Complex as a Cathode Material for Li–O2 Battery Applications. *Polym J* **2022**, *54* (11), 1355–1366. https://doi.org/10.1038/s41428-022-00699-9.

(38) Komaba, S.; Yabuuchi, N.; Ozeki, T.; Okushi, K.; Yui, H.; Konno, K.; Katayama, Y.; Miura, T. Functional Binders for Reversible Lithium Intercalation into Graphite in Propylene Carbonate and Ionic Liquid Media. *J Power Sources* **2010**, *195* (18), 6069–6074. https://doi.org/10.1016/j.jpowsour.2009.12.058.

(39) Porcher, W.; Chazelle, S.; Boulineau, A.; Mariage, N.; Alper, J. P.; Van Rompaey, T.; Bridel, J.-S.; Haon, C. Understanding Polyacrylic Acid and Lithium Polyacrylate Binder Behavior in Silicon

Based Electrodes for Li-Ion Batteries. *J Electrochem Soc* **2017**, *164* (14), A3633–A3640. https://doi.org/10.1149/2.0821714jes.

(40) Wang, A.; Kadam, S.; Li, H.; Shi, S.; Qi, Y. Review on Modeling of the Anode Solid Electrolyte Interphase (SEI) for Lithium-Ion Batteries. *npj Computational Materials*. Nature Publishing Group December 1, 2018. https://doi.org/10.1038/s41524-018-0064-0.

(41) Mishra, S. N.; Punyasloka, S.; Mantripragada, B. S.; Pradhan, A.; Matsumi, N. Enabling Ultrafast Charging in Graphite Anodes Using BIAN-Based Conjugated Polymer/Lithium Polyacrylate as a Binder. *ACS Appl Energy Mater* **2023**. https://doi.org/10.1021/acsaem.3c02129.

(42) Okubo, M.; Tanaka, Y.; Zhou, H.; Kudo, T.; Honma, I. Determination of Activation Energy for Li Ion Diffusion in Electrodes. *Journal of Physical Chemistry B* **2009**, *113* (9), 2840–2847. https://doi.org/10.1021/jp8099576.

(43) Jow, T. R.; Delp, S. A.; Allen, J. L.; Jones, J.-P.; Smart, M. C. Factors Limiting Li + Charge Transfer Kinetics in Li-Ion Batteries . *J Electrochem Soc* **2018**, *165* (2), A361–A367. https://doi.org/10.1149/2.1221802jes.

(44) Jow, T. R.; Allen, J. L.; Deveney, B.; Nechev, K. Charge Transfer and Charge-Discharge Kinetics in Lithium-Ion Batteries. *ECS Trans* **2009**, *16* (35), 163–169. https://doi.org/10.1149/1.3123137.

(45) An, S. J.; Li, J.; Daniel, C.; Mohanty, D.; Nagpure, S.; Wood, D. L. The State of Understanding of the Lithium-Ion-Battery Graphite Solid Electrolyte Interphase (SEI) and Its Relationship to Formation Cycling. *Carbon*. Elsevier Ltd August 1, 2016, pp 52–76. https://doi.org/10.1016/j.carbon.2016.04.008.

(46) Patnaik, S. G.; Vedarajan, R.; Matsumi, N. BIAN Based Functional Diimine Polymer Binder for High Performance Li Ion Batteries. *J Mater Chem A Mater* **2017**, *5* (34), 17909–17919. https://doi.org/10.1039/c7ta03843g.

(47) Zhang, S. S.; Xu, K.; Jow, T. R. Evaluation on a Water-Based Binder for the Graphite Anode of Li-Ion Batteries. *J Power Sources* **2004**, *138* (1–2), 226–231. https://doi.org/10.1016/j.jpowsour.2004.05.056.

(48) Bleda-Martínez, M. J.; Lozano-Castelló, D.; Morallón, E.; Cazorla-Amorós, D.; Linares-Solano, A. Chemical and Electrochemical Characterization of Porous Carbon Materials. *Carbon N Y* **2006**, *44* (13), 2642–2651. https://doi.org/10.1016/j.carbon.2006.04.017.

(49) Versaci, D.; Nasi, R.; Zubair, U.; Amici, J.; Sgroi, M.; Dumitrescu, M. A.; Francia, C.; Bodoardo, S.; Penazzi, N. New Eco-Friendly Low-Cost Binders for Li-Ion Anodes. *Journal of Solid State Electrochemistry* **2017**, *21* (12), 3429–3435. https://doi.org/10.1007/s10008-017-3665-5.

(50) Tan, K. L.; Tan, B. T. G.; Kang, E. T.; Neoh, K. G. *X-Ray Photoelectron Spectroscopy Studies of the Chemical Structure of Polyani»ne*; Vol. 39.

(51) Pohjalainen, E.; Sorsa, O.; Juurikivi, J.; Kallio, T. Water-Soluble Acrylate Binder for Graphite Electrodes in Lithium-Ion Batteries. *Energy Technology* **2016**, *4* (4), 470–472. https://doi.org/10.1002/ente.201500371.

(52) Wang, H.; Zhang, C.; Liu, Z.; Wang, L.; Han, P.; Xu, H.; Zhang, K.; Dong, S.; Yao, J.; Cui, G. Nitrogen-Doped Graphene Nanosheets with Excellent Lithium Storage Properties. *J Mater Chem* **2011**, *21* (14), 5430–5434. https://doi.org/10.1039/c1jm00049g.

(53) Buqa, H.; Holzapfel, M.; Krumeich, F.; Veit, C.; Novák, P. Study of Styrene Butadiene Rubber and Sodium Methyl Cellulose as Binder for Negative Electrodes in Lithium-Ion Batteries. *J Power*

Sources **2006**, *161* (1), 617–622. https://doi.org/10.1016/j.jpowsour.2006.03.073.

(54) Lu, M.; Cheng, H.; Yang, Y. A Comparison of Solid Electrolyte Interphase (SEI) on the Artificial Graphite Anode of the Aged and Cycled Commercial Lithium Ion Cells. *Electrochim Acta* **2008**, *53* (9), 3539–3546. https://doi.org/10.1016/j.electacta.2007.09.062.

(55) Wang, L.; Fu, Y.; Battaglia, V. S.; Liu, G. SBR-PVDF Based Binder for the Application of SLMP in Graphite Anodes. *RSC Adv* **2013**, *3* (35), 15022–15027. https://doi.org/10.1039/c3ra42773k.

(56) Leroy, S.; Blanchard, F.; Dedryvère, R.; Martinez, H.; Carré, B.; Lemordant, D.; Gonbeau, D. Surface Film Formation on a Graphite Electrode in Li-Ion Batteries: AFM and XPS Study. *Surface and Interface Analysis* **2005**, *37* (10), 773–781. https://doi.org/10.1002/sia.2072.

(57) Jayakumar, T. P.; Badam, R.; Matsumi, N. Allylimidazolium-Based Poly(Ionic Liquid) Anodic Binder for Lithium-Ion Batteries with Enhanced Cyclability. *ACS Appl Energy Mater* **2020**, *3* (4), 3337–3346. https://doi.org/10.1021/acsaem.9b02376.

(58) Erk, C.; Brezesinski, T.; Sommer, H.; Schneider, R.; Janek, J. Toward Silicon Anodes for Next-Generation Lithium Ion Batteries: A Comparative Performance Study of Various Polymer Binders and Silicon Nanopowders. *ACS Appl Mater Interfaces* **2013**, *5* (15), 7299–7307. https://doi.org/10.1021/am401642c.

(59) Jia, H.; Xu, Y.; Burton, S. D.; Gao, P.; Zhang, X.; Matthews, B. E.; Engelhard, M. H.; Zhong, L.; Bowden, M. E.; Xiao, B.; Han, K. S.; Wang, C.; Xu, W. Enabling Ether-Based Electrolytes for Long Cycle Life of Lithium-Ion Batteries at High Charge Voltage. *ACS Appl Mater Interfaces* **2020**, *12* (49), 54893–54903. https://doi.org/10.1021/acsami.0c18177.

(60) Xing, J.; Bliznakov, S.; Bonville, L.; Oljaca, M.; Maric, R. A Review of Nonaqueous Electrolytes, Binders, and Separators for Lithium-Ion Batteries. *Electrochemical Energy Reviews*. Springer December 1, 2022. https://doi.org/10.1007/s41918-022-00131-z.

(61) Choi, J.; Kim, K.; Jeong, J.; Cho, K. Y.; Ryou, M. H.; Lee, Y. M. Highly Adhesive and Soluble Copolyimide Binder: Improving the Long-Term Cycle Life of Silicon Anodes in Lithium-Ion Batteries. *ACS Appl Mater Interfaces* **2015**, *7* (27), 14851–14858. https://doi.org/10.1021/acsami.5b03364.

(62) Song, Z.; Wang, L.; Yang, K.; Gong, Y.; Yang, L.; Liu, X.; Pan, F. Intermolecular Chemistry for Designing Functional Binders in Silicon/Carbon Composite Anodes. *Materials Today Energy*. Elsevier Ltd December 1, 2022. https://doi.org/10.1016/j.mtener.2022.101153.

(63) Zhao, Y. M.; Yue, F. S.; Li, S. C.; Zhang, Y.; Tian, Z. R.; Xu, Q.; Xin, S.; Guo, Y. G. Advances of Polymer Binders for Silicon-Based Anodes in High Energy Density Lithium-Ion Batteries. *InfoMat*. Blackwell Publishing Ltd May 1, 2021, pp 460–501. https://doi.org/10.1002/inf2.12185.

(64) Choi, N. S.; Ha, S. Y.; Lee, Y.; Jang, J. Y.; Jeong, M. H.; Shin, W. C.; Ue, M. Recent Progress on Polymeric Binders for Silicon Anodes in Lithium-Ion Batteries. *Journal of Electrochemical Science and Technology*. Korean Electrochemical Society June 1, 2015, pp 35–49. https://doi.org/10.5229/JECST.2015.6.2.35.

(65) Eshetu, G. G.; Figgemeier, E. Confronting the Challenges of Next-Generation Silicon Anode-Based Lithium-Ion Batteries: Role of Designer Electrolyte Additives and Polymeric Binders. *ChemSusChem*. Wiley-VCH Verlag June 21, 2019, pp 2515–2539. https://doi.org/10.1002/cssc.201900209.

(66) Li, Z.; Zhang, Y.; Liu, T.; Gao, X.; Li, S.; Ling, M.; Liang, C.; Zheng, J.; Lin, Z. Silicon Anode

with High Initial Coulombic Efficiency by Modulated Trifunctional Binder for High-Areal-Capacity Lithium-Ion Batteries. *Adv Energy Mater* **2020**, *10* (20). https://doi.org/10.1002/aenm.201903110.

(67)   Mantripragada, B. S.; Badam, R.; Matsumi, N. BIAN-Based Porous Organic Polymer as a High-Performance Anode for Lithium-Ion Batteries. *ACS Appl Energy Mater* **2022**, *5* (6), 6903–6912. https://doi.org/10.1021/acsaem.2c00530.

(68)   Gupta, A.; Badam, R.; Matsumi, N. Heavy-Duty Performance from Silicon Anodes Using Poly(BIAN)/Poly(Acrylic Acid)-Based Self-Healing Composite Binder in Lithium-Ion Secondary Batteries. *ACS Appl Energy Mater* **2022**, *5* (7), 7977–7987. https://doi.org/10.1021/acsaem.2c00278.

(69)   Li, S.; Liu, Y. M.; Zhang, Y. C.; Song, Y.; Wang, G. K.; Liu, Y. X.; Wu, Z. G.; Zhong, B. H.; Zhong, Y. J.; Guo, X. D. A Review of Rational Design and Investigation of Binders Applied in Silicon-Based Anodes for Lithium-Ion Batteries. *Journal of Power Sources*. Elsevier B.V. February 15, 2021. https://doi.org/10.1016/j.jpowsour.2020.229331.

(70)   Preman, A. N.; Lee, H.; Yoo, J.; Kim, I. T.; Saito, T.; Ahn, S. K. Progress of 3D Network Binders in Silicon Anodes for Lithium Ion Batteries. *Journal of Materials Chemistry A*. Royal Society of Chemistry December 28, 2020, pp 25548–25570. https://doi.org/10.1039/d0ta07713e.

(71)   Patnaik, S. G.; Vedarajan, R.; Matsumi, N. BIAN Based Electroactive Polymer with Defined Active Centers as Metal-Free Electrocatalysts for Oxygen Reduction Reaction (ORR) in Aqueous and Nonaqueous Media. *ACS Appl Energy Mater* **2018**, *1* (3), 1183–1190. https://doi.org/10.1021/acsaem.7b00293.

(72)   Gupta, A.; Badam, R.; Nag, A.; Kaneko, T.; Matsumi, N. Bis-Imino-Acenaphthenequinone-Paraphenylene-Type Condensation Copolymer Binder for Ultralong Cyclable Lithium-Ion Rechargeable Batteries. *ACS Appl Energy Mater* **2021**, *4* (3), 2231–2240. https://doi.org/10.1021/acsaem.0c02742.

(73)   Patnaik, K. S.; Badam, R.; Peng, Y.; Higashimine, K.; Kaneko, T.; Matsumi, N. Extremely Fast Charging Lithium-Ion Battery Using Bio-Based Polymer-Derived Heavily Nitrogen Doped Carbon. *Chemical Communications* **2021**, *57* (100), 13704–13707. https://doi.org/10.1039/d1cc04931c.

(74)   Badam, R.; Shibuya, M.; Mantripragada, B. S.; Ohira, M.; Zhou, L.; Matsumi, N. BIAN-Based Durable Polymer Metal Complex as a Cathode Material for Li–O2 Battery Applications. *Polym J* **2022**, *54* (11), 1355–1366. https://doi.org/10.1038/s41428-022-00699-9.

(75)   Shen, H.; Wang, Q.; Chen, Z.; Rong, C.; Chao, D. Application and Development of Silicon Anode Binders for Lithium-Ion Batteries. *Materials*. MDPI June 1, 2023. https://doi.org/10.3390/ma16124266.

(76)   Wang, H.; Wu, B.; Wu, X.; Zhuang, Q.; Liu, T.; Pan, Y.; Shi, G.; Yi, H.; Xu, P.; Xiong, Z.; Chou, S. L.; Wang, B. Key Factors for Binders to Enhance the Electrochemical Performance of Silicon Anodes through Molecular Design. *Small*. John Wiley and Sons Inc January 1, 2022. https://doi.org/10.1002/smll.202101680.

(77)   Li, B.; Li, C.; Cao, Z.; Wang, J.; Zhao, J. *Improving Electrochemical Performance of Li 1.2 Mn 0.52 Co 0.13 Ni 0.13 O 2 by Surface Nitrogen Doping via the Plasma Treatment*; 2016.

(78)   Chen, S.; Song, Z.; Wang, L.; Chen, H.; Zhang, S.; Pan, F.; Yang, L. Establishing a Resilient Conductive Binding Network for Si-Based Anodes via Molecular Engineering. *Acc Chem Res* **2022**,

55 (15), 2088–2102. https://doi.org/10.1021/acs.accounts.2c00259.

(79) Li, Z.; Tang, W.; Yang, Y.; Lai, G.; Lin, Z.; Xiao, H.; Qiu, J.; Wei, X.; Wu, S.; Lin, Z. Engineering Prelithiation of Polyacrylic Acid Binder: A Universal Strategy to Boost Initial Coulombic Efficiency for High-Areal-Capacity Si-Based Anodes. *Adv Funct Mater* **2022**, *32* (40). https://doi.org/10.1002/adfm.202206615.

(80) Niesen, S.; Fox, A.; Murugan, S.; Richter, G.; Buchmeiser, M. R. Multifunctional Self-Cross-Linked Copolymer Binder for High-Loading Silicon Anodes. *ACS Appl Energy Mater* **2022**. https://doi.org/10.1021/acsaem.2c01867.

(81) He, J.; Das, C.; Yang, F.; Maibach, J. Crosslinked Poly(Acrylic Acid) Enhances Adhesion and Electrochemical Performance of Si Anodes in Li-Ion Batteries. *Electrochim Acta* **2022**, *411*. https://doi.org/10.1016/j.electacta.2022.140038.

(82) Pan, Y.; Ge, S.; Rashid, Z.; Gao, S.; Erwin, A.; Tsukruk, V.; Vogiatzis, K. D.; Sokolov, A. P.; Yang, H.; Cao, P. F. Adhesive Polymers as Efficient Binders for High-Capacity Silicon Electrodes. *ACS Appl Energy Mater* **2020**, *3* (4), 3387–3396. https://doi.org/10.1021/acsaem.9b02420.

(83) Xiong, J.; Dupré, N.; Moreau, P.; Lestriez, B. From the Direct Observation of a PAA-Based Binder Using STEM-VEELS to the Ageing Mechanism of Silicon/Graphite Anode with High Areal Capacity Cycled in an FEC-Rich and EC-Free Electrolyte. *Adv Energy Mater* **2022**, *12* (12). https://doi.org/10.1002/aenm.202103348.

(84) Li, Z.; Wu, G.; Yang, Y.; Wan, Z.; Zeng, X.; Yan, L.; Wu, S.; Ling, M.; Liang, C.; Hui, K. N.; Lin, Z. An Ion-Conductive Grafted Polymeric Binder with Practical Loading for Silicon Anode with High Interfacial Stability in Lithium-Ion Batteries. *Adv Energy Mater* **2022**, *12* (29). https://doi.org/10.1002/aenm.202201197.

(85) Guo, M. J.; Xiang, C. C.; Hu, Y. Y.; Deng, L.; Pan, S. Y.; Lv, C.; Chen, S. X.; Deng, H. T.; Sun, C. D.; Li, J. T.; Zhou, Y.; Sun, S. G. A Dual Force Cross-Linked γ-PGA-PAA Binder Enhancing the Cycle Stability of Silicon-Based Anodes for Lithium-Ion Batteries. *Electrochim Acta* **2022**, *425*. https://doi.org/10.1016/j.electacta.2022.140704.

(86) Lee, H. A.; Shin, M.; Kim, J.; Choi, J. W.; Lee, H. Designing Adaptive Binders for Microenvironment Settings of Silicon Anode Particles. *Advanced Materials* **2021**, *33* (13). https://doi.org/10.1002/adma.202007460.

(87) Huang, H.; Wei, D.; Zhu, X.; Wu, Z.; Ling, M. Calcium Ions Modification Polyacrylamide Grafted Protein Binder for Silicon Anode in Lithium-Ion Battery. *Mater Chem Phys* **2023**, *295*. https://doi.org/10.1016/j.matchemphys.2022.127129.

(88) Lai, Y.; Li, H.; Zhang, Y.; Yang, Q.; Li, H.; Sun, Y.; Liu, Y.; Zhong, B.; Wu, Z.; Guo, X. Investigation of Effective Bonding between Varied Binders and Si Anode with Different Particle Sizes. *Appl Phys Lett* **2022**, *121* (18). https://doi.org/10.1063/5.0119372.

(89) Wang, F.; Ma, X.; Li, Y.; Liu, H.; Wu, Q.; Guan, X.; Liu, H.; Wang, X. X.; Xu, J. Room-Temperature Rapid Self-Healing Polymer Binders for Si Anodes in Highly Cycling-Stable and Capacity-Maintained Lithium-Ion Batteries. *ACS Appl Energy Mater* **2023**, *6* (6), 3538–3548. https://doi.org/10.1021/acsaem.3c00161.

(90) Liu, T.; Chu, Q.; Yan, C.; Zhang, S.; Lin, Z.; Lu, J. Interweaving 3D Network Binder for High-Areal-Capacity Si Anode through Combined Hard and Soft Polymers. *Adv Energy Mater* **2019**, *9* (3). https://doi.org/10.1002/aenm.201802645.

(91)   Zheng, F.; Tang, Z.; Lei, Y.; Zhong, R.; Chen, H.; Hong, R. PAAS-β-CDp-PAA as a High-Performance Easily Prepared and Water-Soluble Composite Binder for High-Capacity Silicon Anodes in Lithium-Ion Batteries. *J Alloys Compd* **2023**, *932*. https://doi.org/10.1016/j.jallcom.2022.167666.

(92)   Hu, Z.; Zhao, R.; Yang, J.; Wu, C.; Bai, Y. Binders for Si Based Electrodes: Current Status, Modification Strategies and Perspective. *Energy Storage Materials*. Elsevier B.V. May 1, 2023. https://doi.org/10.1016/j.ensm.2023.102776.

(93)   Luo, C.; Du, L.; Wu, W.; Xu, H.; Zhang, G.; Li, S.; Wang, C.; Lu, Z.; Deng, Y. Novel Lignin-Derived Water-Soluble Binder for Micro Silicon Anode in Lithium-Ion Batteries. *ACS Sustain Chem Eng* **2018**, *6* (10), 12621–12629. https://doi.org/10.1021/acssuschemeng.8b01161.

(94)   Kim, W. J.; Kang, J. G.; Kim, D. W. Blood Clot-Inspired Viscoelastic Fibrin Gel: New Aqueous Binder for Silicon Anodes in Lithium Ion Batteries. *Energy Storage Mater* **2022**, *45*, 730–740. https://doi.org/10.1016/j.ensm.2021.12.024.

(95)   Abe, T.; Sagane, F.; Ohtsuka, M.; Iriyama, Y.; Ogumi, Z. Lithium-Ion Transfer at the Interface Between Lithium-Ion Conductive Ceramic Electrolyte and Liquid Electrolyte-A Key to Enhancing the Rate Capability of Lithium-Ion Batteries. *J Electrochem Soc* **2005**, *152* (11), A2151. https://doi.org/10.1149/1.2042907.

…….…………………………………. The End ……….……………………….……..…